



**Universidade do Minho**  
Escola de Medicina

**Fernando António Faria-Correia**

**ROLE OF THE SCHEIMPFLUG-BASED LENS  
DENSITOMETRY IN PREOPERATIVE  
ASSESSMENT OF AGE-RELATED NUCLEAR  
CATARACTS**

Tese de Doutoramento em Medicina

Trabalho realizado sob a orientação de:

**Professor Doutor Renato Ambrósio Júnior**

Professor Associado da Universidade de Federal de São Paulo (UNIFESP), São Paulo, Brasil

E co-orientação de:

**Professor Doutor Jorge Correia-Pinto**

Professor Catedrático da Escola de Medicina da Universidade do Minho, Braga, Portugal

fevereiro de 2017

## **Declaração**

**Nome:** Fernando António Faria Correia

**Endereço electrónico:** id5684@alunos.uminho.pt

**Telefone:** (+351) 919896521

**Número de Bilhete de Identidade:** 12314973

**Título da dissertação:** Role of Scheimpflug-based lens densitometry in preoperative assessment of age-related nuclear cataract.

**Orientação:** Professor Doutor Renato Ambrósio Júnior

**Co-orientação:** Professor Doutor Jorge Correia Pinto

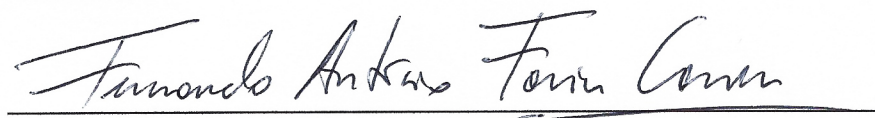
**Ano Conclusão:** 2017

**Designação do Ramo de Conhecimento do Doutoramento:** Medicina

DE ACORDO COM A LEGISLAÇÃO EM VIGOR, NÃO É PERMITIDA A  
REPRODUÇÃO DE QUALQUER PARTE DESTA TESE/TRABALHO

Universidade do Minho, 03 / Maio / 2017

Assinatura



*Fernando António Faria Correia*

## STATEMENT OF INTEGRITY

I hereby declare having conducted my thesis with integrity. I confirm that I have not used plagiarism or any form of falsification of results in the process of the thesis elaboration.

I further declare that I have fully acknowledged the Code of Ethical Conduct of the University of Minho.

University of Minho, 4 / 5 / 2017

Full name: FERNANDO ANTONIO FARIA CORREIA

Signature: Fernando Antonio Faria Correia



“Everything should be made as simple as possible, but not simpler”

Albert Einstein



## **AGRADECIMENTOS**

Esta tese não sendo um trabalho individual mas resultando da colaboração de diversas instituições e pessoas, não posso deixar de dirigir algumas palavras de agradecimento a todos que ajudaram de diferentes formas à sua concretização.

À Professora Doutora Cecília Leão, Presidente da Escola de Medicina da Universidade do Minho, agradeço a possibilidade de ser aluno de doutoramento desta Escola, que sabe incentivar o interesse pela investigação de excelência. É um orgulho para mim fazer parte dos seus doutorandos.

Ao Professor Doutor Jorge Pedrosa, Director do Instituto de Ciências da Vida e da Saúde (ICVS) da Escola de Medicina da Universidade do Minho, agradeço a possibilidade de concretizar os trabalhos científicos que apresento nesta Tese. O ICVS é atualmente uma instituição com créditos afirmados internacionalmente, com as melhores condições para se efectuarem investigações de alto nível científico.

Ao Professor Doutor Renato Ambrósio Júnior, meu Orientador, e também meu Mestre na área do diagnóstico e tratamento da patologia do segmento anterior ocular, devo muitos agradecimentos. Este projecto teve início em março de 2012 aquando da minha chegada ao Rio de Janeiro, para realizar o meu fellowship sob a sua orientação. Sempre confiou em mim, sempre incentivou a criatividade e a perseverança no trabalho de investigação. Proporcionou-me a honra de integrar um grupo científico com a qualidade demonstrada internacionalmente pelo Grupo de Estudo de Tomografia e Biomecânica da Córnea do Rio de Janeiro. Agradeço todas as oportunidades que me concedeu em trabalhar com ele, como também a forte amizade que nos une. Quero deixar uma palavra de simpatia e de amizade à sua esposa, Dra Renata Siqueira, e filhas, Giovanna e Raphaela. Aos restantes colaboradores do grupo de estudo, agradeço a amizade e colaboração nos diversas projetos de investigação que realizamos.

Ao Professor Doutor Jorge Correia Pinto, meu Co-Orientador deste percurso enquanto doutorando, Coordenador do Domínio de Investigação em Ciências

Cirúrgicas do ICVS e Director de Serviço de Cirurgia Pediátrica no Hospital de Braga, quero expressar o meu agradecimento por me ter acompanhado neste caminho. Para além do seu exemplo clínico e científico, sublinho a sua disponibilidade e a inesgotável motivação transmitida.

Ao Dr. Fernando Vaz, Director de Serviço de Oftalmologia do Hospital de Braga, quero manifestar o meu reconhecimento por me ter proposto o desafio para realizar a tese de doutoramento. Quero assinalar que o serviço que dirige foi a base da recolha de todos os dados apresentados neste tese, pelo que deixo aqui a minha mais profunda gratidão ao Dr. Fernando Vaz por todas as facilidades que me concedeu.

A todos os meus colegas e pessoal do Serviço de Oftalmologia do Hospital de Braga, especialmente à secção de córnea e implanto-refractiva (Dr. Tiago Monteiro e Dr. Nuno Franqueira), agradeço a amizade, colaboração e disponibilidade demonstradas durante este percurso.

Ao Dr. George O. Waring IV, professor assistente de Oftalmologia e diretor do Departamento de Cirurgia Refrativa na Medical University of South Carolina, agradeço a partilha de conhecimentos que me proporcionou durante o meu fellowship em 2013, essencialmente na área da avaliação do cristalino disfuncional/catarata.

A toda a minha família quero agradecer o conforto que recebi nas horas mais difíceis deste percurso. Ao meu Pai, minha referência ética e profissional na Oftalmologia, pelos seus conselhos, orientação e entusiasmo que sempre me soube transmitir. À minha Mãe por me ter acompanhado desde criança, pela sua bondade, preocupação e princípios que me transmitiu ao longo dos anos.

À Sara, minha mulher e também minha colega, pelo seu carinho, compreensão, entusiasmo e conselhos para a realização desta tese.

Ao meu filho António Pedro, que me dá força para ir mais além.



## **TITLE: ROLE OF SCHEIMPFLUG-BASED LENS DENSITOMETRY IN PREOPERATIVE ASSESSMENT OF AGE-RELATED NUCLEAR CATARACT.**

**ABSTRACT:** Opacification of the crystalline lens is a commonly observed age-related process and contributes for visual acuity and contrast sensitivity degradation. Cataract surgery is considered to be the most performed surgical procedure worldwide, accounting for about 22 million interventions. In Portugal, about 75.000 cataract surgeries are performed each year. The most widely used clinical method to assess the crystalline lens opacification is the Lens Opacities Classification System III grading system. Scheimpflug imaging enables objective lens densitometry evaluation, which is not susceptible to observer variability and is considered to be a more sensitive and repeatable approach. An extensive literature review related to this topic revealed that objective assessment of cataract with Scheimpflug imaging offers a considerable opportunity for various scientific researches, especially regarding the functional status of the crystalline lens and cataract surgery planning. Several factors compromise the comparison of results and conclusions of previous research studies, such as different densitometric evaluation methods and metrics. The relative absence of studies analyzing a relationship between crystalline lens densitometry and its functional state is also noted, especially when considering ray-tracing aberrometry. This PhD thesis pretend to analyze the application of Scheimpflug imaging in the preoperative evaluation of age-related nuclear cataracts, regarding functional status of the crystalline lens based on ray-tracing wavefront analysis and phacodynamics prediction. In this thesis, we have confirmed that Scheimpflug-based lens densitometry presented a strong association with aging, corrected distance visual acuity decrease, and slit lamp evaluation. A significant and positive relationship was also described between the Scheimpflug-based lens densitometry variables and the internal high-order aberrations, including coma and trefoil. We also studied the relationship between the Scheimpflug-based lens densitometry and a new parameter (Dysfunctional Lens Index) based on ray-tracing wavefront findings. Regarding phacodynamics, we selected different lens densitometric modes to analyze the hardness of the nucleus that were described and used in previous studies. Our results revealed that parameters derived from specific modes, such as three-dimensional and region of interest modes, yielded

the highest correlations coefficients with the ultrasound energy consumed during phacoemulsification. In another study, we also demonstrated that the Dysfunctional Lens Index and the Scheimpflug-derived average density based on three-dimensional presented a similar relationship with phacodynamics. Our findings presented in this thesis suggest that Scheimpflug-based lens densitometry is useful for demonstrating the functional status of the crystalline lens. Scheimpflug-based densitometry also showed to be useful concerning phacodynamics prediction. The data presented also warns for the proper use of the lens densitometry software, regarding selection and placement of the densitometry template, as well as the density metric adopted.

## **TÍTULO: APLICAÇÃO DA DENSITOMETRIA DO CRISTALINO BASEADA NO PRÍNCÍPIO DE SCHEIMPFLUG NA AVALIAÇÃO PRÉ-OPERATÓRIA DE CATARATA NUCLEAR SENIL.**

**RESUMO:** A opacificação do cristalino é um processo relacionado com a idade e contribui para a degradação da acuidade visual e da sensibilidade ao contraste. A cirurgia de catarata é considerada o procedimento cirúrgico mais realizado em todo o mundo, contabilizando cerca de 22 milhões de intervenções. Em Portugal, aproximadamente 75.000 cirurgias de catarata são realizadas anualmente. O método clínico mais amplamente utilizado para avaliar a opacificação do cristalino é o sistema de classificação Lens Opacities Classification System III. O princípio de Scheimpflug permite a avaliação objetiva da densitometria do cristalino, que não é suscetível à variabilidade do observador e é considerada uma abordagem mais sensível e reproduzível. Uma extensa revisão da literatura relacionada com este tópico revelou que a avaliação objetiva da catarata com esta tecnologia oferece uma oportunidade considerável para inúmeras pesquisas científicas, especialmente no que se refere ao estado funcional do cristalino e ao planeamento cirúrgico. Vários fatores comprometem a comparação de resultados e conclusões de pesquisas anteriores, tais como diferentes métodos de avaliação e parâmetros de densitometria. A ausência relativa de estudos que analisam a relação entre a densitometria do cristalino e o seu estado funcional também é evidente, especialmente quando se considera a aberrometria por traçado de raios. Esta tese de doutoramento tem como objetivo analisar a aplicação da imagem Scheimpflug na avaliação pré-operatória de cataratas nucleares senis, no que diz respeito ao estado funcional do cristalino com base na análise de frente de onda por traçado de raios e na previsão da energia ultrassónica consumida durante a facoemulsificação. Confirmamos que a densitometria do cristalino baseada na imagem de Scheimpflug apresentou forte associação com o envelhecimento, a diminuição da melhor acuidade visual corrigida e a avaliação da lâmpada de fenda. Uma relação significativa e positiva também foi descrita entre as variáveis de densitometria baseada no princípio de Scheimpflug e as aberrações de alta ordem internas, incluindo o coma e o trefoil. Também estudamos a relação entre a densitometria do cristalino e um novo parâmetro (Dysfunctional Lens Index)

baseado em achados da frente de onda por traçado de raios. Quanto à facodinâmica, foram selecionados diferentes modos densitométricos do cristalino para analisar a dureza do núcleo, os quais tinham sido descritos e utilizados em estudos anteriores. Os nossos resultados revelaram que os parâmetros derivados de certos modos de análise, tais como os modos tridimensional e de região de interesse, obtiveram os maiores coeficientes de correlação com a energia ultrassónica consumida durante a facoemulsificação. Noutro estudo, também demonstramos que o Dysfunctional Lens Index e a densidade média baseada na análise densitométrica tridimensional apresentaram uma relação similar com a facodinâmica. Os resultados apresentados nesta tese sugerem que a densitometria do cristalino baseado no princípio de Scheimpflug é útil para demonstrar o seu estado funcional. Esta tecnologia também mostrou ser útil em relação à previsão da facodinâmica. Os dados apresentados alertam para o uso adequado do programa de densitometria do cristalino, quanto à seleção e colocação do modelo de densitometria e, os parâmetros de densidade adotados.

## ABREVIATIONS

ADP – Adenosine diphosphate

AQP0 – Aquaporin-0

ATP – Adenosine triphosphate

ATPase – Adenosine triphosphatase

Ca<sup>2+</sup> – calcium

CDE – Cumulative dissipative energy

CDVA – Corrected distance visual acuity

Cl<sup>-</sup> – chloride

CO<sub>2</sub> – carbon dioxide

Da – Dalton

DGS – Direção-Geral da Saúde

DLI – Dysfunctional lens index

DLS – Dysfunctional lens syndrome

G6P – Glucose-6-phosphate

GSH – reduced glutathione

GSSG – oxidized glutathione disulfide

H<sub>2</sub>O – water

H<sub>2</sub>O<sub>2</sub> – hydrogen peroxide

HMP – Hexose monophosphate

HOAs – High-order aberrations

IOL – Intraocular lens

K<sup>+</sup> – Potassium

LOCS – Lens Opacities Classification System

MAPKs – Mitogen-activated protein kinases

mg - Milligrams

MIP – Major intrinsic protein

mL – Mililiters

mm – Milimeters

MTF – Modular transfer function

Na<sup>+</sup> – Sodium

NADP – nicotinamide-adenine dinucleotide phosphate

NADPH - reduced form of nicotinamide adenine dinucleotide phosphate

NC – Nuclear colour  
NF- $\kappa$ B – Nuclear Factor- $\kappa$ B  
nm – Nanometer  
NO – Nuclear opalescence  
OQAS - Optical Quality Analysis System  
OSI – Ocular scatter index  
PNS – Pentacam nuclear staging  
PO<sub>4</sub> – phosphate  
PSF – Point spread function  
RMS – Root mean square  
ROI – Region of interest  
US – Ultrasound  
WHO – World Health Organization  
ZC – Zernike coefficient  
3D – Three-dimensional  
 $\mu$ L – Microliter  
 $\mu$ m – Micrometer  
° – Degrees

## INDEX

<b>CHAPTER I – Introduction and Purposes</b> .....	<b>1</b>
1 – Anatomic and physiological concepts of the crystalline lens .....	3
1.1 – Anatomy of the human eye .....	3
1.2 – Crystalline lens .....	10
1.2.1 – Embryology .....	10
1.2.2 – Morphology .....	11
1.2.3 – Anatomical location .....	12
1.2.4 – Histological structure .....	14
1.2.5 – Vascularization and innervation .....	17
1.2.6 – Biochemistry composition .....	17
1.2.7 – Physiology of the crystalline lens .....	19
1.2.7.1 – Communications between the lens cells .....	19
1.2.7.2 – Electrolyte and hydric balance .....	20
1.2.7.3 – Glucose metabolism .....	23
1.2.7.4 – Protective mechanisms against oxidative damage .....	24
1.2.8 – Functions of the crystalline lens .....	25
2 – Cataract .....	27
2.1 – Definition .....	27
2.2 – Types of cataract .....	29
2.3 – Pathophysiological mechanisms of age-related nuclear cataract .....	30
2.4 – Complementary exams for cataract evaluation .....	33
2.4.1 – Lens Opacities Classification System III grading system .....	35
2.4.2 – Wavefront analysis .....	36
2.4.2.1 – Optical aberrations .....	36
2.4.2.2 – Wavefront surface evaluation .....	37
2.4.2.3 – Optical quality measurement .....	38
2.4.2.4 – Wavefront sensors .....	41
2.4.2.5 – iTrace Visual Function Analyzer .....	42
2.4.2.6 – Wavefront analysis in patients with nuclear cataracts .....	44
2.4.3 – Scheimpflug imaging .....	45
2.4.3.1 – Scheimpflug's principle and its application in Ophthalmology .....	45
2.4.3.2 – Pentacam® HR imaging system .....	52
2.4.3.3 – Lens densitometry software .....	53
2.4.3.4 – Scheimpflug-based lens densitometry in patients with age-related nuclear cataracts .....	56
3 – Cataract surgery .....	57
3.1 – Brief historical background .....	57
3.2 – Nucleus management techniques in phacoemulsification .....	62

3.3 – Scheimpflug-based lens densitometry and its relationship with Phacodynamics .....	63
4 – Purposes .....	64
<b>CHAPTER II – Relationship between Scheimpflug Optical Densitometry And Ocular High-Order Aberrations In Patients With Mild Nuclear Cataract .....</b>	<b>65</b>
<b>CHAPTER III – Relationship between the Dysfunctional Lens Index with Lens Grading Based on the Lens Opacities Classification System III and the Scheimpflug-based Lens Densitometry .....</b>	<b>75</b>
<b>CHAPTER IV – Relationship between Preoperative Scheimpflug-Based Lens Densitometry Metrics And Phacodynamics .....</b>	<b>83</b>
<b>CHAPTER V – Relationship between Objective Metrics for Quantifying Crystalline Lens Dysfunction with Visual Impairment and Phacodynamics Parameters in Patients with Age-related Nuclear Cataract .....</b>	<b>93</b>
<b>CHAPTER VI – Discussion .....</b>	<b>101</b>
<b>CHAPTER VII – Conclusions .....</b>	<b>113</b>
<b>References .....</b>	<b>119</b>



# **CHAPTER I**

## INTRODUCTION AND PURPOSES



## CHAPTER I – INTRODUCTION AND PURPOSES

### 1 – Anatomic and physiological concepts of the crystalline lens

#### 1.1 – Anatomy of the human eye

The human eye presents as an oblate spheroid shape, because of the distinct radii of curvature of the cornea and sclera (8 millimeters (mm) and 12 mm, respectively; Figure 1). Usually, the adult human eye has an anteroposterior diameter of 23 – 25 mm and a transverse diameter of 24 mm. The average total volume of an adult eyeball is approximately 6.5 – 7.0 milliliters (mL). The eyeball presents two main compartments (Figure 1): the anterior segment, which is comprised of the anterior and posterior chambers (Figure 2); the posterior segment, which is composed by the vitreous cavity. (Snell et al. 1998; Riordan-Eva 2011)

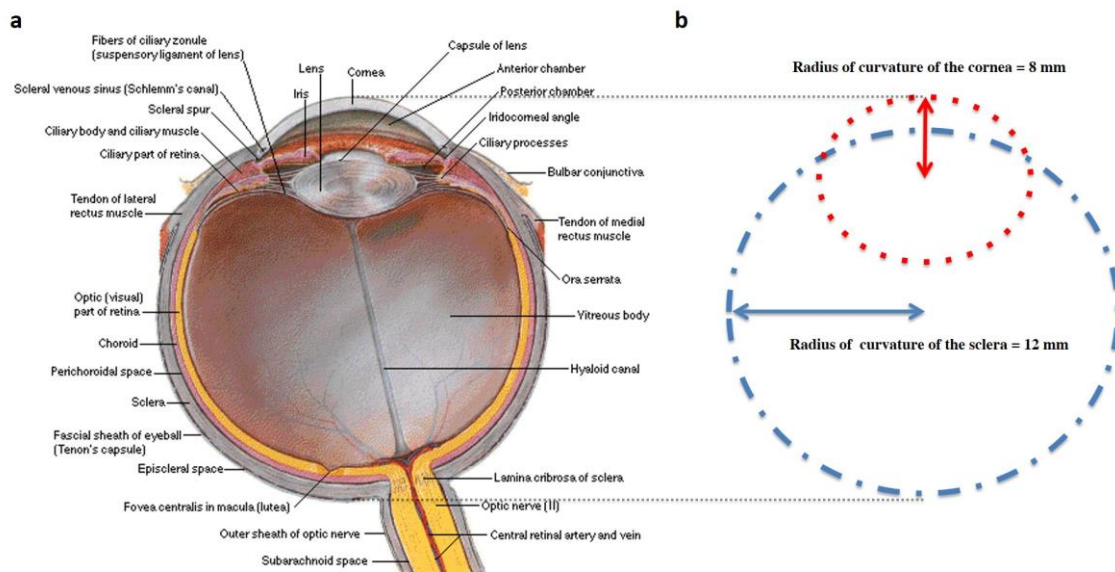


Figure 1 – a) Anatomy of the eye globe; b) Radii of curvature of the cornea and sclera. (Netter, 2011)

The anterior chamber is the space between the cornea and the iris, presenting approximately 3.0 – 3.5 mm of anterior-posterior depth and an average volume of 200 microliter ( $\mu\text{L}$ ). The posterior chamber is the space limited by the iris and the crystalline lens and vitreous face, with approximately 50 – 60  $\mu\text{L}$  of volume. Both chambers are filled with aqueous fluid, being useful to maintain the shape of the eyeball and to provide nutrients and oxygen to the cornea and the crystalline lens. (Snell et al. 1998; Riordan-Eva 2011)

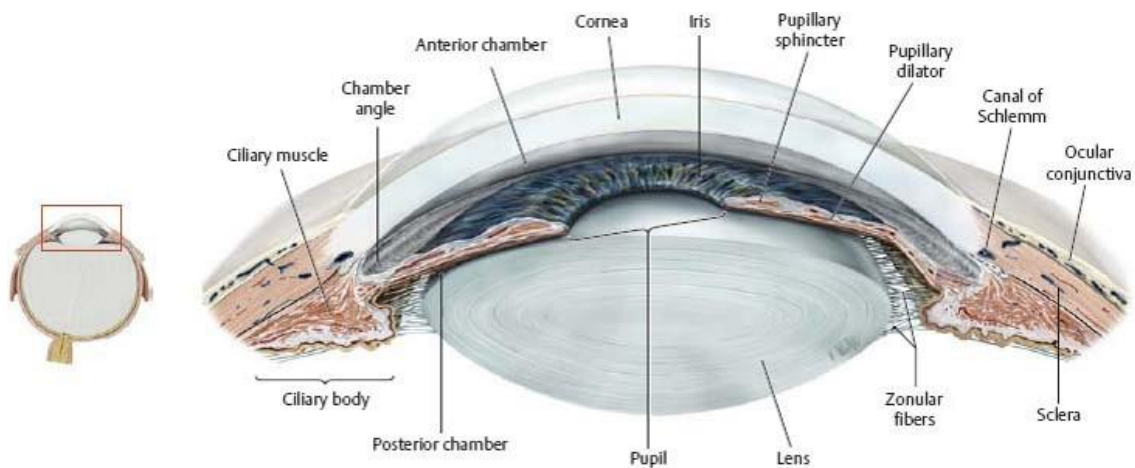


Figure 2 – Anterior segment of the eye formed by the anterior and posterior chambers.(Gilroy *et al.*, 2009)

The vitreous cavity (also known as the posterior segment) is the largest compartment of the eyeball, accounting for more than two-thirds of its volume (5 – 6 mL). This space is filled with vitreous gel, which is a transparent and gelatinous substance that helps in maintaining the retina pushed against the choroid. Unlike the aqueous fluid, which is continuously renewed, the vitreous gel is formed during the embryonic phase and is not replenished.(Snell *et al.* 1998; Riordan-Eva 2011; Mescher *et al.* 2015)

The eyeball is composed of 3 concentric layers (Figure 3). The external layer, also known as the fibrous tunic, is formed by the cornea and the sclera.(Mescher *et al.*, 2015; Riordan-Eva, 2011)

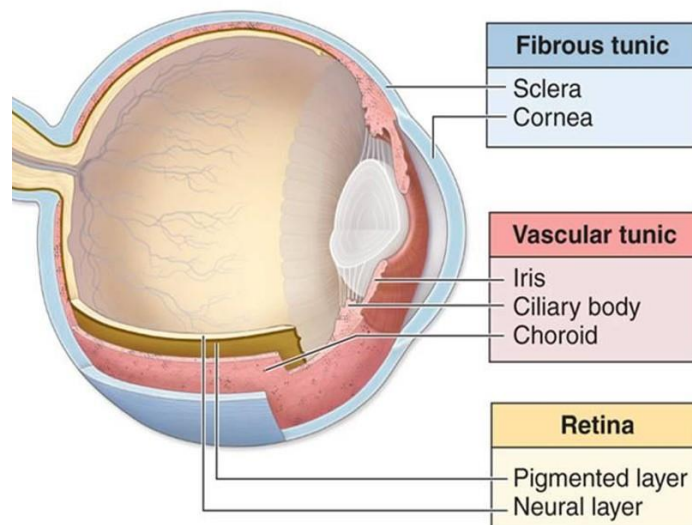


Figure 3 – Layers of the eye globe.(Mescher *et al.*, 2015)

The cornea is a transparent non-vascularized layer and occupies the center of the anterior pole of the eyeball. Its front surface is in direct contact with the tear film and the back surface of the superior eyelid, while its back surface limits the anterior chamber of the eye and is in contact with the aqueous fluid.(Riordan-Eva, 2011; Mescher *et al.*, 2015) The cornea is essential to maintain the intraocular pressure, to support the internal structures of the eye and to protect against ocular trauma. Besides its mechanical functions, this component of the eyeball performs two crucial functions for the ocular vision.(Riordan-Eva, 2011) Its transparency enables the passage of light rays to the retina, and the air-tear film interface on the front surface of the cornea is the main refractive component of the eye, being identical to a positive lens of approximately 43 diopters.(Courville *et al.*, 2004) The anterior surface of the cornea has an elliptical shape, measuring the horizontal and vertical meridians 12.6 mm and 11.7 mm, respectively, while the posterior surface is circular with a diameter of approximately 11.7 mm.(Ambrósio, Nogueira, *et al.*, 2011; Koch *et al.*, 2012; Riordan-Eva, 2011) The corneal thickness is not uniform across the cornea, being the periphery thicker than the central zone (0.65 mm and 0.52 mm, respectively).(Ambrósio, Caiado, *et al.*, 2011; Ambrósio *et al.*, 2003; Riordan-Eva, 2011) Likewise, the curvature is not constant along the anterior surface. The cornea becomes flatter in the periphery, presenting an asymmetrical rate of flattening. It is more pronounced superiorly and nasally compared to the other quadrants.(Riordan-Eva, 2011)

The sclera is a fibrous and practically acellular connective tissue with higher water content than the cornea.(Foster & Sainz de la Maza, 1994; Rada & Johson, 2011; Riordan-Eva, 2011; Mescher *et al.*, 2015) This structure is also avascular, except for the intrascleral vascular plexus and the superficial episcleral vessels adjacent to the limbus.(Foster & Sainz de la Maza, 1994; Rada & Johson, 2011; Riordan-Eva, 2011; Mescher *et al.*, 2015) The whitish-opaque appearance of the sclera is distinct from the corneal transparency because of the high percentage of interweaving between the collagen fibrils and the marked variation in fibril diameter and separation.(Foster & Sainz de la Maza, 1994; Rada & Johson, 2011; Riordan-Eva, 2011; Mescher *et al.*, 2015) The sclera involves the posterior four-fifths of the ocular globe. It helps to keep the shape of the eyeball, protects the inner structures and also provides the support for the tendons of the

extraocular muscles.(Foster & Sainz de la Maza, 1994; Rada & Johson, 2011; Riordan-Eva, 2011) The Tenon capsule is a fascial sheath that covers the sclera up to limbal region, where it merges with the bulbar conjunctiva. This sheath, which separates the eyeball from the periorbital fat, is connected to the sclera by a thin layer of loose connective tissue, known as episclera.(Foster & Sainz de la Maza, 1994; Rada & Johson, 2011; Riordan-Eva, 2011) The thickest parts (1 mm) of the sclera are located anteriorly at the limbus of the cornea, where it joins the corneal stroma, and at the posterior pole.(Riordan-Eva, 2011; Rada & Johson, 2011) The thinnest areas of the sclera are just beneath the insertions of the extraocular muscles, where it measures approximately 0.3 mm.(Riordan-Eva, 2011; Rada & Johson, 2011) The sclera is perforated by the optic nerve, anterior ciliary arteries, vortex veins and ciliary nerves. Lamina cribrosa is the region where the optic nerve penetrates the sclera, being located approximately 1 mm superior and 3 mm medial regarding to the anatomical posterior pole.(Riordan-Eva, 2011; Rada & Johson, 2011) The anterior ciliary arteries penetrate the sclera at the insertions of the rectus muscles. The vortex veins leave the ocular globe 4 mm posterior to the equator. The short and long ciliary nerves traverse the scleral layer near the optic nerve head.(Foster & Sainz de la Maza, 1994; Rada & Johson, 2011; Riordan-Eva, 2011)

The middle layer of the eye is designated by vascular tunic or uveal tract, comprising the choroid, ciliary body, and iris.(Mescher *et al.*, 2015) The iris is the most anterior part of the uveal tract and is a contractile, tympanic-like structure with a central aperture designated by the pupil. The normal surface of the iris has a richly textured surface structure with crypts (tissue gaps) and interlinked trabeculae. Besides the vascular and connective tissues, the iris also presents pigmented cells with melanocytes that are responsible for its distinct color.(Mescher *et al.*, 2015; Riordan-Eva, 2011) In the cross-section view, the iris consists of two layers (Figure 4): the anterior stromal layer and the posterior pigmented epithelial layer.(Bye, 2013)

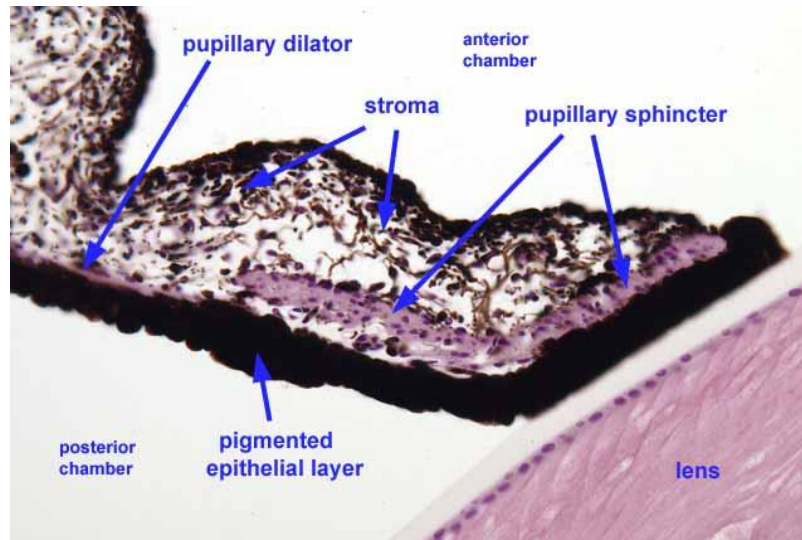


Figure 4 – Cross section view of the iris. (King, 2014)

The anterior stroma is formed by a muscle layer and connective tissue, which contains collagen, nerve fibers, and vascular vessels. The collarette of the iris, that covers the lesser arterial circle of the iris, is located about 2 mm from the pupillary margin. It divides the anterior stroma into the pupillary zone and the ciliary zone. The former is located between the pupillary margin and the collarette, and contains the sphincter pupillae muscle. This autonomic smooth muscle is concentrically disposed and induces pupil constriction by parasympathetic innervation. The ciliary zone is located from the collarette to the iris root. The dilator pupillae is within this area and is supplied by the postganglionic sympathetic fibers from the superior cervical ganglion. The posterior pigmented epithelial layer is limited to the posterior surface of the iris and protects the eye against the excessive incident light. It is continuous with the non-pigmented epithelium of the iris and the ciliary body. The apical membrane of the posterior pigmented epithelial layer is adherent to the anterior pigmented epithelium. The basal membrane of the posterior pigmented epithelial cells confines the posterior chamber. (Mescher *et al.*, 2015; Bye, 2013)

The ciliary body (Figure 5) is also part of the uveal tract. (Mescher *et al.*, 2015) It has a triangular shape in cross-section view, presenting 6-7 mm in width. Its base provides the only attachment to the sclera by the longitudinal muscle fibers, being inserted into the scleral spur. (Mescher *et al.*, 2015; Riordan-Eva, 2011) The base is directed anteriorly and is closely connected to the iris, while the apex is oriented posteriorly to the ora serrata. The ciliary body has three principal functions: aqueous fluid formation, lens accommodation, and aqueous fluid drainage by the

uveoscleral outflow and trabecular system.(Riordan-Eva, 2011; Bye, 2013) The ciliary body is divided into two regions: pars plicata and pars plana.(Riordan-Eva, 2011; Bye, 2013) The former presents a highly vascularized network and a rough presentation due to its radial ciliary processes. These ciliary processes are the primary anchor sites for the lens zonules, but some also insert into the pars plana. The latter region is a relatively avascular and pigmented area with 4 mm wide, extending from the ora serrata to the ciliary processes of the pars plicata. The ora serrata represents the boundary between the ciliary body and the retina.(Mescher *et al.*, 2015; Riordan-Eva, 2011)

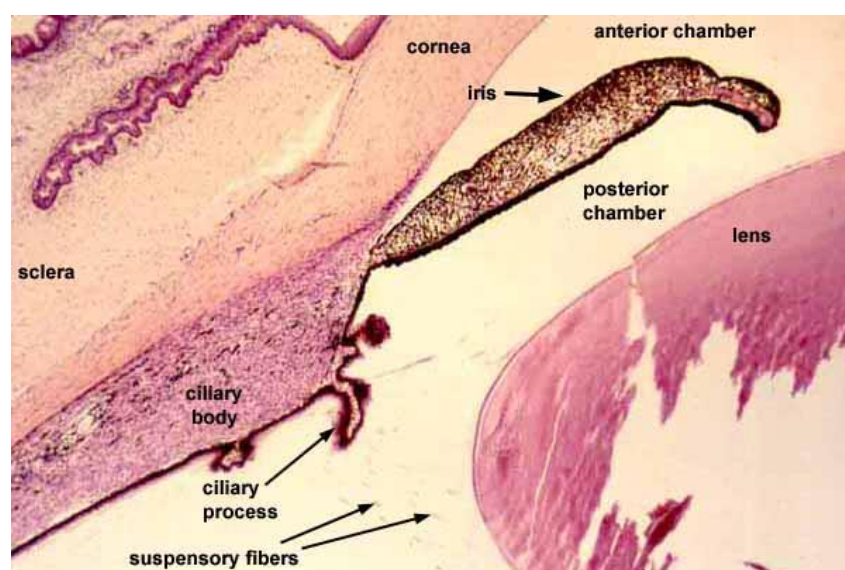


Figure 5 – Meridional section through the anterior eye highlighting the ciliary body and drainage apparatus.(King, 2004)

The choroid is the posterior part of the uveal tract and lies between the retinal pigment epithelium and the sclera.(Mescher *et al.*, 2015) It is attached to the sclera at two regions: at the optic nerve head and at the exit points of the vortex veins. This layer presents an average thickness of 0.25 mm and consists of 2 compartments: vascular layer and Bruch's membrane.(Mescher *et al.*, 2015; Riordan-Eva, 2011) The choroid is responsible for the blood supply of the outer third of the retina and the anterior part of the ocular globe. Due to its high pigmentation degree and high vascular flow, the choroid is also responsible for light block and temperature regulation.(Mescher *et al.*, 2015; Riordan-Eva, 2011) The retina (Figure 6) is the innermost layer of the ocular globe and is responsible for the photochemical transduction, where the neuronal impulses are generated and transmitted along the visual pathways.(Mescher *et al.*, 2015) The retinal



thickness varies from 0.56 mm near the optic disc to 0.1 mm at the ora serrata, being the thinnest point located at the fovea. The inner surface of the retina is in contact with the vitreous gel, and the outer surface is in contact with Bruch's membrane of the choroid. (Mescher *et al.*, 2015; Riordan-Eva, 2011) The retina englobes two portions: the external retinal pigment epithelium (non-visual region) and the internal neuronal (visual). The latter portion is composed by the photoreceptors, such as the rods and the cones, and by the ganglion cells that are responsible for transmitting the visual inputs by their axons, which constitute the optic nerve. (Mescher *et al.*, 2015; Riordan-Eva, 2011)

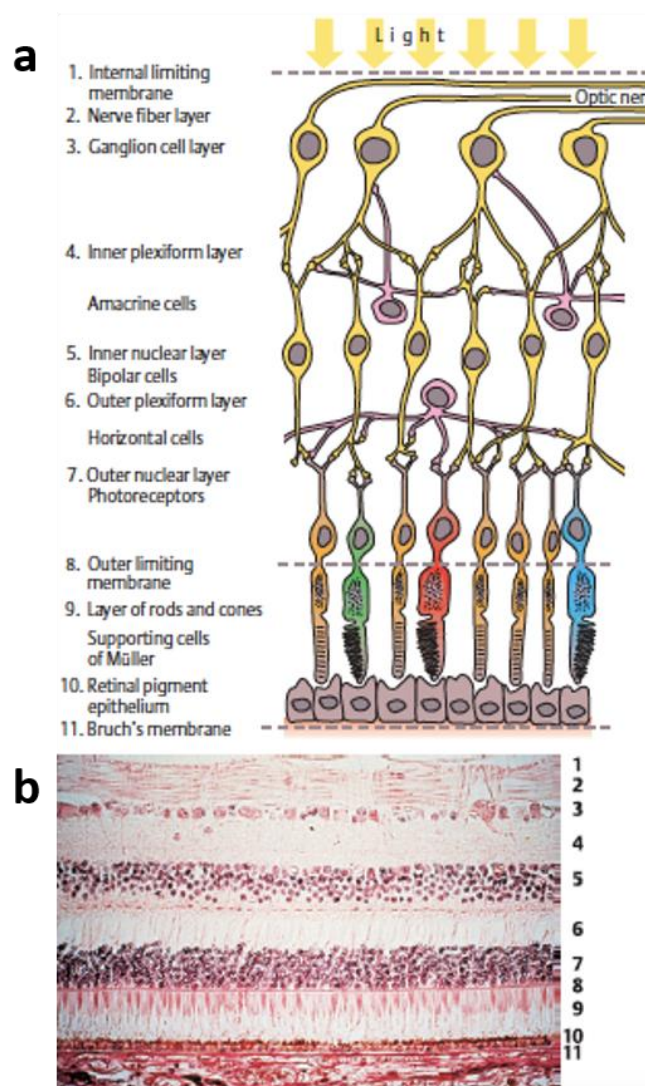


Figure 6 – Schematic layers of the retina (a) with the corresponding histological image (b). (Lang, 2007)

## 1.2– Crystalline lens

### 1.2.1 – Embryology

At the 22nd day of embryonic development, the newly formed optical vesicles come into contact with the surface ectoderm. Simultaneously with the changes that occur in each optic vesicle, the ectodermal cells are induced to increase in size, forming the lens placode (Figure 7 – a).(Riordan-Eva, 2011; Kuszak & Costello, 2002)

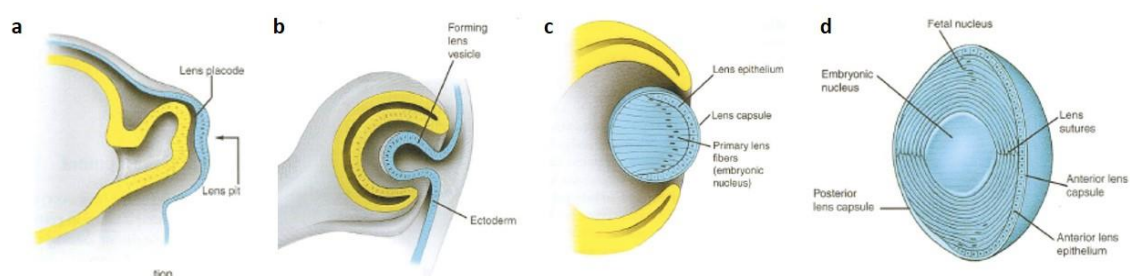


Figure 7 – Embryology development of the crystalline lens: a) formation of the lens placode; b) formation of the lens vesicle; c) formation of the embryonic nucleus; d) formation of the fetal nucleus.(Bobrow *et al.*, 2014)

On the 29th day, this placode begins to invaginate, which will result in the lens vesicle (Figure 7 – b).(Riordan-Eva, 2011; Kuszak & Costello, 2002) During this phase, it separates entirely from the superficial ectoderm and is formed by a sphere of a single layer of cuboid cells. The apical surfaces of these cells are directed toward the lumen, whereas their basal surfaces are directed toward the outer surface and are involved by a basement membrane designated by lens capsule.(Riordan-Eva, 2011; Kuszak & Costello, 2002) Simultaneously, the optic vesicle is also submitted to an invagination process to form the two-layered optic cup. The lens vesicle is placed in the opening of the optic cup. Before this phase, the posterior layer cuboidal cells begin to elongate anteriorly, filling the lumen of the lens vesicle. These cells originate the primary lens fibers and constitute the embryonic nucleus of the crystalline lens (Figure 7 – c).(Riordan-Eva, 2011; Kuszak & Costello, 2002) The cuboidal cells of the anterior part of the lens vesicle form the lens epithelium. At the equator level, these cells proliferate and elongate to form secondary lens fibers. These fibers formed during gestation compose the fetal nucleus (Figure 7 – d). Their anterior and posterior ends are extended toward the anterior and posterior poles, respectively, and interdigitate with the

ends of the fibers from the opposite side, forming the lens sutures. (Riordan-Eva, 2011; Kuszak & Costello, 2002)

### 1.2.2 – Morphology

The crystalline lens is a transparent and biconvex structure, presenting an anterior and posterior curvature radii of approximately 10 mm and 6 mm, respectively. (Riordan-Eva, 2011; Bye, 2013) The maximum curvature points of both surfaces represent the anterior and posterior poles of the crystalline lens, being connected by an imaginary line designated by the axis of the lens or the optical axis (Figure 8). The meridians are defined as lines on the surface that pass from one pole to the other. Its peripheral and circumferential edge represents the equator of the lens, which is parallel to the plane that passes through the equator of the ocular globe. (Beebe, 2011)

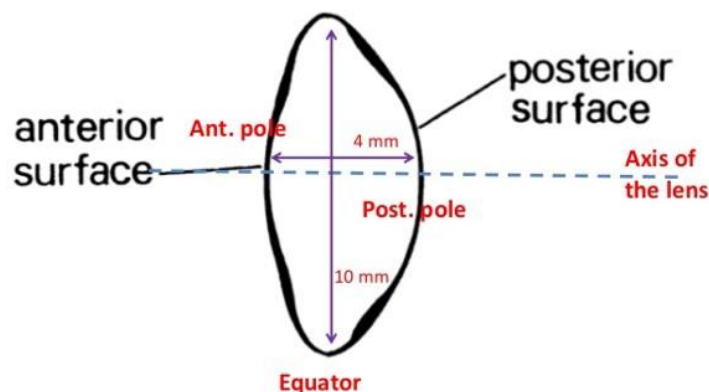


Figure 8 – Schematic of an adult crystalline lens, showing the relationship between the anterior and posterior poles, the equator and the axis of the lens. (Bobrow *et al.*, 2014)

In this way, the crystalline lens assumes an almost vertical position and its axis substantially overlaps with the anteroposterior axis of the ocular globe but shows a slight difference. Its maximum deviation consists of a slight rotation around its vertical axis, in such a way that its temporal side is displaced posteriorly about 3 – 7 degrees ( $^{\circ}$ ). Moreover, sometimes a rotation around the transverse axis occurs, so that the superior part leans forward (about  $3^{\circ}$ ). (Beebe, 2011; Rosales & Marcos, 2009)

Some features of the crystalline lens undergo changes throughout life. In the newborn, the crystalline lens presents 6.5 mm of equatorial diameter, increasing to approximately 9 - 10 mm in adulthood. Its anteroposterior measure or thickness

also increases from 3.5 - 4 mm at birth to about 5 mm in adults. The weight of the crystalline lens also increases with age. It weights approximately of 65 mg (miligrams) in the newborn and nearly 255 mg in adults.(Duncan *et al.*, 1997; Beebe, 2011)

### 1.2.3 – Anatomical location

Anterior to the crystalline lens is the anterior chamber of the eye and the iris diaphragm. It is held in position by its attachments to the vitreous body, and by the suspensory apparatus or the zonules of Zinn or zonula ciliaris, that extends from the equator of the lens to the ora serrata (Figure 9).(Zinn & Mockel-Pohl, 1973; Marshall *et al.*, 1982) These zonular fibers are a set of microfibrils, arising from the basal laminae of the nonpigmented epithelium of the pars plana and pars plicata of the ciliary body.

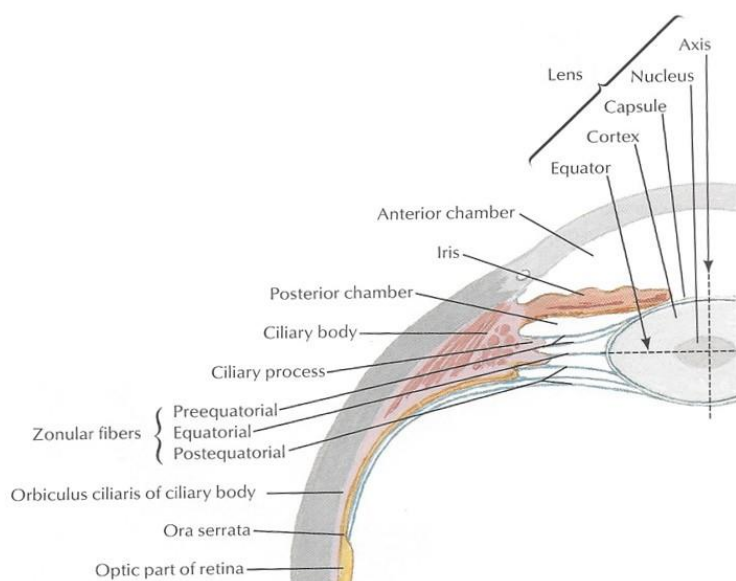


Figure 9 – Horizontal section of the crystalline lens and the supporting structures. (Netter, 2011)

These zonular fibres are 5-30 micrometer ( $\mu\text{m}$ ) in diameter and are composed of multiple filaments of fibrillin, being immersed in a compact gel formed by glycoproteins and glycosaminoglycans.(Zinn & Mockel-Pohl, 1973; Mecham *et al.*, 1988; Hanssen *et al.*, 1998; Canals *et al.*, 1996) The suspensory apparatus of the eye can be divided into the following sections (Figure 10): pars orbicularis (zonules that lie over pars plana); zonular plexus (zonules that lie between the ciliary processes); zonular fork (point of angulation of the zonule, lying in the mid zone of ciliary valleys and consolidates to zonular bundles); zonular

limbs.(Beebe, 2011; Majumder, 2008) The latter is further divided into three segments: anterior zonular limb that passes from pars plana to preequatorial part of the lens capsule; posterior zonular limb that passes from pars plicata to postequatorial part of the lens capsule; equatorial zonular limb which passes from pars plicata to the lens equator.(Majumder, 2008) Most of the zonules fibers anchor to the pre and postequatorial area of the lens capsule (approximately 1.5 mm anterior and posterior from the equator, respectively).(Canals *et al.*, 1996; Beebe, 2011)

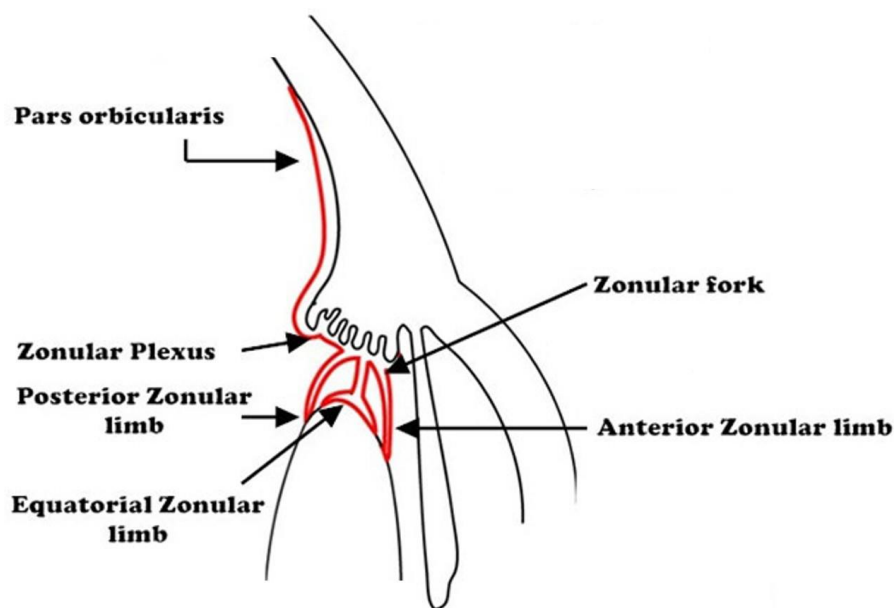


Figure 10 – Schematic of the suspensory apparatus and its components. (Majumder, 2008)

Depending on their attachment, zonules can also be divided into three groups (Figure 11): primary zonules, secondary zonules and tension zonules. The primary zonules are those attached to the lens capsule. The secondary zonules are fibers that connect the primary zonules to each other. The tension zonules are fibers which attach the primary zonules to the basement membrane of the ciliary processes.(Majumder, 2008)

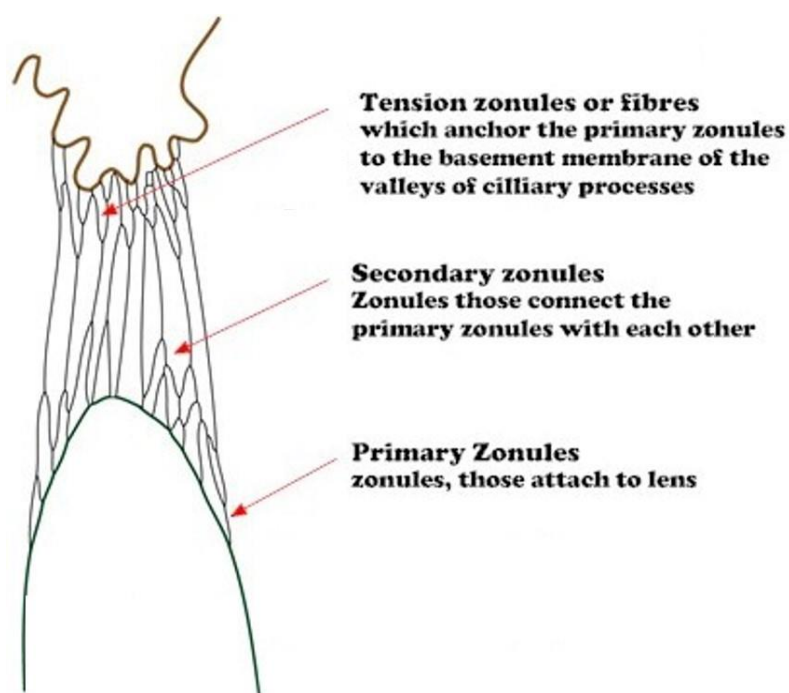


Figure 11 – Schematic of the zonules classification based on their attachment in the crystalline lens. (Majumder, 2008)

There are spaces defined by the network distribution of the zonular fibers. The canal of Hannover is the space between the pre and postequatorial zonules and is filled with equatorial zonule fibers. The space between postequatorial zonules and hyaloid zonules is known as canal of Petit. The hyaloid zonules are fibers that connect the anterior hyaloid of the vitreous gel at the border of the patellar fossa to the pars plana and pars plicata. (Majumder, 2008)

#### 1.2.4 – Histological structure

In cross-section view, the crystalline lens is composed by the capsule, lens epithelium, cortex and nucleus (Figure 12). (Taylor *et al.*, 1996; Duncan *et al.*, 1997)

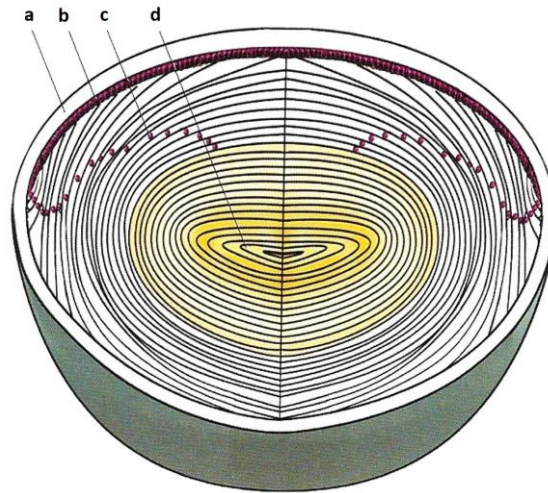


Figure 12 – Schematic representation of the crystalline lens: a – capsule, b – epithelium, c – cortex; d – nucleus. (Lorente & Mendicuti, 2008)

The capsule formed by a transparent basement membrane and is produced by the lens epithelium. (Danysh & Duncan, 2009) Histologically, it is composed by laminin, and types I, II and IV collagen. (Danysh & Duncan, 2009; Kelley *et al.*, 2002) Concerning the permanent increasing volume of the crystalline lens, the synthesis of the anterior capsule persists throughout life. In adulthood, the anterior lens capsule presents 14  $\mu\text{m}$  thickness compared to the 2 – 4  $\mu\text{m}$  of the posterior lens capsule. Due to its elastic properties, the capsule can mold the lens substance during the accommodative stimulus. (Fisher & Pettet, 1972; Kelley *et al.*, 2002; Danysh & Duncan, 2009) The *zonular lamellae* represent the outer layer of the capsule and play an essential role as anchoring points for the zonular fibers. (Danysh & Duncan, 2009)

As mentioned before, lens fibers can be classified as primary or secondary. The first lens cells to be transformed into fibers during embryogenesis are designated by primary lens fibers. The cells of the lens vesicle that were not induced to form primary fibers remain as lens epithelium, which covers the anterior surface of the primary fiber mass. The lens epithelium is located in close relation with the inner surface of the basement membrane, being only present at the level of the anterior surface and the equator of the crystalline lens (ends 0.5 mm posteriorly to the equator). (Fagerholm & Philipson, 1981; Marshall *et al.*, 1982; Kuszak, 1995; Lin *et al.*, 2016) It consists of a single layer of cuboidal cells, being supported by the basement membrane on its base and attached by *zonulae occludens* at the level of the subapical surfaces. (Lo & Harding, 1986; Bassnett *et al.*, 1994; Kuszak, 1995) The epithelial cells present round and central nuclei. (Fagerholm &

Philipson, 1981; Marshall *et al.*, 1982; Balaram *et al.*, 2000) At the equator level, these cells increase in height and show frequent mitosis, forming the germinative center. (Kuszak, 1995; Hejtmancik & Shiels, 2015; Beebe, 2011; Lin *et al.*, 2016) They determine a constant cell proliferation and progressive increase of the size of the crystalline lens. These new cells further differentiate into lens fibers. Due to their basal ends extension, these cells migrate on the inner surface of the capsule, in a U-shaped, forming highly elongated cells (about 10 – 12  $\mu\text{m}$ ). The fiber cells are hexagonal in cross-view, spindle-shaped and present several interlocking projections. (Kuszak *et al.*, 1983; Kuszak, 1995; Taylor *et al.*, 1996) After the fiber elongation process, terminal differentiation continues as the newly formed fibers routinely eliminate their nuclei and organelles, such as Golgi bodies, mitochondria, rough and smooth endoplasmic reticulum. The removal of these organelles is necessary because their retention would cause a significant diffraction of light and thereby compromise the crystalline lens function. (Bassnett, 1992; Bassnett & Beebe, 1992; Bassnett, 1995) This dynamic process also induces the cells to move inwardly from the equator to the center of the crystalline lens, defining the areas of the cortex (newly divided cells that have nuclei) and the nucleus (enucleated cells). Thus, the lens fibers are arranged in concentric lamellae, like onion peel, and their ends are faced at the level of the crystalline lens sutures. (Kuszak *et al.*, 1984; Kuszak, 1995; Kuszak *et al.*, 2004) The anterior suture has a Y-shape, while the posterior suture presents an inverted Y-shape. This appearance is consequence of the pattern of the lens fibers, since they are internally displaced from the periphery to the center by younger fibers and are parallel to the anteroposterior axis of the crystalline lens. (Kuszak *et al.*, 1984; Kuszak, 1995; Taylor *et al.*, 1996; Kuszak *et al.*, 2004) As mentioned previously, the lens nucleus grows to fill the entire crystalline lens throughout life, being the oldest layers of lens fibers the most central. (Kuszak, 1995; Taylor *et al.*, 1996; Bassnett & Costello, 2016) The embryonic and fetal nuclei are produced during the embryonic life and persist in the center of the crystalline lens (Figure 13). (Garland *et al.*, 1996; Taylor *et al.*, 1996) Only primary lens fibers form the embryonic nucleus, and they do not form sutures. (Taylor *et al.*, 1996; Shestopalov & Bassnett, 2000) The fetal nucleus is constituted by all the secondary fibers formed until birth, and they contribute to the lens suture formation. (Kuszak *et al.*, 1984; Kuszak, 1995; Taylor *et al.*, 1996; Kuszak *et al.*, 2004) The fibers formed



after birth and through sexual maturation are juvenile nuclear fibers. Because the length of time to complete the sexual maturation is not constant, juvenile nuclear dimensions have broader boundaries compared to the fetal and embryonic nuclei. The adult lens nucleus is formed by all secondary fibers formed after sexual maturation excluding the fibers of the cortex (Figure 13).(Taylor *et al.*, 1996)

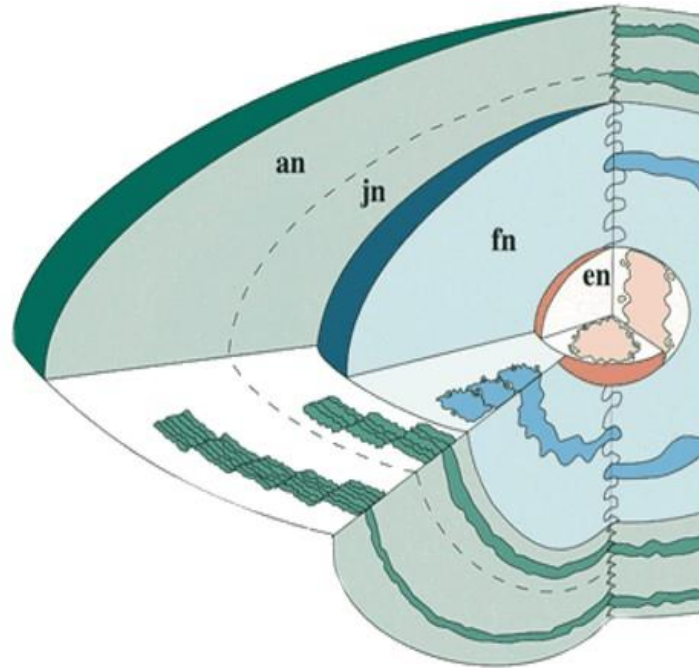


Figure 13 – Schematic representation of the nucleus. Embryonic nucleus (en) is formed by primary fibers. The fetal nucleus (fn), juvenile nucleus (jn), adult nucleus (an), and cortex (c) are composed of secondary fibers formed during specific periods of development.(Taylor *et al.*, 1996)

### 1.2.5 – Vascularization and innervation

The crystalline lens has a high dynamic capacity in its structural remodeling, requiring oxygen and nutrients, primarily destined for the lens epithelium cells and the nucleated cells of the cortex. However, the lens is avascular and is nourished by diffusion from the aqueous humor and vitreous body. In adulthood, the lens is completely devoid of nerves, blood and lymph vessels.(Mathias *et al.*, 1997; Mathias *et al.*, 2007)

### 1.2.6 – Biochemistry composition

In the adult lens, the water defines 65% of the wet weight, and the proteins make up the remaining 35%.(Bloemendal *et al.*, 2004; Hejtmancik *et al.*, 2015; Hejtmancik & Shiels, 2015) Interestingly, the protein concentration inside the

crystalline lens is approximately three times greater than the standard protein concentration of the most human cells.(Fagerholm *et al.*, 1981; Bloemendal *et al.*, 2004; Hejtmancik & Shiels, 2015) The lens proteins (Figure 14) are divided into two groups based on the water solubility: water soluble; water insoluble.

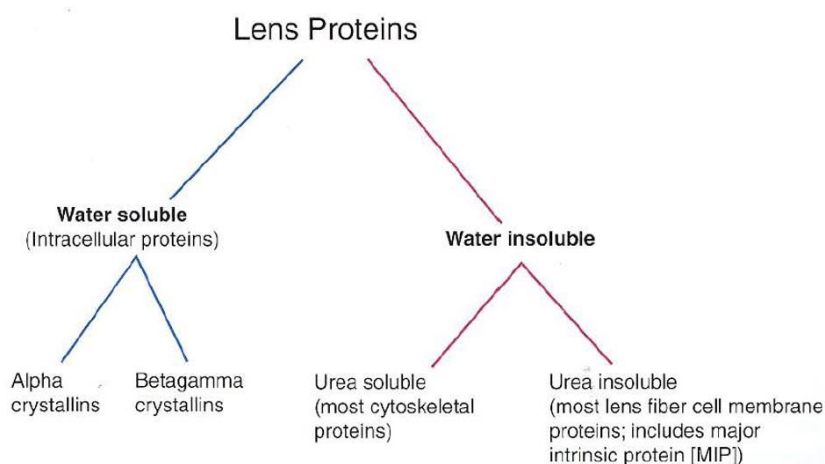


Figure 14 – Overview of the crystalline lens proteins.(Bobrow *et al.*, 2014)

The former group, also designated by crystallins, represents approximately 80% of total lens protein, and it is further divided into two subgroups: Alpha crystallins and Betagamma crystallins.(Piatigorsky, 1989; Sharma & Santhoshkumar, 2009; Mathias & Rae, 2004; Hejtmancik *et al.*, 2015) The Alfa crystallins define about one-third of the total lens protein mass, and they prevent the denaturation and insolubilization of other crystallins and partially denatured proteins. The subunits of this type of crystallins, AlphaA and AlphaB, constitute heteromeric complexes with approximately 30 subunits.(Liang & Li, 1991; Bloemendal *et al.*, 2004; Laganowsky *et al.*, 2010; Hejtmancik *et al.*, 2015) The Betagamma crystallins are divided into two groups, depending on molecular weight and isoelectric points. The Beta crystallins represent 55% of yhe wet weight of the water-soluble lens proteins and constitute complex forms by associating with other proteins.(Bloemendal *et al.*, 2004; Hejtmancik *et al.*, 2015) The Gamma crystallins are the smallest and the least heavy of the crystalline proteins, and they do not tend to combine with each other or with other types of proteins. The water-insoluble fraction represents about 1.5% of the total lens protein.(Bloemendal *et al.*, 2004; Hejtmancik *et al.*, 2015) This group can also be divided into two subgroups, depending on urea solubility property. The urea-soluble group is mainly formed by cytoskeletal proteins, presenting proteins rich

in vimentin, phakinin and filensin.(Maisel, 1984; Su *et al.*, 2011) The urea-insoluble group contains the plasma membrane proteins of the lens fibers cells, including the major intrinsic protein (MIP).(Varadaraj *et al.*, 1999; Bassnett *et al.*, 1999; Mathias & Rae, 2004; Mathias *et al.*, 2007) Other minor components of the crystalline are anions, cations, acid ascorbic and glutathione, which are essential to the lens metabolism, in order to to maintain its transparency and to avoid oxidative damage.

## **1.2.7 – Physiology of the crystalline lens**

### **1.2.7.1 – Communications between the crystalline lens cells**

The lens physiology mechanisms are essential to control water and electrolyte balance to maintain its transparency. To achieve this purpose, the inner cells need to communicate with the external ones and the fluids outside the lens.(Kuszak *et al.*, 1989; Bassnett *et al.*, 1994; Shestopalov & Bassnett, 2003; Hejtmancik *et al.*, 2015) Differentiated lens fibers are separated by a well-defined extracellular space, except at the intercellular junctions. As a result of terminal differentiation, the extracellular space between mature fibers is minimized as plasma membranes are transformed into a complex pattern involving several intercellular junctional contacts.(Kuszak, 1995; Taylor *et al.*, 1996; Hejtmancik *et al.*, 2015; Hejtmancik & Shiels, 2015; Audette *et al.*, 2016) Using scanning electron microscopy is possible to identify different types of junctions between lens fibers. The lens fiber gap junction is typically 16-18 nm thick and is formed by connexins.(al-Ghoul & Costello, 1996; Hejtmancik *et al.*, 2015) These proteins, located in opposed regions from neighboring fibers, are conjoined across a narrowed extracellular space that measures 1 to 2 nanometer (nm).(Lo & Harding, 1986) Its pore size allows passage of 1000 to 1500 Dalton (Da) molecules. Thus, charge- and size-restricted substances may transfer from fiber to fiber without energy consumption.(Cheng *et al.*, 2008; Slavi *et al.*, 2014; Hejtmancik *et al.*, 2015) The fiber lens gap junctions differ from other gap junctions in their amino acid sequence, ultrastructure and permeation properties.(Hejtmancik *et al.*, 2015) Thin asymmetric junction designates another type of junctions with a similar appearance to the gap junctions. These junctions consist of proteins aggregates derived from the aquaporin-0 (AQP0) family, also referred as MIP.(Varadaraj *et al.*, 1999; Mathias & Rae, 2004; Varadaraj *et al.*,

2005; Hejtmancik *et al.*, 2015) These proteins play a dual role: single membrane water transport channels that remove water from the extracellular space; adhesive function between the cells.(Scheuring *et al.*, 2007; Hejtmancik *et al.*, 2015) After the terminal differentiation of the lens fibers, the lateral membrane of these cells suffers a dramatic remodeling process, featuring polygonal domains of furrowed membrane. This ultrastructural change may result from the redistribution of the AQP0 channels.(Simon *et al.*, 1982; Fotiadis *et al.*, 2000) Fusion zones are another type of junction between the lens fibers, which occur between the lateral membranes from neighboring fibers.(Kuszak *et al.*, 1985; Kuszak *et al.*, 1989) These are common among the anterior or posterior segments of fiber cells as they approach their sutural locations. Though being necessary for the suture modeling required for the lens function, the fusion zones also enable intercellular transport between fibers for larger substances.(Kuszak *et al.*, 1985; Kuszak *et al.*, 1989)

### 1.2.7.2 – Electrolyte and hydric balance

In contrast to the surrounding aqueous fluid and vitreous gel, the crystalline lens has higher levels of potassium (K<sup>+</sup>) and lower levels of sodium (Na<sup>+</sup>), chloride and water (Figure 15).(Duncan, 1969b; Duncan, 1969a; Paterson & Maurice, 1971; Paterson, 1972; Patterson, 1988)

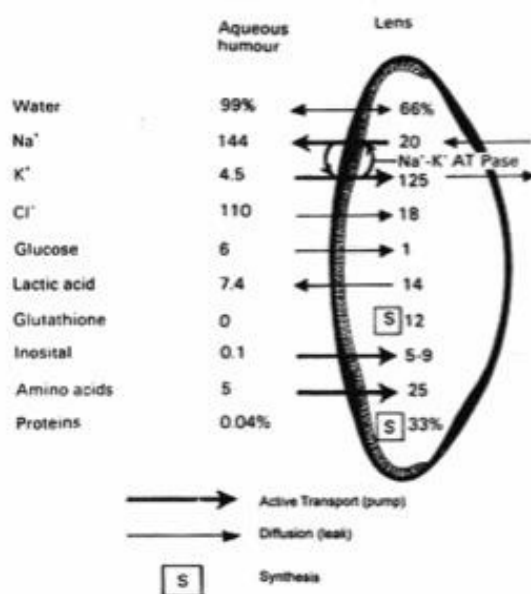


Figure 15 – Chemical composition of the crystalline lens (all values in mmol/kg of lens water, unless otherwise stated)(Cl<sup>-</sup> – chloride; K<sup>+</sup> – potassium; Na<sup>+</sup> – sodium; Na<sup>+</sup>/K<sup>+</sup> ATPase – sodium/potassium adenosine triphosphatase).(Agarwal *et al.*, 2002)

To maintain electrolyte and hydric balance, the crystalline lens generates chemical and electrical energy. For example,  $\text{Na}^+/\text{K}^+$ adenosine triphosphatase (ATPase) is linked to cation pumps and its activity is dependent on energy consumption, to allow the influx of  $\text{K}^+$  and efflux of  $\text{Na}^+$ .(Garner & Kong, 1999; Fischbarg *et al.*, 1999; Paterson & Delamere, 2004) This enzyme was also identified in the membrane of equatorial fiber cells.(Garner & Kong, 1999; Fischbarg *et al.*, 1999; Danysh & Duncan, 2009) When  $\text{Na}^+$  is actively exchanged by  $\text{K}^+$  by the epithelial cells, a chemical gradient promotes a diffusion of  $\text{Na}^+$  into the crystalline lens and  $\text{K}^+$  out of the primarily through the posterior surface. The anterior location of the  $\text{Na}^+/\text{K}^+$ ATPase is responsible for the anteroposterior gradient of the  $\text{Na}^+$  and  $\text{K}^+$  ions and has been designated by “pump and leak” theory of cation transport (Figure 16).(Paterson, 1972; Paterson & Delamere, 2004; Mathias & Rae, 2004; Mathias *et al.*, 2007)

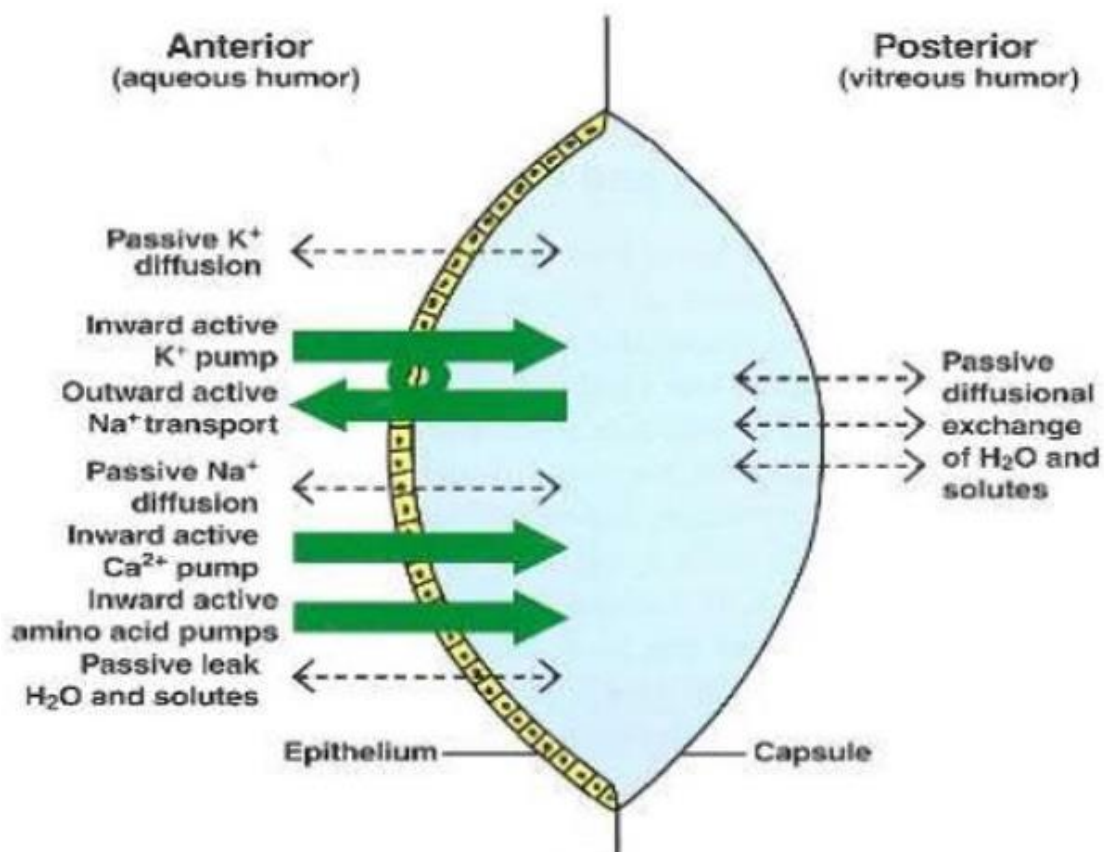


Figure 16 – Anteroposterior gradient of sodium and potassium enables the solute movement through the crystalline lens ( $\text{Ca}^{2+}$ – calcium;  $\text{H}_2\text{O}$  – water;  $\text{K}^+$  – potassium;  $\text{Na}^+$  – sodium).(Bobrow *et al.*, 2014)

Based on this concept, the  $\text{Na}^+$  is concentrated in the posterior part of the crystalline lens, and the inverse occurs with the  $\text{K}^+$ , which is more concentrated

in the anterior part of the organelle.(Duncan, 1969b; Duncan, 1969a; Paterson, 1972; Mathias & Rae, 2004; Mathias *et al.*, 2007) The “pump and leak” theory is essential for three important roles: regulation of the water content of the crystalline lens; maintenance of the electrical potential difference between the inside and outside the lens (approximately -70 millivolts); preservation of the physiochemical environment inside the crystalline lens to maintain transparency and enzymatic activity. The basal membrane of the epithelial cells allows the entrance of others substances essential for the metabolism of the epithelial and fiber cells, by secondary active transportation (against the concentration gradient). This type of transfer is ensured while the Na<sup>+</sup> gradient is maintained (higher Na<sup>+</sup> concentration in the aqueous fluid and lower Na<sup>+</sup> concentration intracellularly). For example, the active transport of amino acid is a mechanism dependent on the Na<sup>+</sup> gradient.(Mackic *et al.*, 1996; Fischbarg *et al.*, 1999; Mathias & Rae, 2004; Paterson & Delamere, 2004) Instead of an active transport mechanism, glucose enters the crystalline lens by both simple and facilitated diffusion, and the metabolism waste products leave the organelle by simple diffusion.(Fischbarg *et al.*, 1999; Mathias & Rae, 2004) In summary, K<sup>+</sup> and other molecules (such as aminoacids, glutathione, glucose) are actively transported into the anterior part of the crystalline lens by the epithelium, being diffused through the lens based on the concentration gradient. Contrariwise, Na<sup>+</sup> flows through the lens from the posterior side due to its concentration gradient, and then is actively exchanged for K<sup>+</sup> by the epithelial cells.

The electrolyte balance is also necessary to maintain the calcium (Ca<sup>2+</sup>) homeostasis, which is critical for the proper function of the crystalline lens.(Paterson & Delamere, 2004; Hejtmancik *et al.*, 2015) The Ca<sup>2+</sup> is actively pumped outwards from the lens cells. Intracellular overload of this ion may trigger a series of enzymatic cascades with activation of Ca<sup>2+</sup>-dependent proteases, such as calpain, resulting in the irreversible breakdown of structural proteins and cell apoptosis.(Borchman *et al.*, 1989; Marcantonio & Duncan, 1991; Gao *et al.*, 2004)

### 1.2.7.3 – Glucose metabolism

The glucose plays an essential role in the crystalline lens metabolism. Inside the lens, the higher percentage of the glucose is phosphorylated to glucose-6-phosphate (G6P) by the hexokinase. Since this enzymatic step is processed at a slow rate, the metabolic pathways are influenced by the availability of the G6P. Once available, it enters one of the two metabolic pathways: anaerobic glycolysis or hexose monophosphate (HMP) shunt (Figure 17). (Kinoshita, 1955; Kinoshita, 1965; Hejtmancik *et al.*, 2015)

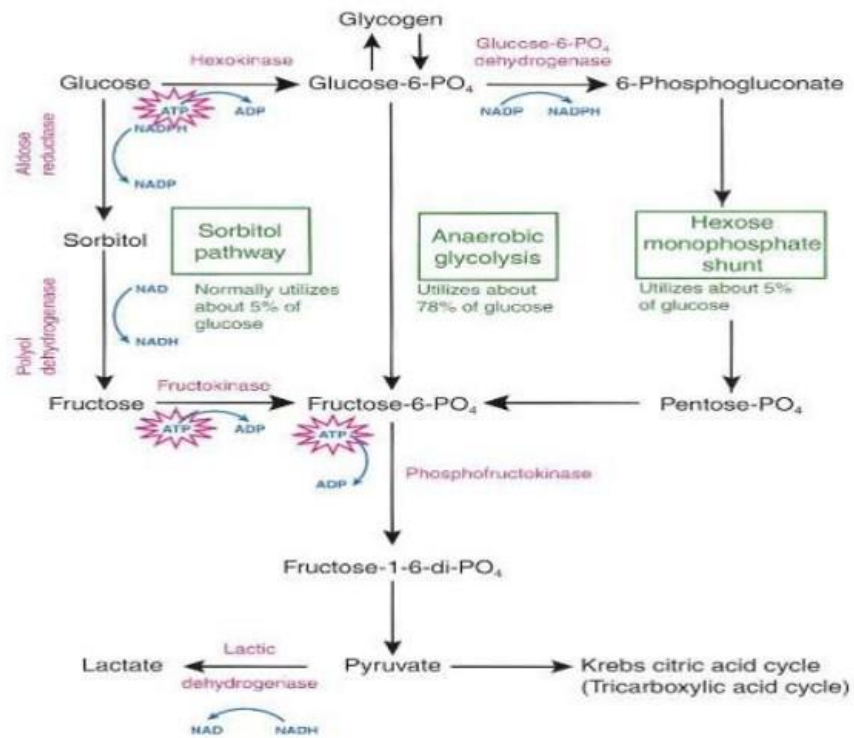


Figure 17 – Different pathways of the glucose metabolism in the crystalline lens (ADP – Adenosine diphosphate; ATP – Adenosine triphosphate; NADP – nicotinamide-adenine dinucleotide phosphate; NADPH – reduced form of nicotinamide adenine dinucleotide phosphate; PO<sub>4</sub> – phosphate). (Bobrow *et al.*, 2014)

Approximately 80% of the glucose is consumed in the anaerobic glycolysis, resulting in only two molecules of adenosine triphosphate (ATP). (Kinoshita, 1965; Hejtmancik *et al.*, 2015) The anaerobic glycolysis is regulated by the enzyme phosphofructokinase, which is sensible to the gradient of the metabolic products of this pathway. The majority of the pyruvate produced by the glycolytic pathway is reduced to lactate, involving the lactic dehydrogenase enzyme. This enzymatic step results in the consumption of the reduced form of nicotinamide adenine dinucleotide phosphate (NADPH). Despite approximately 5% of glucose being

used in the HMP route, this pathway is stimulated by high concentrations of glucose. The HMP shunt plays a significant role in the renewal of NADPH, which is needed for the activities of the aldolase reductase and the glutathione reductase. The resultant metabolites of the HMP shunt are consequently transformed to lactate by the glycolytic pathway. (Kinoshita, 1965; Hejtmancik *et al.*, 2015)

When the glucose concentration is excessive, such as in hyperglycemic states, the sorbitol pathway is activated more than the anaerobic glycolysis, resulting from the down-regulation of the hexokinase by the products derived from the glycolysis (Figure 17). (Kinoshita, 1965) In normal conditions, only 5% of the lens glucose is converted to sorbitol. The aldolase reductase plays a critical role in this pathway, converting glucose into sorbitol, being then metabolized to fructose by the enzyme polyol dehydrogenase. The resultant fructose is converted into fructose – 6 – phosphate that enters the anaerobic glycolysis pathway. (Kinoshita, 1965; Cheng *et al.*, 1983; McLean *et al.*, 1985)

#### **1.2.7.4 – Protective mechanisms against oxidative damage**

Due to external radiations and to metabolic activity, reactive oxygen radicals are generated and may interact with structural components of the lens cells in different ways. (Berthoud & Beyer, 2009; Hejtmancik *et al.*, 2015; Hejtmancik & Shiels, 2015) For example, peroxidation of cellular membranes and proteins makes these components to be unable not to carry out their function properly, due to cross-linking of lipids and proteins. (Jahngen-Hodge *et al.*, 1994; Ahuja *et al.*, 1999) Reactive oxygen species may also damage and distort the DNA of the lens cells. (Osnes-Ringen *et al.*, 2016; Lin *et al.*, 2016) The crystalline lens has protective mechanisms to avoid the oxidative damage. (Brennan *et al.*, 2012; Hejtmancik & Shiels, 2015) For example, the glutathione (L-γ-glutamyl-L-cisteinylglycine) is imported from the aqueous fluid and is present in high concentrations in the crystalline lens. The epithelial cells have higher concentrations of this component compared to cortex and nucleus cells. (Reddy *et al.*, 1973; Reddy, 1990) This element is essential for the protection against oxidative damage and in the maintenance of the reduced state of different proteins, in order to prevent changes of the transparency and metabolism of the crystalline lens. (Reddy, 1990; Kamei, 1993) The levels of reduced glutathione



are kept constant (95% of the total) due to a pathway that involves the glutathione peroxidase and the glutathione reductase sequentially (Figure 18).(Reddy & Giblin, 1984; Reddy, 1990; Hejtmancik & Shiels, 2015)

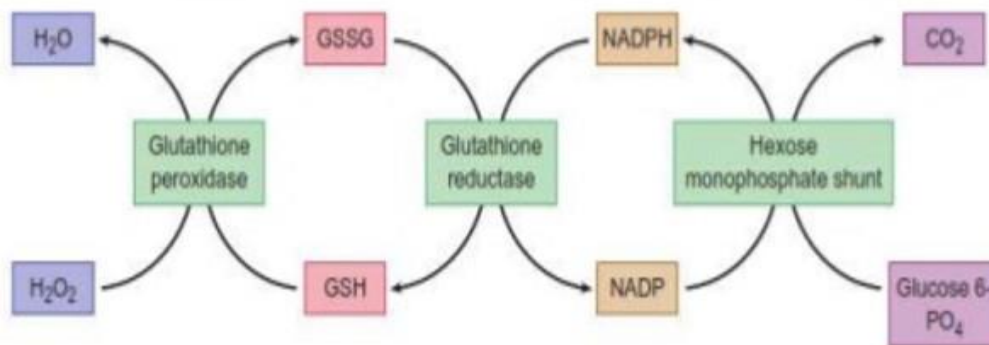


Figure 18 - Glutathione cycle for protection against the oxidative damage ( $CO_2$  – carbon dioxide;  $H_2O$  – water;  $H_2O_2$  – hydrogen peroxide; GSH – reduced glutathione; GSSG – oxidized glutathione disulfide; NADP – nicotinamide-adenine dinucleotide phosphate; NADPH – reduced form of nicotinamide adenine dinucleotide phosphate;  $PO_4$  –phosphate).

The reducing agent in the last step of this pathway is the NADPH derived from the HMP shunt.(Cheng *et al.*, 1983) Another essential protective element against oxidative stress is ascorbic acid, which is also derived from the aqueous fluid. The superoxide dismutase and catalase enzymes have an active role in this mechanism. For example, the pathway involving these enzymes enables the elimination of the superoxide anion.(Bhuyan & Bhuyan, 1978; Varma *et al.*, 1982)

### 1.2.8 – Functions of the crystalline lens

The physiological and biochemical properties of the crystalline lens enable the following functions: 1 – to maintain its transparency to visible light for a long time; 2 – to provide adequate refractive medium of high refractive index, being among liquids with refractive index greater than the air; 3 – to vary its focus range through the accommodation process; 4 – to enable metabolic survival of their mature or differentiated fibers of the central regions that are devoided of subcellular organelles; 5 – to filter out ultraviolet light entering the eye, to avoid damage to the retina.(Hejtmancik & Shiels, 2015; Riordan-Eva, 2011)

Regarding the ocular optics, the crystalline lens acts like a convergent lens, as its index of refraction (approximately 1.4 in the nucleus and 1.36 in the cortex) is distinct from that of the aqueous fluid and vitreous gel. In its nonaccommodative state, the lens contributes about 15–20 diopters of the approximately 60 diopters

of the ocular convergent refractive power. The remaining convergent refractive power derives from the air–cornea interface. The accommodation process that allows the eye to change focus from distance to near images by changing the crystalline lens shape. This mechanism is controlled by the contraction of the ciliary muscles, which are connected to the crystalline lens through the zonular fibers. At a short focal distance the ciliary muscle contracts, zonule fibers loosen, and the lens becomes more spherical, increasing its refractive power. When changing focus to a distant object, relaxation of the ciliary muscle occurs, and the crystalline lens becomes flatter.(Riordan-Eva, 2011; Bobrow *et al.*, 2014) The pathophysiology of the crystalline lens is related to mechanisms that lead to accommodation disability and transparency loss.(Taylor *et al.*, 1996; Mathias *et al.*, 1997; Duncan *et al.*, 1997; Hejtmancik & Shiels, 2015)

Presented in 2013, the Dysfunctional Lens Syndrome (DLS) concept helps to explain the age-related and progressive visual deterioration and difficulty for near vision that patients experience after their 40s.(Waring IV, 2013) The pathophysiological mechanisms associated with this entity are loss of accommodation, reduction of crystalline lens transparency and change of the internal aberrations profile.(Waring IV, 2013) The DLS features three sequential stages.(Waring IV, 2013; Waring IV, 2014) In the first stage, patients usually complain mild loss of near vision and present a clear crystalline lens with minimal light scattering. Most people at this stage will start to use readers or bifocals. Interestingly, the early visual losses are largely unnoticed. The further stages are characterized by progressive loss of transparency of the crystalline lens, which leads to cataract development in the third stage. Due to the age-related nature of the disorder, patients may complain progressive halos, glare and decreased visual quality.(Waring IV, 2013; Waring IV, 2014).

## 2 – Cataract

### 2.1 – Definition

A cataract is usually defined as any opacity in the crystalline lens (Figure 19).(Hejtmancik & Shiels, 2015; Beebe, 2011)

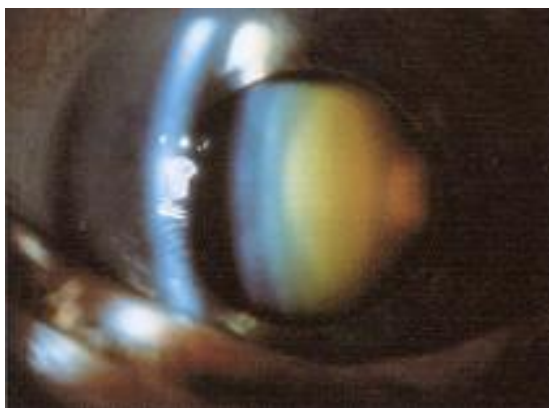


Figure 19 – Slit lamp image of eye with opacity of the crystalline lens (cataract).(Bobrow *et al.*, 2014)

The prevalence and incidence of cataract is not clear to define. The main challenge is to define diagnostic criteria. The size, shape, location and density of these opacities are age-related and are not uniform. In the majority of the studies, cataract is defined as an opacity of the crystalline lens at the slit lamp, being associated with visual acuity reduction.(Beebe, 2011; Hockwin, 1994; Sasaki *et al.*, 1989) According to data from the Direção-Geral da Saúde (DGS), it is estimated approximately 170,000 cases, of which 6 out of 10 patients over 60 years-old have signs of cataract.(Direção-Geral da Saúde, 2005; Direção-Geral da Saúde, 2007) Based on the epidemiological data provided by the World Health Organization (WHO), cataract is considered to be the leading cause of blindness worldwide, being responsible for 51% of the total cases. Concerning visual impairment, cataract represents the cause in 33% of the cases, surpassed only by uncorrected refractive errors (43%).(World Health Organization, 2013; World Health Organization, 2016; World Health Organisation, 2016) Derived from the aging of the population, the prevalence of cataracts gradually increases each year. For example, WHO pointed out that 17 million of 37 million blind people worldwide were caused by cataract in 2002. Predictions indicate an increase of over 3 million cases in 2020.(World Health Organization, 2016)

Although 90% of this disease is diagnosed in developing countries, it has a social and financial impact in developed world countries, affecting the older populations

mostly. Patients suffering from cataract are more likely to have significantly reduced quality of life derived from low vision. Concerning medical costs, a large percentage of these costs are unrelated with ocular problems.(Holden, 2007; Frick & Foster, 2003; Rosenberg & Sperazza, 2008) For example, approximately 75% of visually impaired people required assistance with everyday tasks as blindness restricts mobility. Some reports also pointed towards to the adverse impact on productivity, but it may also be considered a cause of mortality increase.(Javitt *et al.*, 1983)

Cataract surgery is estimated to be the most common surgery performed in developed countries, specially due to the increasing volume of out-patient procedures.(World Health Organization, 2016) In Portugal, the number of cataract surgeries performed is approximately 75,000 per year.(Mertens, 2015) Interestingly, previous studies analyzed the impact of cataract surgery. After the surgical procedure, patients were more prone to perform productive activities and quality of life had also improved.(Frick & Foster, 2003; Smith & Smith, 1996) Thus, proper diagnosis and treatment of this ocular disease are essential for health programs, since it has tremendous economic and social impacts and may dramatically affect the quality of life of patients and their families

## 2.2 – Types of cataract

To describe this ocular pathology, the literature review reveals multiple terms and classifications that sometimes may overlap.(Sasaki, 1991; Gupta *et al.*, 2011)

Table 1 refers to the etiologic classification of cataracts.

Table 1 – Classification of cataracts according to etiology

<b>Acquired cataracts</b> (over 99% of cataracts)	<b>Age-related</b> (over 90% of cataracts)
	<b>Secondary to systemic conditions</b> <ul style="list-style-type: none"> <li>– Diabetes mellitus</li> <li>– Galactosemia</li> <li>– Renal insufficiency</li> <li>– Mannosidosis</li> <li>– Fabry disease</li> <li>– Lowe syndrome</li> <li>– Wilson disease</li> <li>– Myotonic dystrophy</li> <li>– Tetany</li> <li>– Skin disorders</li> </ul>
	<b>Secondary to ocular disease</b> <ul style="list-style-type: none"> <li>– Heterochromia</li> <li>– Uveitis</li> <li>– Retinal vasculitis</li> <li>– Retinitis pigmentosa</li> </ul>
	<b>Secondary to ocular surgery</b> <ul style="list-style-type: none"> <li>– Vitrectomy and silicone oil retinal tamponade</li> <li>– Filtering operations</li> </ul>
	<b>Traumatic</b> <ul style="list-style-type: none"> <li>– Contusion</li> <li>– Perforation</li> <li>– Infrared radiation</li> <li>– Electrical injury</li> <li>– Ionizing radiation</li> </ul>
<b>Congenital cataracts</b> (fewer than 1% of cataracts)	<b>Toxic</b> <ul style="list-style-type: none"> <li>– Corticosteroids</li> <li>– Chlorpromazine</li> <li>– Miotic agents</li> </ul>
	<b>Hereditary</b> <ul style="list-style-type: none"> <li>– Autosomal-dominant</li> <li>– Autosomal-recessive</li> <li>– Sporadic</li> <li>– X-linked</li> </ul>
	<b>Cataracts due to early embryonic damage</b> <ul style="list-style-type: none"> <li>– Rubella</li> <li>– Mumps</li> <li>– Hepatitis</li> <li>– Toxoplasmosis</li> </ul>

In an attempt to eliminate the subjectivity of the evaluations, clinical researchers established the anatomical location of the lens opacity as a reference. This consensus divides the cataract into three main types: cortical, nuclear and posterior subcapsular.(Chylack *et al.*, 1993; Chylack, 1984) For example, classifications were developed based on this approach, such as the Lens

Opacities Classification System (LOCS) II and III, the Oxford Cataract Classification System, Beaver Dam Eye Study and Age-Related Eye Disease Study.(Hall *et al.*, 1997; Chylack *et al.*, 1993; KARBASSI *et al.*, 1993; Klein *et al.*, 1998; Braccio *et al.*, 1998) For the purpose of the present thesis, the description will be focused on age-related nuclear cataract..

### **2.3 – Pathophysiological mechanisms of age-related nuclear cataract**

Transparency of the crystalline lens is possible due to several factors, including the structural organization of the lens fibers, the physiology and the biochemistry components of this organelle.(Mathias *et al.*, 1997; Hejtmancik & Shiels, 2015; Hejtmancik *et al.*, 2015; Lin *et al.*, 2016) Any modification of these factors is associated with the change of the transparency of the crystalline lens, leading to cataract formation.(Mathias *et al.*, 1997; Hejtmancik & Shiels, 2015; Hejtmancik *et al.*, 2015; Lin *et al.*, 2016)

Patients with age-related cataracts may present different symptoms. The most frequent complaint is a gradual and progressive reduction of the visual acuity.(Alió *et al.*, 2005; Chua *et al.*, 2004) Since age-related cataracts course with changes in contrast sensitivity, patients may report disabling glare, especially at night, and decreased ability to discern colors.(Chua *et al.*, 2004; Adamsons *et al.*, 1992) Owing to refraction changes in the crystalline lens, symptoms related to myopic shift and monocular diplopia may also be reported.(Archer, 2007)

The pathophysiological mechanisms of age-related cataracts are not entirely understood, and the multifactorial interactions between physiological processes of the lens, environmental, nutritional and systemic factors may have an essential role in the pathogenesis.(Chylack, 1984; Mathias & Rae, 2004; Hejtmancik & Shiels, 2015; Leinfelder, 1953; Lampi *et al.*, 1998; Gao *et al.*, 2013; Eckerskorn *et al.*, 1987; Duncan *et al.*, 1997; Bloemendal *et al.*, 2004; Berthoud & Beyer, 2009)

Aging contributes to several changes of the crystalline lens, such as accommodative range reduction and weight and thickness increase.(Alió *et al.*, 2005; Taylor *et al.*, 1996) Due to the unceasing proliferation at the equator level, new fibers layers are added in a concentric pattern, inducing compression and hardening of the central nucleus.(Kuszak, 1995; Hejtmancik & Shiels, 2015) This

process of nucleus sclerosis is associated with other changes. For example, the nucleus becomes yellow in color, tending toward brown with increasing age. There is also an increase of water-insoluble proteins with age that also contributes for the lens opacification and consequently for the light scattering. Therefore, the process of nuclear cataractogenesis may represent an exacerbation of changes related to aging.(Chylack, 1984; Sharma & Santhoshkumar, 2009; Sethna *et al.*, 1982; Gao *et al.*, 2013; Ferrer *et al.*, 1990; Duncan *et al.*, 1997)

Understanding the oxidant-antioxidant imbalance is essential for the pathophysiological mechanisms of the progressive loss of lens transparency. Since the crystalline lens is more susceptible to oxidative attack from reactive oxygen radicals, it has enzymatic antioxidants, such as superoxide dismutase, glutathione peroxidase or glutathione reductase, that protect the crystalline lens from oxidative damage.(Reddy, 1990; Hejtmancik *et al.*, 2015) Previous studies demonstrated that deprivation of reduced glutathione plays a predominant role in the pathogenic mechanisms of age-related nuclear cataracts.(Zhang & Augusteyn, 1994; Kamei, 1993; Reddy, 1990) For example, hardening of the nucleus related with aging contributed for a declined diffusion of reduced glutathione towards the nucleus, making the central area of the crystalline lens more susceptible to oxidative damage, resulting ultimately in nuclear cataract.(Gao *et al.*, 2013; Slavi *et al.*, 2014) Reduction in the protective activity of these pathways is associated with cataract formation, by causing fiber cells disruption, cellular membrane breakdown or rearrangement, and accumulation of abnormal crystalline proteins (Figure 20).(Varma *et al.*, 1982; Hejtmancik *et al.*, 2015; Brennan *et al.*, 2012; Jahngen-Hodge *et al.*, 1994)

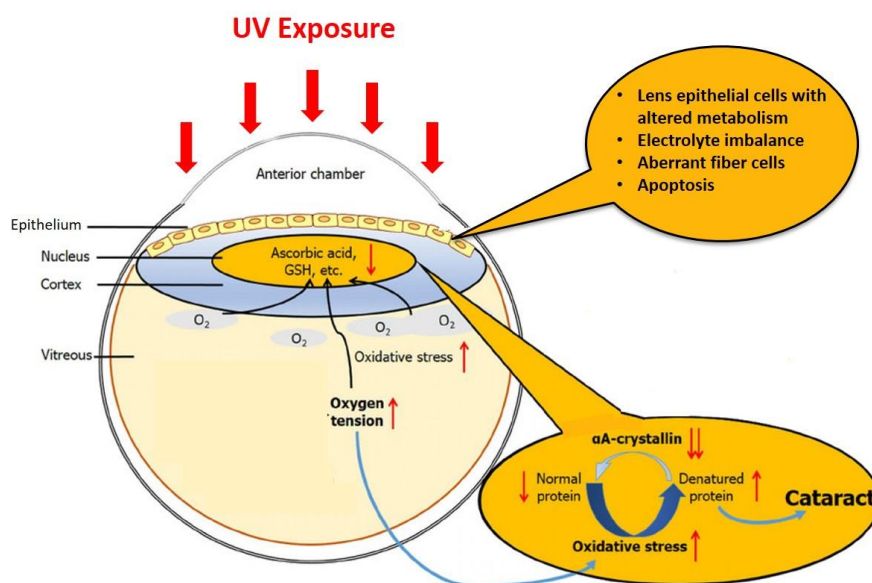


Figure 20 – Oxidative damage in the crystalline lens inducing accumulation of abnormal crystalline proteins, electrolyte imbalance and aberrant lens cells (GSH – reduced glutathione; O<sub>2</sub> – oxygen).(Zhu *et al.*, 2013)

The protein content of the crystalline lens is essential for the maintenance of transparency and refractive index, considering the crystallins as the most common structural proteins of the lens.(Hejtmancik *et al.*, 2015; Mathias & Rae, 2004) Structural and functional modification of these proteins may derive from different processes, such as oxidation, phosphorylation or transamidation, leading to insoluble and high-molecular-weight proteins. The resulting changes induce fluctuations in the refractive index of the crystalline lens, light scattering and transparency reduction.(Sharma & Santhoshkumar, 2009; Chylack, 1984) For example, the reduction of Alpha-crystallin results in increased protein insolubility and aggregation, inducing subsequently light scattering and loss of lens transparency.(Chylack, 1984; Bloemendal *et al.*, 2004; Jahngen-Hodge *et al.*, 1994; Lampi *et al.*, 1998; Sharma & Santhoshkumar, 2009) The functions of proteins associated with channels membranes and cytoskeletal system are also altered in the nuclear cataract formation.(Hejtmancik *et al.*, 2015; Maisel, 1984; Su *et al.*, 2011) To keep the electrolyte homeostasis, a process, which is driven by energy consumption, allows K<sup>+</sup> to accumulate intracellularly by the outflow of Na<sup>+</sup> and Ca<sup>2+</sup>.(Hejtmancik *et al.*, 2015; Paterson & Delamere, 2004) Ionic imbalance, resulting from a progressive decrease of K<sup>+</sup> and increase of Na<sup>+</sup> and of Ca<sup>2+</sup> intracellularly, contributes for the loss of transparency. For example, an increase in the Ca<sup>2+</sup> concentration induces irreversible modification of structural



proteins due to proteases activation.(Ahuja *et al.*, 1999; Gao *et al.*, 2004; Marcantonio & Duncan, 1991)

Other pathways may influence the cataractogenesis by different modes. The Nuclear Factor- $\kappa$ B (NF- $\kappa$ B) and mitogen-activated protein kinases (MAPKs) pathways are also activated by oxidative stress and have a crucial role in stress signaling and cell apoptosis. Both mechanisms were reported to be present in lens epithelial cells and are necessary for their normal function. Thus, activation of these pathways by oxidative stress may also affect the transparency of the crystalline lens, causing a decline of epithelial cell density and an aberrant differentiation of lens fiber cells.(Li *et al.*, 2003; Li *et al.*, 1995; Dudek *et al.*, 2001; Boileau *et al.*, 2003)

#### **2.4 – Complementary exams for cataract evaluation**

Proper classification and grading are essential because the type of cataract determines specific complaints, loss of functional vision and distinct surgical approach.(Chua *et al.*, 2004) Cataract assessment showed to be influenced by the subjectivity of the clinicians.(Chylack *et al.*, 1993; Hall *et al.*, 1997; Karbassi *et al.*, 1993; Wong *et al.*, 2013) To surpass this issue, technological and scientific developments enabled new methods to document the disease and to analyze its impact on visual function and in quality of life.(Lim *et al.*, 2014; Sachdev *et al.*, 2004; Kuroda, Fujikado, *et al.*, 2002a; Magno, Freidlin, *et al.*, 1994; Pei *et al.*, 2008; Gupta *et al.*, 2013; Dicarlo *et al.*, 1999; Rovati & Docchio, 2004; Cotlier, 1999; Pan *et al.*, 2015; Steinberg *et al.*, 1994) Table 2 provides a list of the different evaluation methods. It is worthwhile to mention that no single exam adequately describes the effect of cataract on a patient's visual status or functional ability. In addition to allowing documentation and grading of lens opacities, these assessment techniques must be integrated with clinical data, such as visual acuity and functional impairment tests, to understand the effect of the cataract on the patient's daily needs and quality of life.(Pan *et al.*, 2015; Rosenberg & Sperazza, 2008; D'Ambrósio, 1999) Concerning anterior segment imaging, technological developments enabled to visualize and quantify detailly specific features of the anterior ocular segment.(Salomao *et al.*, 2009) For example, corneal topography became popular in the mid-1980s, when surface reconstruction algorithms enabled color-coded maps and indices derived from

the acquired reflection image of the Placido photokeratoscope. (Ambrósio & Belin, 2010) This ancillary tool provided more accuracy in the diagnosis and management of corneal disease. Other important application of this device was in screening refractive surgery patients, as well as evaluating and improving the outcomes of corneal and cataract surgeries. (Salomao *et al.*, 2009; Ambrósio *et al.*, 2013; Ambrósio, Nogueira, *et al.*, 2011) In the last two decades, technological developments of the anterior segment imaging enabled increased speed and resolution scans, enhanced microstructural imaging, and marked increase of data available on the three-dimensional representations of the anterior segment. In addition to improve the analysis of the cornea, the advances also allowed more precise and detailed measurements of the anterior chamber and the crystalline lens. Currently, the data offered by these tools is useful for the diagnosis and the clinical decision-making in the cataract, cornea and refractive surgery subspecialties. (Salomao *et al.*, 2009; Ambrósio *et al.*, 2013; Ambrósio, Nogueira, *et al.*, 2011) For the purpose of this thesis, the LOCS III grading system, the wavefront analysis and the Scheimpflug imaging will be described.

Table 2 – Complementary exams for cataract evaluation

<p><b>Standardized clinical grading and photographic systems (comparing a patient's cataract with standard photographs)</b></p> <p>Lens Opacities Classification System (LOCS) III Grading system          Wisconsin Clinical and Photographic Cataract Grading system          Wilmer Clinical and Photographic Cataract Grading system          Oxford Clinical Cataract Grading system          Age-Related Eye Disease Study (AREDS) Cataract Grading System</p>
<p><b>Contrast sensitivity test</b></p> <p>Vision contrast test system (VCTS)          CSV-1000®          Pelli Robson test          Bailey Lovie chart          Cambridge low contrast grating          Regan charts          Functional acuity contrast testing (FACT) charts</p>
<p><b>Glare test</b></p> <p>Brightness Acuity Test          CSV-1000®          Straylight meter</p>
<p><b>Functional impairment and quality of life questionnaires</b></p> <p>National Eye Institute Function Questionnaire – 25 items (VFQ-25)          Visual Function Questionnaire – 14 items (VF-14)</p>
<p><b>Scheimpflug imaging</b></p>
<p><b>Optical coherence tomography</b></p>
<p><b>Ultra-high frequency ultrasound</b></p>
<p><b>Wavefront sensors</b></p>
<p><b>Autofluorescence</b></p>

### 2.4.1 – LOCS III grading system

The LOCS III was developed in 1993 by Chylack et al. and represents an improved method to classify and compare the type and severity of age-related cataract based on slit lamp examination. This system derived from the LOCS II, which was introduced in 1989. Some adjustments were made to enable a better characterization of the cataracts. For example, the LOCS III uses standardized six pictures obtained by a slit-lamp to classify nuclear opalescence (NO) and nuclear color (NC), and five retroillumination images to scale cortical and posterior subcapsular cataract (Figure 21).(Chylack *et al.*, 1993)

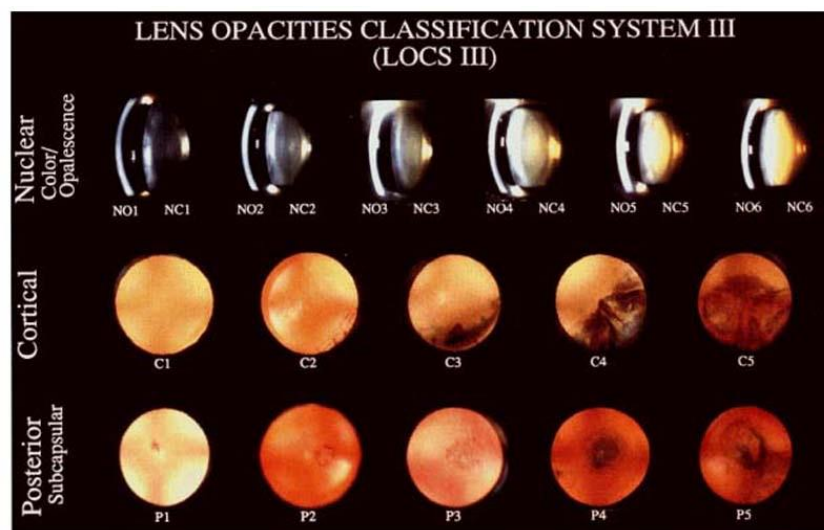


Figure 21 – Lens Opacities Classification System (LOCS) III grading system.(Chylack *et al.*, 1993)

The degree of cataract is obtained from a decimal scale at equally spaced intervals, where NO and NC are characterized on a scale from 0.1 to 6.9 (based on six standard photographs), and cortical and posterior subcapsular are graded on a scale from 0.1 to 5.9, based on the five standard pictures.(Chylack *et al.*, 1993) The LOCS III grading system is a more objective method of analyzing the lens opacity and can provide information about possible complications of cataract surgery. For example, previous studies have reported that the degree of NO correlates with the incidence of capsular rupture during phacoemulsification.(Bencic *et al.*, 2005; Davison & Chylack, 2003)

## 2.4.2 – Wavefront analysis

### 2.4.2.1 – Optical aberrations

A perfect optical system would be one able to converge exactly in a focal image point all the rays of light from an object or a point light source. However, that ideal focus is given rarely in the real world. Instead, we usually find a light spot more or less homogenous, being its shape and intensity dependent on optical imperfections of the system, which are generically known as optical aberrations.(Applegate & Howland, 1997; Oliveira *et al.*, 2012) Based on this concept, each focus point from the image also will also form a flat surface in a perfect optical system. Considering a complex optical system as the eye, the resultant wavefront will be not plane due to optical aberrations (Figure 22).(Pepose & Applegate, 2005; Applegate & Howland, 1997; Oliveira *et al.*, 2012)

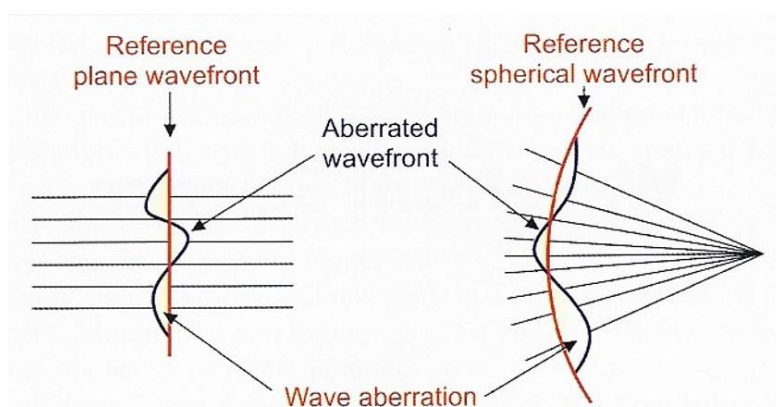


Figure 22 – Aberrated or imperfect wavefront are deviated from the ideal reference wavefront.(Sinjab, 2014)

The difference of the actual wavefront shape and the ideal flat reference represents the amount of deviation or aberration in the wavefront.(Applegate & Howland, 1997; Oliveira *et al.*, 2012) When the wavefront surface is regularly deformed in a spherical or cylindrical fashion, the optical system can be corrected spherical-cylindrical lenses. These aberrations are designated by low-order aberrations. The low-order aberrations are known in ophthalmology as spherical (hyperopia and myopia) and cylindrical (regular astigmatism) components. The optical aberrations that are not corrected by spherical-cylindrical lenses are known as high-order aberrations (HOAs).(Applegate *et al.*, 2014; Applegate, Marsack, *et al.*, 2003; Applegate *et al.*, 2002) These aberrations play an essential role in the reduction of the optical performance in different types of patients,



As a general rule, the value of the aberration decreases with the increase of the order of Zernike. Thus, above the 4th order, the impact of the aberrations is minimal. In healthy eyes, it has been estimated that the terms up to the 4th order entirely represent the total aberrations for a small and medium pupil, and the 99% of total aberrations for a 6-mm pupil. Considering the same magnitude, the visual impact of the peripheral aberrations also appears to be less than the central ones of each order.(Applegate *et al.*, 2002; Oliveira *et al.*, 2012) In clinical practice, the primary source of aberrations in the eye is the anterior surface of the cornea followed by the lens.(Artal *et al.*, 2002; Applegate *et al.*, 2000; Oshika *et al.*, 1999) In young adults, the total aberration of the eye (without defocus) is less than the corneal or the internal ones, when considered separately. This fact is explained by the opposite sign of the spherical aberrations and astigmatisms of the cornea and the crystalline lens.(Artal *et al.*, 2002; Oshika *et al.*, 1999; Wang *et al.*, 2005)

#### **2.4.2.3 – Optical quality measurement**

Wavefront analysis is one method to objectively assess vision impairment by quantifying the total aberrations and HOAs of the optical system of the eye. The influence of these aberrations in an optical system can be measured by different forms. All these measurements are affected by two main factors, particularly the magnitude of irregularities and pupil diameter.(Thibos *et al.*, 2002; Fang *et al.*, 2013; Oliveira *et al.*, 2012)

The Point Spread Function (PSF) is a mathematical tool that evaluates the response of an optical system to a point object or source. The PSF can be demonstrated considering all ocular aberrations or just the high-order aberrations. The PSF charts present variable scales in minutes of arc. To allow comparisons, usually is added to the chart a reference scale with an optotype equivalent to 1.0 of visual acuity, which measures 5 minutes of arc (Figure 24).(Cheng *et al.*, 2003; Marsack *et al.*, 2004)

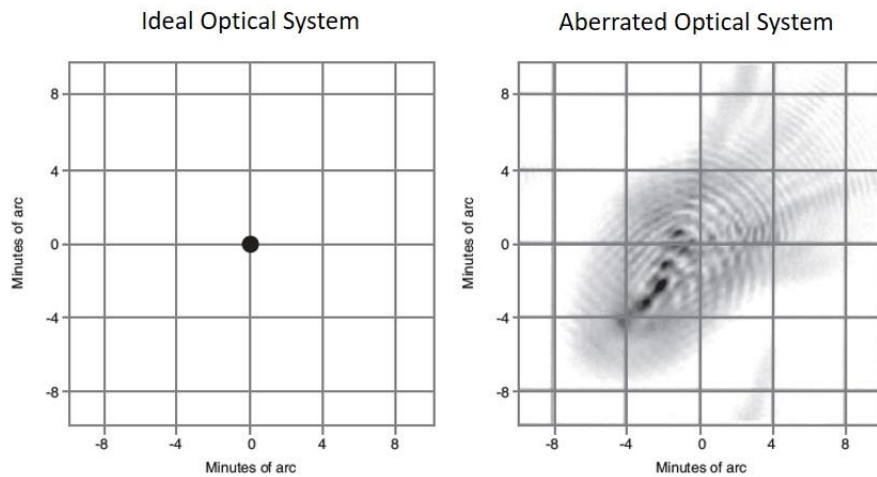


Figure 24 - Point spread function (PSF) in a perfect optical system without aberrations (left) and an eye with severe aberrations (right). In the ideal system, the image the point remains true to the object, while in the eye with aberrations this point is seen as a shapeless blurring. (Ambrósio *et al.*, 2012)

The Modulation Transfer Function (MTF) is the ratio of the contrast of the object and image. An image generated by an optical system will be perfect if the contrast found in the image is identical to the object. In this condition, the MTF is equal to 1.0, meaning that the image has the same contrasting tones of the object. The contrast (or modulation) of an object or an image is measured by the intensity and distribution of dark and light shades. If, after passing through an optical system, the image does not present the same contrast properties of the object, the optical system influenced the final image of the object, or the modulation was not transferred correctly (Figure 25). (Marsack *et al.*, 2004; Applegate *et al.*, 2000)

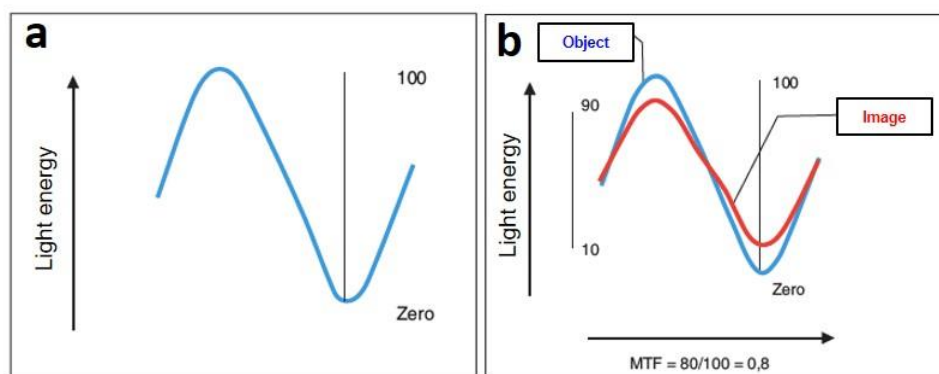


Figure 25 – Contrast representation of an object or its modulation (A). Note that the higher light energy (lighter) is represented on the ordinate with the value 100. (B) has the representation of the modulation of the same object (blue line) and his image, after passing through an optical system (red line). Note that after passing through the optical system this hypothetical picture does not have the same energy levels and their modulation is 80 (maximum energy = 90 and minimum power = 10). The modulation transfer function (MTF) in this case is 0.8 (80/100).

(Ambrósio *et al.*, 2012)

As previously mentioned, ocular aberrations can be analyzed as the difference between the actual wavefront of an optical system and a perfectly flat surface (total aberrations) or the difference between the actual wavefront and a specific spherical-cylindrical surface (high-order aberrations). The farther from the reference surface is the real wavefront, the greater the optical aberrations. Thus, if the average of the distances is performed, point by point, from the reference surface to the real wavefront, the ocular aberrations can be quantified. Nevertheless, as some portions of the wavefront will be anterior or posterior regarding the reference surface and will present opposite signs, before performing the average of these distances it is necessary to override signals (by calculating the square of the distances). The Root Mean Square (RMS) is the root mean square of the (squared) distances between the reference plane and the wavefront (Figure 26). Although RMS is a reliable measure of the amount of aberration of an optical system, it is generic and does not consider specific qualitative characteristics of aberrations.(Oliveira *et al.*, 2012; Applegate, Ballentine, *et al.*, 2003)

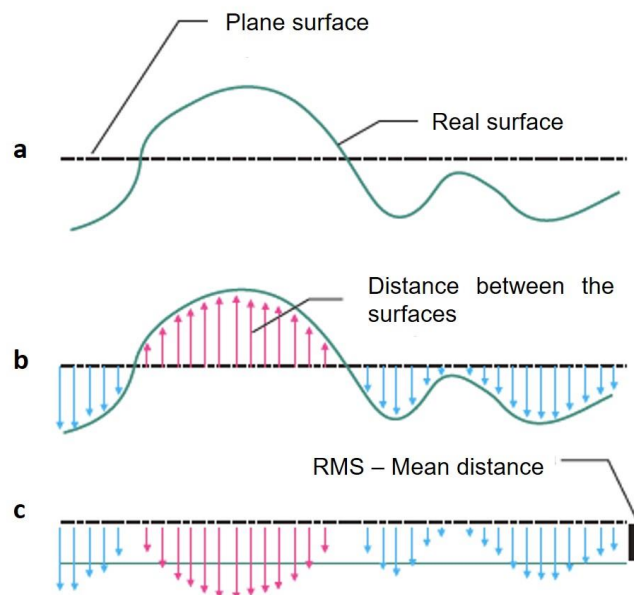


Figure 26 – Schematic representation of calculating the root of mean square (RMS). To calculate the area between the actual surface (blue) and the reference surface (dotted), the values have to be considered in module, because otherwise, the upper portion would nullify the lower, concluding erroneously that both surfaces would be identical. RMS equal to the average of the distances represented by the blue and red arrows.(Ambrósio *et al.*, 2012)



The Zernike Coefficient (ZC) is an expression of the magnitude of each aberration. Unlike RMS, the ZC can be presented in negative and positive values (Figure 27). (Applegate, Ballentine, *et al.*, 2003; Oliveira *et al.*, 2012)

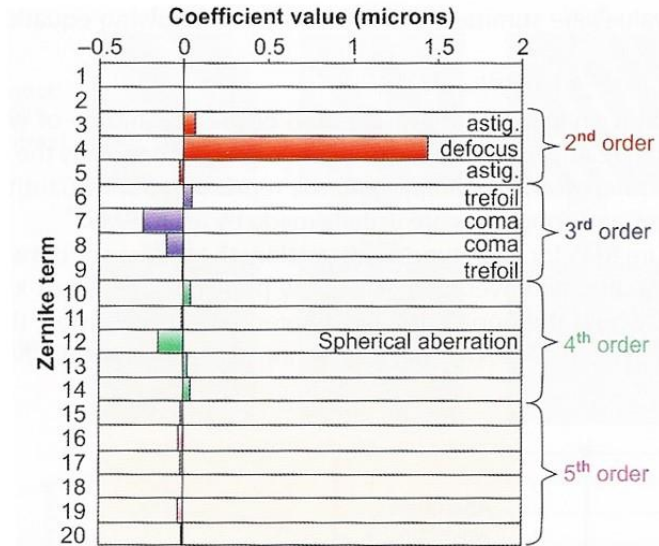


Figure 27 – Zernike Coefficients is an expression if the amount of each individual aberration.

#### 2.4.2.4 – Wavefront sensors

Currently, there are several systems available for the analysis of the wavefront. All the different methods have the common objective to analyze the deviations of wavefronts that cross the human eye compared to a standard reference. Such shifts and distortions of the light beams are measured and reconstructed into a map of aberrations. (Cheng *et al.*, 2003; Marsack *et al.*, 2004; Oliveira *et al.*, 2012) Deviations are decomposed using mathematical formulas and translated numerically into the different ways of optical quality analysis. (Marsack *et al.*, 2004; Oliveira *et al.*, 2012), The wavefront analysis systems can be divided in output and input optical systems. (Cervino *et al.*, 2007; Netto *et al.*, 2005; Rozema *et al.*, 2005) The input optical systems evaluate the aberrations of the light beam projected on the retina. (Kaemmerer *et al.*, 2000; Mrochen *et al.*, 2000; Buscemi, 2002; Rozema *et al.*, 2005) Output optical systems assess the wavefront exiting the eye from a light beam projected on the retina and reflected in the opposite direction. (Thibos, 2000; Thibos & Hong, 1999; Rozema *et al.*, 2005) Based on the distinct analysis forms, the devices may be classified according to the operation pattern (Table 3).

Table 3 – Wavefront sensors

<b>1 – Outgoing Optical Systems</b>
<b>Hartmann – Shack principle</b> (LadarWave - Alcon; Zywave - Bausch & Lomb; WaveScan – VISX; Wasca Analyzer – Carl Zeiss-Meditec; KR-9000PW - Topcon)
<b>2 – Ingoing Optical Systems</b>
<b>Tscherning principle</b> (WaveLight Wavefront Analyzer - WaveLight; ORK Wavefront Analyzer - Schwind)
<b>Ray Tracing principle</b> (Tracey VFA; i-Trace – Tracey)
<b>Double pass principle</b> (OPD Scan – Nidek; OQAS - Visionmetrics)

#### 2.4.2.5 – iTrace Visual Function Analyzer

The iTrace Visual Function Analyzer, manufactured by Tracey Technologies (Houston, Texas), combines a Placido-based corneal topographer (EyeSys Vista Vision, Inc., Houston, Texas, USA) and a wavefront analyzer based on the ray-tracing principle (Figure 28). (Rozema *et al.*, 2005)



Figure 28 – iTrace Visual Function Analyzer (Tracey Technologies, Houston, Texas, USA).

This principle measures the aberrations of the light input that passes through the eye sequentially for each point, as opposed to other methods, such as a Hartmann-Shack and Tscherning, which measure the optics of the eye integrally as a single beam light. (Bartsch *et al.*, 2008; Molebny *et al.*, 2000; Pinero *et al.*, 2011) With the ray-tracing system developed, each laser beam is moved to a new position, and the next point on the retina is then determined. This process continues until interrupted 256 points have been projected through the pupil entrance, which occurs in about 100 milliseconds. If the eye is emmetropic, all

256 points fall on the same point that represents the center of the macula. When a series of points is projected sequentially through the pupil, a location profile of these points is then created on the retina, designated by the retinal spot diagram (Figure 29). (Bartsch *et al.*, 2008; Pinero *et al.*, 2011) The intensity of energy detected at each point of the retina is also determined.

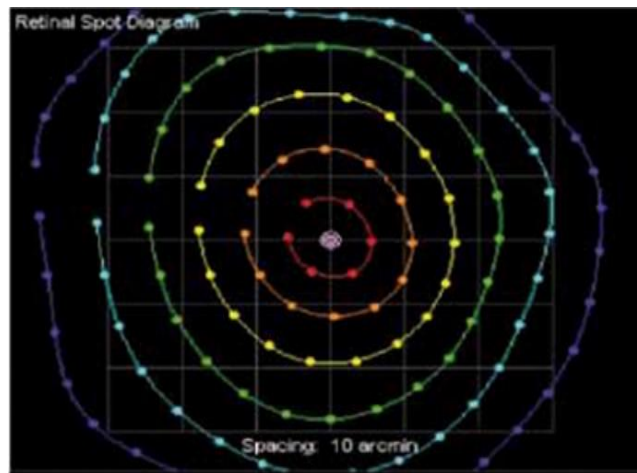


Figure 29 – Retinal Spot Diagram. (Gomez *et al.*, 2012)

The ray-tracing system has some advantages over other technologies. First, the fast capture means that there is no confusion in the analysis of the original location of these points on the pupil entrance with the reflected location on the retina, once each section is analyzed sequentially and separately. This method explains the easy measurement of highly aberrated eyes with ray-tracing system. Then, due to the fast control of the laser spots profile projected on the pupil entrance, the software can track the pupil size and design all 256 points in small to large pupils (from 2 mm to 8 mm). (Bartsch *et al.*, 2008; Molebny *et al.*, 2000; Rozema *et al.*, 2005)

As mentioned before, this wavefront analyzer integrates an aberrometer with corneal topography. The internal aberrations are calculated by subtracting the corneal aberrations derived from the topography data from those of the entire eye measured by the ray-tracing aberrometer. Therefore, the total aberrations and HOAs derived from the crystalline lens can be measured (Figure 30). (Rozema *et al.*, 2005; Bartsch *et al.*, 2008)

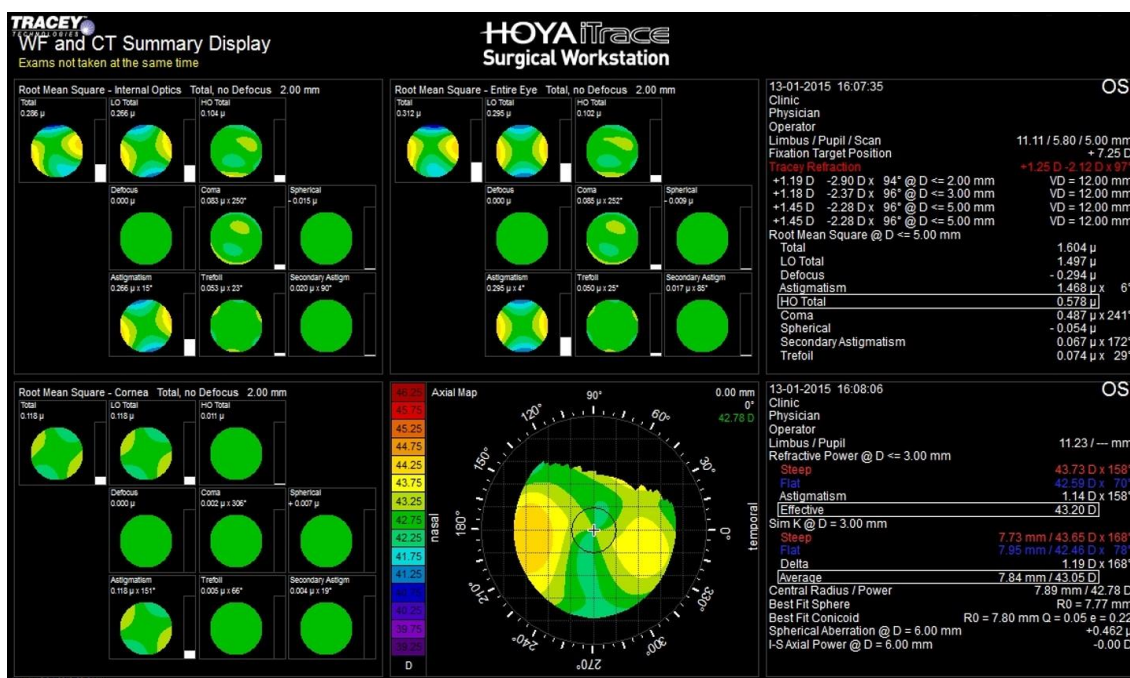


Figure 30 – Total, corneal and internal aberrations analysis provided by the iTrace Visual Function Analyzer.

#### 2.4.2.6 – Wavefront analysis in patients with nuclear cataracts

Internal HOAs change and mild crystalline lens opacification could explain some symptoms reported by patients with mild cataracts, even with unnoticeable findings in visual acuity measurements. (Alió *et al.*, 2005; Rocha *et al.*, 2007) Aging causes deterioration of the optical quality of the eye, which is mainly due to progressive changes in the structure of the lens, causing an increase in HOAs and light scattering. (Alió *et al.*, 2005; Rocha *et al.*, 2007) For example, the cornea has a RMS spherical aberration of  $+0.28 \mu\text{m}$ , considering a 6.0-mm pupil. In young adults, this aberration is compensated by the negative ( $-0.27 \mu\text{m}$ ) spherical aberration derived from the crystalline lens. With aging, the crystalline lens decreases its negative spherical aberration, neutralizing it at 40 years and becoming positive after 60 years. (Artal *et al.*, 2002) Thus, in the presence of corneal aberrations within the normal range, modification of the internal aberrations profile indicates refractive changes in the crystalline lens, suggesting a nuclear sclerosis process, although its transparency is not significantly altered. These studies used different types of wavefront devices, including Hartmann-Shack sensors. (Alió *et al.*, 2005; Kuroda, Fujikado, *et al.*, 2002b; Kuroda, Fujikado, Ninomiya, *et al.*, 2002; Ortiz *et al.*, 2008; Rocha *et al.*, 2007; Sachdev *et al.*, 2004) Using the i-Trace Visual Function Analyzer, eyes with nuclear

cataract also registered an increase of the internal HOAs, being the comatic aberration the most predominant aberration.(Lee *et al.*, 2008)

### **2.4.3 – Scheimpflug imaging**

#### **2.4.3.1 – Scheimpflug’s principle and its application in Ophthalmology**

The Scheimpflug principle is a geometric rule commonly used in photography and offers an extension of depth of focus and more sharpness to points of the image located in different planes.(Scheimpflug, 1904; Carpentier, 1901) In 1973, the first Scheimpflug imaging system was used for evaluation of the crystalline lens in a laboratory setting.(Brown, 1973b; Brown, 1973a) Scheimpflug devices, such as the Nidek EAS 1000 (Gamagori, Japan) and the Topcon SL-45 (Tokyo, Japan), only became commercially available in the 80s and 90s. These systems enabled the detection of changes in lens transparency over time by measuring the scattered light along the optical axis.(Kojima *et al.*, 1990; Wegener *et al.*, 1992) Currently, Scheimpflug imaging was subjected to various developments and has several applications in Ophthalmology

# Clinical applications of the Scheimpflug principle in Ophthalmology

## *Aplicações clínicas do princípio de Scheimpflug na Oftalmologia*

---

Fernando Faria-Correia<sup>1</sup>, Renato Ambrósio Jr.<sup>2</sup>

### ABSTRACT

*This article presents a review of the principles and clinical applications of the Scheimpflug principle in the anterior segment imaging. By providing a three-dimensional image of the anterior segment, this technology provides elevation and curvature data of the anterior and posterior surfaces of the cornea, pachymetric mapping, the total refractive power of the cornea and the anterior segment biometry. For the refractive surgery sub-specialty, this approach improves the ability to identify cases at risk of ectasia, as well as the planning and evaluation of the results of surgical procedures. Recently, this technology was introduced in corneal biomechanical in vivo evaluations and in femtosecond laser-assisted cataract surgery.*

**Keywords:** Scheimpflug; Tomography; Biomechanics; Cornea; Cataract; Refractive surgery

### RESUMO

Este artigo apresenta uma revisão dos princípios e das aplicações clínicas do princípio de Scheimpflug na área da imagiologia do segmento anterior. Ao disponibilizar uma imagem tridimensional do segmento anterior, esta tecnologia permite a caracterização da elevação e curvatura das superfícies anterior e posterior da córnea, o mapeamento paquimétrico, o cálculo do poder refrativo total da córnea e a biometria do segmento anterior. Na subespecialidade de cirurgia refrativa, esta abordagem melhora a capacidade de identificação de casos com risco de desenvolver ectasia, bem como de planejamento e de avaliação dos resultados dos procedimentos cirúrgicos. Recentemente, esta tecnologia foi introduzida na avaliação biomecânica *in vivo* da córnea e na cirurgia de catarata assistida por laser de femtossegundo.

**Descritores:** Scheimpflug; Tomografia; Biomecânica; Córnea; Catarata; Cirurgia refrativa

---

<sup>1</sup> Escola das Ciências da Saúde, Universidade do Minho, Braga, Portugal; Study Group on Corneal Tomography and Biomechanics of Rio de Janeiro, Rio de Janeiro, RJ, Brazil.

<sup>2</sup> Universidade Federal de São Paulo, São Paulo, SP, Brazil; Study Group on Corneal Tomography and Biomechanics of Rio de Janeiro, Rio de Janeiro, RJ, Brazil

**The authors declare no conflicts of interests.**

Received for publication 10/07/2015 - Accepted for publication 07/10/2015

## INTRODUCTION

Advances in diagnostic capabilities have been critical to the evolution of refractive surgery, which emerged as a new subspecialty in the early 1980s.<sup>1</sup> Improving imaging methods of the cornea and the anterior segment is related to the continuous need to increase the safety and effectiveness of surgical procedures.<sup>2</sup> Linked to a better selection of candidates for refractive surgery, the development of diagnostic technologies dramatically favored surgical planning capabilities, including personalization of laser ablation treatment and the evaluation of results and complications of these procedures.<sup>3-8</sup> This knowledge also had an impact on the selection of the type and power of the intraocular lens to be implanted in the cataract surgery.<sup>9,10</sup> In addition, the treatment of complex cases such as keratoconus, corneal dystrophies and other causes of irregular astigmatism also has developed due to advances in the imaging of the cornea and anterior segment.<sup>11-15</sup>

Initially, the main obstacle was the limitations inherent in the computer technology. The technological development has allowed the acquisition and analysis of images, having been key to the development of corneal topography. Stephen Klyce, PhD, is known for having developed derivative color maps of quantitative analysis of various points of the corneal curvature maps.<sup>16</sup> The analysis of the reflected images of the Placido's disk has been the dominant technique for the analysis of the anterior corneal surface.<sup>2</sup> Alternatively, the scan photogrammetry uses a stereo triangulation technique wherein a regular pattern consisting of horizontal and vertical lines is projected onto the eye surface to reconstruct the elevation of the anterior corneal surface.<sup>17</sup> Michael Belin, MD, developed the basis for calculating the elevation maps in relation to a reference surface being defined by a geometric shape (spheric, aspheric or toric ellipsoid) which best fits the actual corneal surface.<sup>17,18</sup> ENREF<sup>17</sup> Both the Placido's disk and the scan photogrammetry are able to calculate the maps of axial (sagittal) and tangential (instantaneous) curvature of elevation and refraction of the anterior corneal surface. Other systems, such as the Hartmann-Shack sensor for analysis of front-of-wave, also incorporate a device for corneal topography analysis.<sup>2</sup> However, these devices are limited to the analysis of the anterior corneal surface.<sup>19</sup>

Regarding the measurement of the thickness of the cornea, the optical pachymeter was presented by David Maurice, PhD in 1955.<sup>20</sup> The ultrasonic technique has demonstrated greater repeatability than the optical pachymeter, but only provided data of a single point.<sup>19,21</sup> Mandell e Polse proposed a study of the horizontal profile of the corneal thickness using a modified optical pachymeter. In this context, the variation of thickness in the horizontal meridian proved to be a feature for the diagnosis of keratoconus.<sup>22</sup>

The development of the anterior segment tomography allowed the assessment of the profile of the corneal thickness from the pachymetry mapping.<sup>23,24</sup> Tomography (from the Greek: "tomos" means slice and "grafia" means describe) is a concept that represents the three-dimensional reconstruction of the cornea, providing detailed information on the thickness and the anterior and posterior surfaces of the cornea.<sup>19</sup> Different technologies such as the horizontal slit scanning, the rotating Scheimpflug camera, high frequency ultrasounds, and optical coherence tomography are commercially available from various instruments.<sup>19,25</sup>

Advances in corneal imaging were beyond the tomographic characterization. The concept of customized biomechanics in refractive surgery was introduced by Cynthia Roberts, PhD, in 2005.<sup>26</sup> The Ocular Response Analyzer (ORA - Reichert Inc., Depew, USA) was introduced as the first device to assess in vivo the biomechanics of the cornea.<sup>27,28</sup> ORA is a non-contact tonometer (NCT) which uses an electro-quantitative system for controlling the deformation of the cornea by the corneal reflection of infrared light. Other technologies, such as the Scheimpflug image and optical

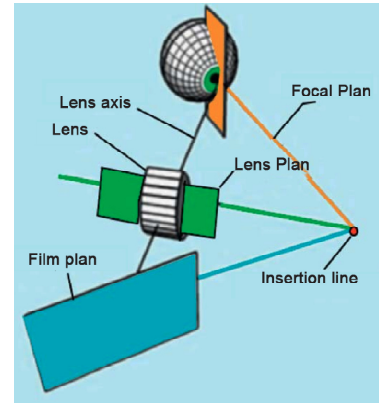


Figure 1: Scheme of the Scheimpflug principle.

coherence tomography, have also been recently introduced to provide dynamic measurements of the corneal deformation.<sup>29,30</sup> Finally, imaging of the cornea and the anterior segment was also used in cataract surgery assisted by femtosecond laser.<sup>31-33</sup>

This review focuses on the application of the Scheimpflug principle for laser refractive surgery, including its diagnostic capability and biomechanical assessment of the cornea, as well as its recent use in the planning of assisted cataract surgery by femtosecond laser.

### Scheimpflug Principle

The Scheimpflug principle is a geometric rule commonly used in photography. This concept was first described by Jules Carpentier in 1901, having been cited and credited in the original patent by Theodor Scheimpflug in 1904.<sup>34</sup> In this technique, three imaginary planes - the film plane, the lens plane and the focal plane - are arranged in a non-parallel way (Figure 1). The lens is tilted so that the resulting plane of the lens intercept the planes of the film and focus in a line of intersection known as Scheimpflug line. In a typical photographic camera, the film plane and the lens plane are parallel to each other, and also relative to the focal plane. This principle allows increasing the depth of focus and sharpness of image points located on different planes.<sup>34</sup>

### Scheimpflug images of the corneal and anterior segment

The Scheimpflug photography was used in the imaging of the anterior segment by devices EAS 1000 by Nidek (Gamagori, Japan) and SL-45 by Topcon (Tokyo, Japan).<sup>35,36</sup> These systems have the ability to measure the dispersion of light along the optical axis, allowing the detection of changes in the transparency of the lens over time.<sup>35</sup> Associated to the optical densitometry, recording these images also offer biometric measurements of the anterior segment such as the anterior chamber depth and peripheral angle measurements.<sup>37</sup> However, these systems did not hold the three-dimensional reconstruction of the anterior segment.

In 1995, the optical cross-sectioning for examination of the cornea was first introduced commercially with the Orbscan [(originally Orbtex, Inc.) Bausch & Lomb Surgical, Salt Lake City, USA].<sup>38-42</sup> ENREF<sup>39</sup> ENREF<sup>39</sup> This instrument is designed to provide tomographic data (three-dimensional reconstruction), but the nomenclature regarding the CT concept was not set yet, so that it was still referred as topography.<sup>19,38,42</sup> This system introduced the slit-scanning imaging technique or the cobblestone methodology, involving the projection of 40 slits (12.50 mm height and 0.30 mm wide) with a Scheimpflug angle of 45 degrees. However, Orbscan slit images do not exhibit the same depth of field as compared to those obtained by the Scheimpflug systems (Figure 2). In its first version, the Orbscan

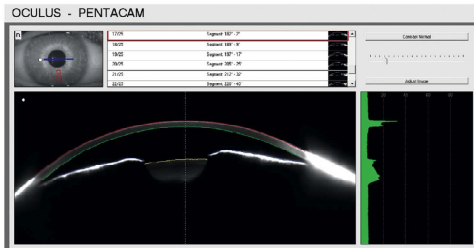


Figure 2: Scheimpflug image of the cornea and anterior segment

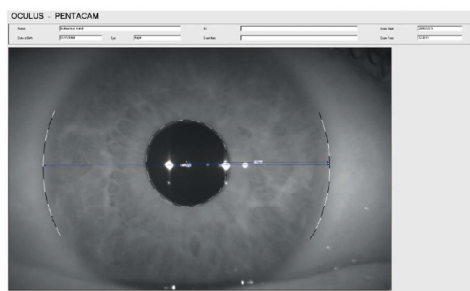


Figure 3: High-resolution front iris camera.

provided information from the anterior curvature extrapolated from elevation data. In 1999, a Placido disk was integrated into the Orbscan II to obtain data directly from the anterior curvature.

The digital tomography with rotating Scheimpflug camera has been recognized as an evolution of the horizontal cross section (cobblestone methodology) in the tomographic assessment of the cornea and anterior segment. Although the capture of horizontal images does not have points in common, the system has a rotating center common to all the images, which makes the registration more precise.<sup>43,44</sup> The Pentacam (Oculus, Wetzlar, Germany) was the first system available to perform digital tomography of the cornea and anterior segment using rotational

Scheimpflug photography. This device was introduced in 1999, and introduced commercially in 2002. Pentacam, along with the rotating Scheimpflug camera, is part of a second front chamber to control the attachment and compensate the ocular alignment.

In the acquisition mode, optimal alignment is obtained with the first Purkinje reflection of the cornea using both the front chamber and the Scheimpflug one before automatically initiating the exam. A second high-resolution front camera records the size and orientation of the pupillary opening, serving as a guide for three-dimensional reconstruction. This camera also provides black-and-white measurements of the pupil size (Figure 3). The analysis of the three-dimensional Scheimpflug image provides data from the anterior and posterior surface of the cornea, anterior surface of the iris and the crystalline. As the system employs blue visible light (wavelength of 475 nm, free from ultraviolet radiation in Pentacam), that is sensitive to corneal opacities, resulting in hyperreflective images of inaccurate contour. Due to total internal reflection in the peripheral cornea, direct visualization of the anterior chamber angle is not possible. However, the extrapolation software is able to provide an estimate of the iris-corneal angle with relatively high accuracy.<sup>45</sup> Currently, there are other business units that incorporate rotational Scheimpflug imaging technology, and in particular Galilei (Ziemer, Switzerland), TMS-5 (Tomey, Nagoya, Japan); Sirius (CSO; Florence, Italy) and Preciso (Ivis Technologies, Taranto, Italy). Table 1 presents the diagnostic capabilities of all devices with Scheimpflug imaging technology.

**Corneal tomography using the Scheimpflug principle for screening ectasia**

One of the most important applications of corneal computed tomography relates to the diagnosis of keratoconus and other ectasia diseases of the cornea.<sup>3,46-49</sup> Pachymetry and elevation indices proved to be effective to detect keratoconus.<sup>50-52</sup> The graphics of the spatial profile and the percentage increase in corneal thickness describe the ring pachymetry increase since the thinnest point.<sup>23,24,51</sup> These charts are available on Pentacam and have been used successfully in the diagnosis of keratoconus.<sup>24,50,53</sup> Pachymetry progression indices (PPI) are calculated for all semi-meridians of the cornea, such that the average of all meridians (PPI Ave) and the meridian with maximum pachymetry progression (PPI max) are reported. The “Ambrósio Relational Thickness” (ART) parameter is the ratio

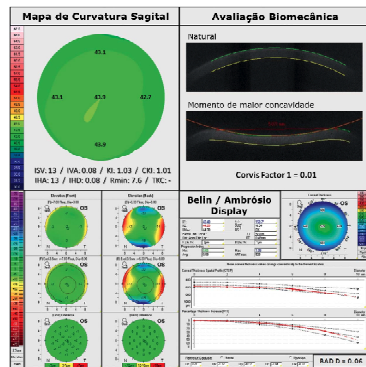


Figure 4: Detailed analysis of a normal cornea, including the map of front curve (sagittal) using the absolute scale of Smolek-Klyce, BAD and biomechanical evaluation with CorVIS ST. BAD-D <1.45, ART-Max >412 e “Corvis Factor 1” <0.2 are the most relevant findings. ART, Ambrosio Relational Thickness; BAD, Belin-Ambrosio Enhanced Ectasia Display

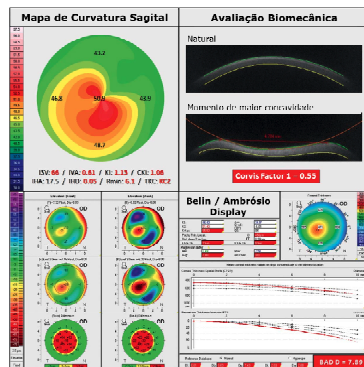
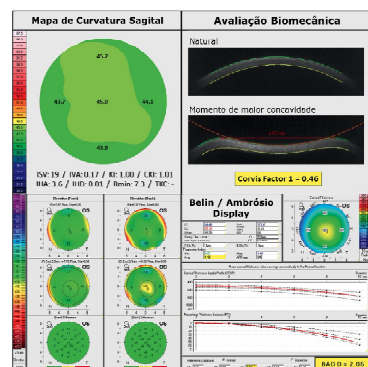


Figure 5: Detailed analysis of both eyes in the same patient with very asymmetrical keratoconus. A. Keratoconus in the anterior curvature map, BAD-D > 2.5, ART-Max <360 and “Corvis Factor 1” > 0.35; B. Forme fruste keratoconus with a relatively normal anterior curvature map, but with BAD-D >1.45, ART-Max <412 and “Corvis Factor 1” >0.25. ART, Ambrosio Relational Thickness; BAD, Belin-Ambrosio Enhanced Ectasia Display





**Table 1**  
Comparative table of instruments with Scheimpflug image

Company	Pentacam Oculus, Germany Rotational	Galilei Ziemer, Switzerland Rotational	TMS-5 Tomey, Japan Rotational	Precisio Ivis, Italy Rotational	Sirius CSO, Italy Rotational	Orbscan Bausch&Lomb, USA Horizontal cross section
Placido's disk	No	Yes	Yes	Yes	Yes	Yes
Elevation maps	Yes	Yes	Yes	Yes	Yes	Yes
Refractive power map of the cornea	Yes	Yes	Yes	Yes	Yes	Yes
Pachymetric map	Yes	Yes	Yes	Yes	Yes	Yes
Graphic of the space profile of the thickness	No	No	No	No	No	No
Cataract analysis	Yes	Yes	Yes	No	Yes	Yes
Analysis of the anterior chamber	Sim	Sim	Sim	Sim	Sim	Sim

**Table 2**  
Results of the curves "receiver operating characteristic" (ROC) of the parameters  
of Pentacam (331 normal patients vs. 242 patients with bilateral clinical keratoconus)

	Cutoff value	AUC	Standard error <sup>a</sup>	95% CI of AUC <sup>b</sup>	Sensibility	95% CI of sensibility	Specificity	95% IC da specificity
BAD D	>2.11	1	0.0000743	0.993- 1.000	99.59	97.7-100.0	100	98.9-100.0
Posterior elevation in the thinnest point (BFS)	>12	0.991	0.00396	0.979-0.997	96.28	93.1-98.3	98.79	96.9-99.7
Posterior elevation in the thinnest point (BFTE)	>8	0.994	0.00218	0.984-0.999	95.04	91.5-97.4	99.09	97.4-99.8
ART Avg	≤474	0.999	0.000663	0.991-1.000	99.59	97.8-100.0	98.19	96.1-99.3
ART Max	≤386	0.999	0.000674	0.991-1.000	99.17	97.0-99.9	97.28	94.9-98.7
K Max	>47.8	0.978	0.00633	0.963-1.000	90.50	86.1-93.9	97.89	95.7-99.1

a Method for standard error calculation (DeLong, 1988), listed in the software MedCalc.

b 95% CI, confidence interval; AUC, area under the curve "receiver operating characteristic".

ART Ave, Ambrósio's Relational Thickness medium; ART Max, Ambrósio's Relational Thickness maximum; BAD-D, D-final value of Belin-Ambrósio Enhanced Ectasia Display; BFS, Best Fit Sphere; BFTE, Best Fit Toric Ellipsoid; K Max, maximum keratometry value; SE, Standard error calculated by the binomial method.

**Table 3**  
Results of the curves "receiver operating characteristic" (ROC) of the parameters  
of Pentacam (331 normal patients vs. 47 patients with forme fruste keratoconus).

	Cutoff value	AUC	Standard error	95% CI of AUC	Sensibility	95% CI of sensibility	Specificity	95% CI of specificity
BAD D	>1.22	0.975	0.0121	0.954-0.989	93.62	82.5-98.7	94.56	91.5-96.7
Posterior elevation in the thinnest point (BFS)	>5	0.825	0.0348	0.783-0.862	74.47	59.7-86.1	74.92	69.9-79.5
Posterior elevation in the thinnest point (BFTE)	>1	0.849	0.0324	0.809-0.883	80.85	66.7-90.9	72.51	67.4-77.2
ART Avg	≤521	0.956	0.0203	0.930-0.974	91.49	79.6-97.6	93.05	89.8-95.5
ART Max	≤416	0.959	0.0153	0.934-0.977	85.11	71.7-93.8	93.05	89.8-95.5
K Max	>45	0.635	0.0431	0.584-0.683	53.19	38.1-67.9	64.05	58.6-69.2

a Method for standard error calculation (DeLong, 1988), listed in the software MedCalc.

b 95% CI, confidence interval; AUC, area under the curve "receiver operating characteristic".

ART Ave, Ambrósio's Relational Thickness medium; ART Max, Ambrósio's Relational Thickness maximum; BAD-D, D-final value of Belin-Ambrósio Enhanced Ectasia Display; BFS, Best Fit Sphere; BFTE, Best Fit Toric Ellipsoid; K Max, maximum keratometry value; SE, Standard error calculated by the binomial method.

between the PPI and the thinnest point.

The "Belin-Ambrósio Enhanced Ectasia Display" (BAD; Figures 4 and 5) allows an overview of tomographic structure of the cornea by combining data from the anterior and posterior elevation, pachymetry and curvature. The BAD considers deviations from normality for different parameters, so that a zero value represents the mean of the normal population and one is the value of a standard deviation value toward the value

of the disease (ectasia).<sup>3</sup> The final 'D' is calculated based on the regression analysis, weighing differently the various parameters. Alternatively, Saad and Gatnel developed an efficient method of combining pachymetry and elevation data of Orbscan in discriminant functions to detect keratoconus and forme fruste keratoconus (FFKC).<sup>34</sup>

Tables 2 and 3 provide the cutting values and the details of curves "receiver operating characteristic" (ROC) of the most

effective Pentacam parameters for identifying cornea with ectasia. Table 2 refers to a study involving an eye randomly selected from 331 normal patients and 242 patients with bilateral clinical keratoconus.<sup>3</sup>

Interestingly, the fact that the screening of the risk of ectasia should go beyond keratoconus detection is crucial to consider the studies that include mild or subclinical forms of ectasia.<sup>3,55</sup> One of the most important subgroups consists of eyes with relatively normal topography of keratoconus patients detected in the contralateral eye, being referred as FFKC.<sup>3,54,56</sup> Table 3 refers to a study which included 47 corneas with FFKC, and the same control group of study<sup>57</sup> of Table 2. It is critical to adjust the cutoff values to identify such mild cases or those of susceptibility to ectasia. For example, BAD-D has a cutoff value of 2.11 to detect keratoconus (99.59% sensitivity and 100% specificity; Table 2), but the best cutoff value to detect FFKC is 1.22 (93.62% sensitivity and 94.56% specificity). The optimization of the area under the ROC curve can be possible with the cutoff value, but with a minimal and tolerable loss of specificity value. For example, some parameters that are very efficient in the detection of keratoconus, such as the maximum keratometry, may not be useful in identifying cases with FFKC.

#### Dynamic Scheimpflug imaging to assess corneal deformation

CorVIS ST (Oculus, Wetzlar, Germany) is an NCT with a high-speed Scheimpflug camera that was launched in 2010.<sup>3,29</sup> ENREF\_28 The coupled Scheimpflug camera covers the horizontal 8.5 mm of the cornea and captures more than 4300 images per second to monitor the response of the cornea to a collimated and calibrated puff of air. The air pulse has a fixed profile with symmetrical configuration and with maximum internal pressure of the pump of 25 kPa.<sup>29</sup> During the recording time of 30 ms, 140 digital images are acquired with 576 measuring points in each. Advanced algorithms for detecting the cornea contours are applied to each image. The measurement starts with the cornea in its natural convex shape. The puff of air forces the cornea inside (*ingoing phase*), going through a time of applanation (*ingoing applanation*) in a concavity phase until it reaches its peak. There is a period of oscillation before starting the output or return phase (*outgoing phase*). The cornea undergoes a second moment of applanation (*outgoing applanation*) until returning to its natural shape. A possible cam motion can occur in this phase of the measurement. The time and pressure in the first and second applanation moments and when the cornea reaches the maximum point of concavity are recorded. The intraocular pressure (IOP) is based on the deformation data. The amplitude of deformation is detected as the largest displacement of the corneal apex on the image corresponding to the moment of greatest concavity. The radius of curvature in the phase of largest concavity, the lengths and the speeds of the cornea during the applanation phases are also recorded. The lowest value of corneal thickness is also available, and is derived from the first horizontal Scheimpflug image.<sup>29</sup>

Preliminary results have shown that IOP has strong and significant influence on the corneal deformation parameters. In a study involving a model of the eye's anterior chamber composed of hydrophilic contact lenses mounted in a sealed water chamber with adjustable pressure, three lenses with known constitution were evaluated under different pressure levels.<sup>58</sup> Each different lens showed different deformation amplitude in the pressure levels evaluated, which were greater (less rigid behavior) with lower pressure levels ( $P < 0.001$ ; Bonferroni *posthoc* test). Interestingly, when evaluated under the same internal pressure, the deformation amplitude demonstrated to be inversely related to the percentage of polymer in the lens composition. However, the thinner lens and with less polymer had an inferior deformation amplitude (more rigid behavior) at higher pressures than the thicker lenses and with more percentage of polymer in lower pressures. Furthermore, the impact of the IOP reduction in the corneal deformation has been well documented in many clinical

situations, particularly a case of pressure-induced keratopathy.<sup>59</sup> Studies comparing normal and keratoconus corneas show statistically significant differences for most of the deformation parameters provided by CorVIS, but with a relatively high overlay between the groups, which limits their diagnostic applications. The combination of parameters using linear discriminant analysis and other techniques of artificial intelligence has been the subject of intense studies by the *Brazilian Study Group of Artificial Intelligence and Corneal Analysis* (BrAIn). For example, the "Corvis Factor 1" was effective to improve the ability to distinguish normal corneal from those with ectasia, including cases of FFKC ( $P < 0.001$ , Kruskal-Wallis test with Dunn's *post-hoc* test). Along with the diagnosis of ectasia, the biomechanical study with the Scheimpflug technology was effective to assess changes after the crosslinking (Roberts, unpublished data, 2011). In the studies conducted at Ohio State University, in the 1st month after the procedure a smaller deformation amplitude ( $P < 0.0014$ ) was recorded. This result is justified by the increased rigidity of the cornea after the procedure.

The integration between the biomechanical and tomographic data demonstrated a significant improvement in identifying much milder forms of ectasia (Figure 5). This has also to be considered when assessing the risk of progression of ectasia and the prognosis of keratoconus. In a study involving 119 eyes with normal corneas and 19 eyes with FFKC, a combined parameter derived from tomography and biomechanical assessments was designed and presented an area under the ROC curve of 0.999. This combined parameter had a sensitivity of 100% and a specificity of 99.2%.<sup>3</sup>

#### Scheimpflug imae in cataract surgery assisted by femtosecond

Cataract surgery assisted by femtosecond laser depends fundamentally on the imaging of the anterior segment to guide the corneal incisions, the curvilinear and continuous capsulorhexis and the fragmentation of cataracts.<sup>33</sup> LENSAR Laser System (LENSAR Inc., Winter Park, USA) incorporates a three-dimensional confocal illumination (3D-CSI) consisting of an advanced transmitter of scanning lighting which increases the accuracy of the three-dimensional reconstruction using the Scheimpflug imaging technique.<sup>60</sup> The system has a lateral (x, y) and longitudinal (z) resolution of less than 10 microns. The ability to determine the position of the anterior and posterior surfaces of the crystalline is increased due to the high-contrast of the optic system on the anatomical edges, which makes the 3D-CSI relatively less sensitive to the dispersion present in higher density cataracts. Additionally, the 3D-CSI provides detailed structural details of cataract, with the potential of automatic classification of their density. Due to the layout of the optical rays, LENSAR can collect biometric data (including rays of anterior and posterior corneal curvature, corneal thickness, anterior chamber depth, anterior and posterior curvature rays of the crystalline and the thickness of the crystalline), also allowing the detection of the crystalline tilt to the optical axis.<sup>60</sup> Other systems available on the market, and in particular LenSx (Alcon Laboratories, Fort Worth, Texas, USA), Catalys (OptiMedica Corp., California, USA) and Victus Technolas (Bausch & Lomb/Technolas Perfect Vision GmbH, Germany) use optical coherence tomography (OCT) to assess the location of the intraocular structures.<sup>33</sup>

## CONCLUSION

The Scheimpflug imaging technique will coexist with other technologies such as OCT and high-frequency ultrasound, but it will have an evolutive role in the area of laser refractive surgery. Continuous advances are expected to strengthen the diagnostic capabilities and surgical planning. Faster computer systems and high-resolution cameras also have a significant role in this evolution. Furthermore, artificial intelligence is of key importance in order to increase the safety and efficacy of customized refractive treatments.

## REFERENCES

1. Wilson SE, Klyce SD. Advances in the analysis of corneal topography. *Surv Ophthalmol*. 1991;35(4):269-77.
2. Wilson SE, Ambrosio R. Computerized corneal topography and its importance to wavefront technology. *Cornea*. 2001;20(5):441-54.
3. Ambrosio R, Jr., Nogueira LP, Caldas DL, et al. Evaluation of corneal shape and biomechanics before LASIK. *Int Ophthalmol Clin*. 2011;51(2):11-38.
4. Ambrosio R, Jr., Tervo T, Wilson SE. LASIK-associated dry eye and neurotrophic epitheliopathy: pathophysiology and strategies for prevention and treatment. *J Refract Surg*. 2008;24(4):396-407.
5. Lin DT, Holland S, Tan JC, Moloney G. Clinical results of topography-based customized ablations in highly aberrated eyes and keratoconus/ectasia with cross-linking. *J Refract Surg*. 2012;28(11):S841-8.
6. Pasquali T and Krueger R. Topography-guided laser refractive surgery. *Curr Opin Ophthalmol*. 2012;23(4):264-8.
7. Ambrosio R, Jr., Jardim D, Netto MV, Wilson SE. Management of unsuccessful LASIK surgery. *Compr Ophthalmol Update*. 2007;8(3):125-41; discussion 143-4. Review.
8. Ambrosio R, Jr., Wilson SE. Complications of laser in situ keratomileusis: etiology, prevention, and treatment. *J Refract Surg*. 2001;17(3):350-79. Review.
9. Packer M, Fine IH, Hoffman RS. Aspheric intraocular lens selection: the evolution of refractive cataract surgery. *Curr Opin Ophthalmol*. 2008;19(1):1-4.
10. Packer M, Fine IH, Hoffman RS. Aspheric intraocular lens selection based on corneal wavefront. *J Refract Surg*. 2009;25(1):12-20.
11. Kanellopoulos AJ, Binder PS. Management of corneal ectasia after LASIK with combined, same-day, topography-guided partial transepithelial PRK and collagen cross-linking: the athens protocol. *J Refract Surg*. 2010;27(5):323-31.
12. Koller T, Iseli HP, Donitzky C, Ing D, Papadopoulos N, Seiler T. Topography-guided surface ablation for forme fruste keratoconus. *Ophthalmology*. 2006;113(12):2198-202.
13. Reinstein DZ, Archer TJ, Gobbe M. Refractive and topographic errors in topography-guided ablation produced by epithelial compensation predicted by 3D Artemis VHF digital ultrasound stromal and epithelial thickness mapping. *J Refract Surg*. 2012;28(9):657-63.
14. Reinstein DZ, Archer TJ, Gobbe M. Combined corneal topography and corneal wavefront data in the treatment of corneal irregularity and refractive error in LASIK or PRK using the Carl Zeiss Meditec MEL 80 and CRS-Master. *J Refract Surg*. 2009;25(6):503-15.
15. Faria-Correia F, Luz A, Ambrósio Jr R. Managing corneal ectasia prior to keratoplasty. *Expert Rev Ophthalmol*. 2015;10(1):33-48.
16. Klyce SD. Computer-assisted corneal topography. High-resolution graphic presentation and analysis of keratoscopy. *Invest Ophthalmol Vis Sci*. 1984;25(12):1426-35.
17. Belin MW, Litoff D, Strods SJ, Winn SS, Smith RS. The PAR Technology Corneal Topography System. *Refract Corneal Surg*. 1992;8(1):88-96.
18. Belin MW, Khachikian SS. An introduction to understanding elevation-based topography: how elevation data are displayed - a review. *Clin Experiment Ophthalmol*. 2009;37(1):14-29.
19. Ambrosio R, Jr., Belin MW. Imaging of the cornea: topography vs tomography. *J Refract Surg*. 2010;26(11):847-9.
20. Maurice DM, Giardini AA. A simple optical apparatus for measuring the corneal thickness, and the average thickness of the human cornea. *Br J Ophthalmol*. 1951;35(3):169-77.
21. Salz JJ, Azen SP, Bernstein J, Caroline P, Villasenor RA, Schanzlin DJ. Evaluation and comparison of sources of variability in the measurement of corneal thickness with ultrasonic and optical pachymeters. *Ophthalmic Surg*. 1983;14(9):750-4.
22. Mandell RB, Polse KA. Keratoconus: spatial variation of corneal thickness as a diagnostic test. *Arch Ophthalmol*. 1969;82(2):182-8.
23. Ambrosio R, Jr. Percentage thickness increase and absolute difference from thinnest to describe thickness profile. *J Refract Surg*. 2010;26(2):84-6; author reply 86-7.
24. Ambrosio R, Jr., Alonso RS, Luz A, Coca Velarde LG. Corneal-thickness spatial profile and corneal-volume distribution: tomographic indices to detect keratoconus. *J Cataract Refract Surg*. 2006;32(11):1851-9.
25. Salomao MQ, Esposito A, Dupps WJ, Jr. Advances in anterior segment imaging and analysis. *Curr Opin Ophthalmol*. 2009;20(4):324-32.
26. Roberts C. Biomechanical customization: the next generation of laser refractive surgery. *J Cataract Refract Surg*. 2005;31(1):2-5.
27. Luce DA. Determining in vivo biomechanical properties of the cornea with an ocular response analyzer. *J Cataract Refract Surg*. 2005;31(1):156-62.
28. Dupps WJ, Jr., Wilson SE. Biomechanics and wound healing in the cornea. *Exp Eye Res*. 2006;83(4):709-20.
29. Ambrosio R, Jr., Ramos I, Luz A, et al. Dynamic Ultra-High Speed Scheimpflug Imaging for assessing corneal biomechanical properties. *Rev Bras Oftalmol*. 2013;72(2):99-102.
30. Dorronsoro C, Pascual D, Perez-Merino P, Kling S, Marcos S. Dynamic OCT measurement of corneal deformation by an air puff in normal and cross-linked corneas. *Biomed Opt Express*. 2012;3(3):473-87.
31. Schumacher S, Fromm M, Oberheide U, Gerten G, Wegener A, Lubatschowski H. In vivo application and imaging of intralenticular femtosecond laser pulses for the restoration of accommodation. *J Refract Surg*. 2008;24(9):991-5.
32. Palanker DV, Blumenkranz MS, Andersen D, et al. Femtosecond laser-assisted cataract surgery with integrated optical coherence tomography. *Sci Transl Med*. 2010;2(58):58ra85.
33. Roberts TV, Lawless M, Chan CC, et al. Femtosecond laser cataract surgery: technology and clinical practice. *Clin Experiment Ophthalmol*. 2013;41(2):180-6.
34. Wegener A, Laser-Junga H. Photography of the anterior eye segment according to Scheimpflug's principle: options and limitations - a review. *Clin Experiment Ophthalmol*. 2009;37(1):144-54.
35. Foo KP, Maclean H. Measured changes in cataract over six months: sensitivity of the Nidek EAS-1000. *Ophthalmic Res*. 1996;28 Suppl 2: 32-6.
36. Wegener A, Hockwin O, Laser H and Strack C. Comparison of the Nidek EAS 1000 system and the Topcon SL-45 in clinical application. *Ophthalmic Res*. 1992;24 Suppl 1:55-62.
37. Baez KA, Orengo S, Gandham S, Spaeth GL. Intraobserver and interobserver reproducibility of the Nidek EAS-1000 Anterior Eye Segment Analysis System. *Ophthalmic Surg*. 1992;23(6):426-8.
38. Cairns G, McGhee CN, Collins MJ, Owens Hand Gamble GD. Accuracy of Orbscan II slit-scanning elevation topography. *J Cataract Refract Surg*. 2002;28(12):2181-7.
39. Cairns G, McGhee CN. Orbscan computerized topography: attributes, applications, and limitations. *J Cataract Refract Surg*. 2005;31(1):205-20.
40. Kim H, Joo CK. Measure of keratoconus progression using Orbscan II. *J Refract Surg*. 2008;24(6):600-5.
41. Aufarth GU, Tetz MR, Biazid Y, Volcker HE. Measuring anterior chamber depth with Orbscan Topography System. *J Cataract Refract Surg*. 1997;23(9):1351-5.
42. Aufarth GU, Wang L, Volcker HE. Keratoconus evaluation using the Orbscan Topography System. *J Cataract Refract Surg*. 2000;26(2):222-8.
43. Belin MW and Khachikian SS. New devices and clinical implications for measuring corneal thickness. *Clin Experiment Ophthalmol*. 2006;34(8):729-31.
44. Belin MW, Khachikian SS, McGhee CN, Patel D. New technology in corneal imaging. *Int Ophthalmol Clin*. 2010;50(3):177-89.
45. Aptel F, Chiquet C, Beccat S, Denis P. Biometric evaluation of anterior chamber changes after physiologic pupil dilation using Pentacam and anterior segment optical coherence tomography. *Invest Ophthalmol Vis Sci*. 2012;53(7):4005-10.
46. Rao SN, Raviv T, Majmudar PA, Epstein RJ. Role of Orbscan II in screening keratoconus suspects before refractive corneal surgery. *Ophthalmology*. 2002;109(9):1642-6.
47. Lim L, Wei RH, Chan WK, Tan DT. Evaluation of keratoconus in Asians: role of Orbscan II and Tomey TMS-2 corneal topography. *Am J Ophthalmol*. 2007;143(3):390-400.
48. Belin MW, Asota IM, Ambrosio R, Jr., Khachikian SS. What's in a name: keratoconus, pellucid marginal degeneration, and related thinning disorders. *Am J Ophthalmol*. 2011;152(2):157-62 e1.
49. Tummanapalli SS, Maseedupally V, Mandathara P, Rathi VM, Sangwan VS. Evaluation of corneal elevation and thickness indices in pellucid marginal degeneration and keratoconus. *J Cataract Refract Surg*. 2013;39(1):56-65.
50. Faria-Correia F, Ramos IC, Lopes B, et al. Topometric and Tomographic Indices for the Diagnosis of Keratoconus. *Int J Kerat Ect Cor Dis*. 2012;1(2):92-9.
51. Luz A, Ursulio M, Castaneda D, Ambrosio R, Jr. [Corneal thickness progression from the thinnest point to the limbus: study based on a normal and a keratoconus population to create reference values]. *Arq Bras Oftalmol*. 2006;69(4):579-83. Portuguese
52. Ambrosio R, Jr., Caiado AL, Guerra FP, et al. Novel pachymetric parameters based on corneal tomography for diagnosing keratoconus. *J Refract Surg*. 2011;27(10):753-8.
53. Bühren J, Kook D, Yoon G, Kohner T. Detection of subclinical keratoconus by using corneal anterior and posterior surface aberrations and thickness spatial profiles. *Invest Ophthalmol Vis Sci*. 2010;51(7):3424-32.
54. Saad A, Gatinel D. Topographic and tomographic properties of forme fruste keratoconus corneas. *Invest Ophthalmol Vis Sci*. 2010;51(11):5546-55.
55. Ambrosio R, Jr., Dawson DG, Salomao M, Guerra FP, Caiado AL, Belin MW. Corneal ectasia after LASIK despite low preoperative risk: tomographic and biomechanical findings in the unoperated, stable, fellow eye. *J Refract Surg*. 2010;26(11):906-11.
56. Klyce SD. Chasing the suspect keratoconus. *Br J Ophthalmol*. 2009;93(7):845-7.
57. Ambrosio R, Jr., Valbon BF, Faria-Correia F, Ramos I, Luz A. Scheimpflug imaging for laser refractive surgery. *Curr Opin Ophthalmol*. 2013;24(4):310-20.
58. Correia FF, Ramos I, Roberts CJ, Steinmueller A, Krug M, Ambrosio R, Jr. Impact of chamber pressure and material properties on the deformation response of corneal models measured by dynamic ultra-high-speed Scheimpflug imaging. *Arq Bras Oftalmol*. 2013;76(5):278-81.
59. Faria-Correia F, Ramos I, Valbon B, Luz A, Roberts CJ, Ambrosio R, Jr. Scheimpflug-based tomography and biomechanical assessment in pressure-induced stromal keratopathy. *J Refract Surg*. 2013;29(5):356-8.
60. Packer M, Klyce SD, Smith C. The LENSAR Laser System-3D for Femtosecond Cataract Surgery. *US Ophthalmic Review*. 2014;7(2):89-94.

## Corresponding author:

Renato Ambrósio Jr, MD, PhD - Instituto de Olhos Renato Ambrósio  
Rua Conde de Bonfim 211 / 712 - 20520 - 050

Phone: 55 21 2234-4233

E-mail: dr.renatoambrosio@gmail.com

### 2.4.3.2 – Pentacam® HR imaging system

The Pentacam® (Oculus, Wetzlar, Germany), the first system that performed corneal and anterior segment tomography by digital rotating Scheimpflug photography, was first presented in 1999 (Figure 31). (Ambrósio & Belin, 2010; Ambrósio *et al.*, 2013; Wegener & Laser-Junga, 2009)



Figure 31 – Pentacam® system (Oculus, Wetzlar, Germany).

Compared to previous Scheimpflug cameras, the rotational measurement has a common center that makes image registration more accurate. The scan only takes a maximum of 2 seconds and uses visible blue light (475 nm). Any eye movement is detected by a second camera and corrected by ray-tracing algorithms. The Pentacam® calculates a three-dimensional (3D) model of the anterior eye segment from 138.000 distinct elevation points (Figure 32). (Ambrósio & Belin, 2010; Ambrósio *et al.*, 2013)

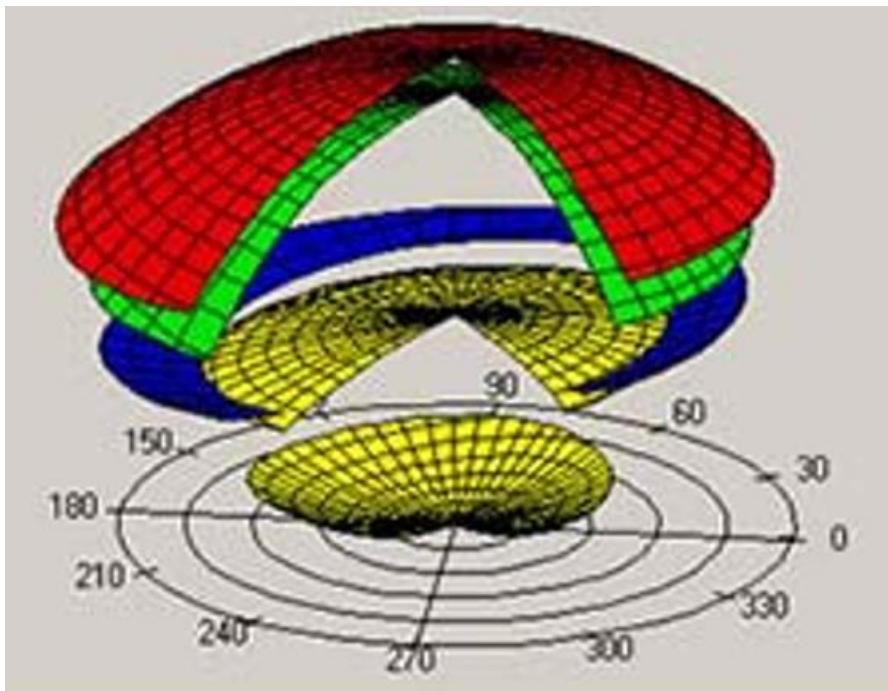


Figure 32 – Three-dimensional eye model provided by the Pentacam® system.

The three-dimensional Scheimpflug image scanning provides detailed data regarding the topography, elevation and pachymetry of the cornea, the depth, angle, and volume of the anterior chamber, and optical density evaluation of the crystalline lens.(Ambrósio & Belin, 2010; Ambrósio *et al.*, 2013)

#### 2.4.3.3 – Lens densitometry software

The Pentacam system can measure the optical density based on the Scheimpflug images analysis.(Handzel *et al.*, 2014; Wegener & Laser-Junga, 2009; Ambrósio *et al.*, 2013; Kirkwood *et al.*, 2009; Weiner *et al.*, 2014) Using blue light illumination, the evaluation of the lens density is based on light scattering.(Handzel *et al.*, 2014; Kirkwood *et al.*, 2009; Weiner *et al.*, 2014) This system evaluates the difference of transmitted and measured lights, providing a value of the optical density on a scale from 0 to 100 points (based on a gray scale).(Kirkwood *et al.*, 2009; Weiner *et al.*, 2014) The Pentacam system also offers objective and distinct densitometric analysis algorithms. The software enables a manual analysis that provides a densitometric assessment in a specific Scheimpflug image (two dimensions analysis), such as the peak, linear and region of interest (ROI) modes. The peak mode (Figure 33) is based on the analysis of a densitometry graph, which measures the optical density from the

anterior surface of the cornea to the posterior lens capsule.(Ortiz *et al.*, 2008)  
This mode only provides the maximum optical density in the region where the cursor is placed in the Scheimpflug image.

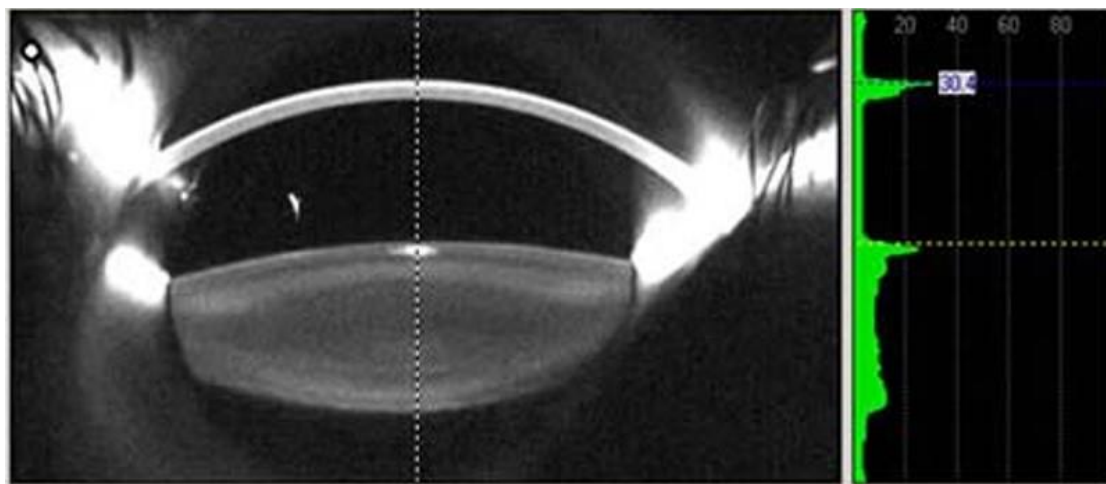


Figure 33 – Peak mode lens densitometry analysis.

The linear mode (Figure 34) evaluates the density of a line manually drawn, and the ROI mode (Figure 34) enables densitometry values inside for a customized drawn area. Both modes provide average density, maximum density, and standard deviation parameters.(Kirkwood *et al.*, 2009; Weiner *et al.*, 2014)

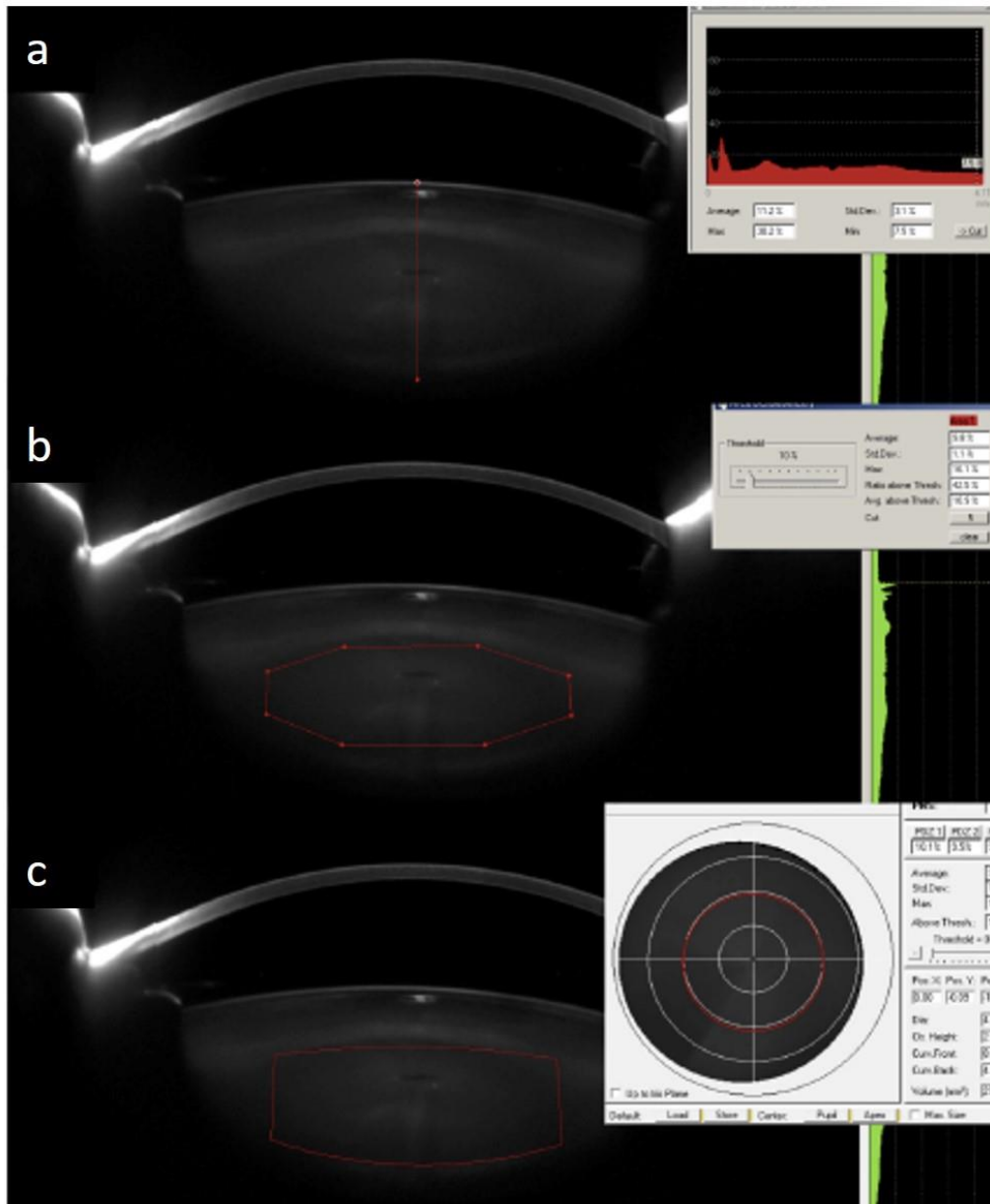


Figure 34 – Linear mode (a), region of interest (ROI) mode (b) and three-dimensional mode (c) lens densitometry analysis.

The 3D mode (Figure 34), also known as Pentacam Nuclear Staging (PNS), automatically generates a cylindrical template for the density measurement. This template can also be customized regarding its position, diameter, height, front and back curvatures. In addition to providing the same metrics as the linear and ROI modes, it also displays a degree of cataract on a scale of 0 to 5, based on the value of the optical density of the lens nucleus. (Kirkwood *et al.*, 2009; Weiner *et al.*, 2014; Nixon, 2010)

#### **2.4.3.4 – Scheimpflug-based lens densitometry in patients with age-related nuclear cataracts**

Precise quantification of the lens density was always considered to be a crucial parameter in studies involving cataracts. The subjectivity of the assessments of the crystalline lens opacity was an issue for the methodology of research in this field.(Kirkwood *et al.*, 2009; Weiner *et al.*, 2014) Despite the classification systems, such as LOCS III grading scale, helped to improve the evaluation of different types of age-related cataracts, studies have shown that these approaches are also subject to inter and intra-individual variability.(Grewal *et al.*, 2009; Gupta *et al.*, 2013; Kim *et al.*, 2009; Pei *et al.*, 2008) Since its introduction, Scheimpflug imaging enabled objective lens density measurements. Scheimpflug devices, as the Pentacam system, demonstrated to be a validated and repeatable lens densitometry method.(Kirkwood *et al.*, 2009; Weiner *et al.*, 2014) Different densitometric modes presented a significant correlation with visual acuity and LOCS III classification in age-related nuclear cataracts.(Datiles *et al.*, 1995; Grewal *et al.*, 2009; Gupta *et al.*, 2013; Pei *et al.*, 2008; Magno, Freidlin, *et al.*, 1994; Magno, Lasa, *et al.*, 1994) Based on the limited number of research studies, the relationship between the wavefront analysis and objective Scheimpflug-based lens densitometry is not yet studied thoroughly. As the wavefront analysis can detect changes in the crystalline lens even before a noticeable reduction in visual acuity, the study of its relationship with lens densitometry is interesting towards the detection of early forms of cataract by Scheimpflug-based densitometry.



### 3 – Cataract surgery

#### 3.1 – Brief historical background

Cataract surgery consists of the removal of the crystalline lens that has developed an opacification. The decrease in visual acuity, glare due to ocular scattering and degradation of contrast sensitivity are the major indications for cataract surgery. In the same procedure and following the surgical removal of the opaque lens, the surgeon implants an artificial intraocular lens inside the capsular bag. Despite being a procedure considered one of the safest and with high success rates worldwide, this technique suffered modifications and innovations over the centuries that allowed reaching this level of excellence.

The earliest form of cataract surgery was designated by 'couching' and was used for the first time in India (Figure 35). The first descriptions related to this technique date the third century BC and were written by the Indian physician Susruta. (Mukhopadhyay & Sharma, 1992)

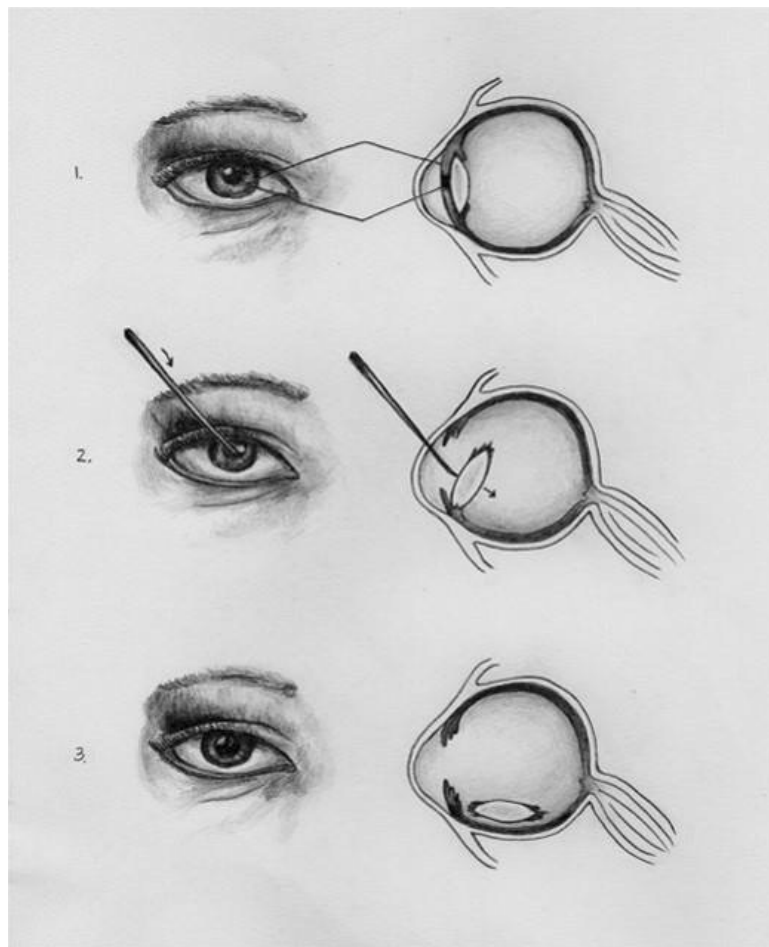


Figure 35 – Couching technique. The surgeon used a curved needle to dislodge the cataract through a corneal or scleral incision. (Lorente & Mendicute, 2008)

The use of this surgical procedure was widespread in the Roman Empire, Middle Age Europe and Africa. The surgery used a curved needle to dislodge the opaque lens, which was thought to be in the middle of the eye globe, through corneal or scleral incision. By pushing the cataract downwards, the light would be enabled to enter the eye. Due to several reasons, including the nonsterilized and rudimentary material and postoperative inflammation, this technique was associated with a high rate of complications, such as endophthalmitis, hyphema, retinal detachment and optic atrophy.(Nieves-Moreno *et al.*, 2015a)

In 1748, Jacques Daviel was the first European physician to extract cataracts from the eye successfully. Based on new anatomical concepts, Daviel developed and revolutionized the surgical technique. Instead of displacing the cataract, these improvements enabled a more accurate and safer surgery by removing the opaque lens. The knowledge introduced by Daviel represented the beginning of the extracapsular cataract extraction. After performing a semicircular corneal incision, the cataract was removed by expression through a circular opening in the anterior lens capsule (Figure 36).(Obuchowska & Mariak, 2005; Daviel, 1967)



Figure 36 – Daviel's extracapsular cataract extraction technique.(Bobrow *et al.*, 2014)

Although this new approach has attained a relative preservation of the anterior segment anatomy, complications were also reported, including wound healing problems, inflammation, endophthalmitis, vitreous loss, retinal detachment and choroid detachment.(Nieves-Moreno *et al.*, 2015a)

In 1753, Samuel Sharp was the first physician to perform an intracapsular cataract extraction successfully. Regarding this procedure, the cataract was removed inside its capsular bag, through a limbal incision. There were different surgical instruments to manipulate the cataract by breaking the zonules.(Thorpe, 1959; Callahan, 1967; Nieves-Moreno *et al.*, 2015b)

Scientific developments, such as the use of sterilized, suture material and operating microscopes, helped to improve the surgical outcomes and to reduce the complications rate. Concerning the intracapsular cataract extraction technique, a cryoprobe was introduced to enable the lens extraction by a cooling mechanism with nitrous oxide.(Krwawicz, 1963; Krwawicz, 1961) After applying the probe to the lens surface, the freezing mechanisms made the cataract adherent to the probe. Using front and back maneuvers with the cryoprobe, the cataract was released from the zonules and vitreous gel.(Krwawicz, 1963; Krwawicz, 1961) The trend for the extracapsular cataract extraction was related to its advantages compared to the intracapsular technique, such as the smaller surgical incision needed and the preservation of the capsular bag.(Jaffe, 1996; Roper, 1954) New instruments, such as the cystitome to open the anterior capsule and cannulas to aspirate the lens material from the chamber, improved the overall outcomes of the extracapsular cataract extraction.(Nieves-Moreno *et al.*, 2015a; Nieves-Moreno *et al.*, 2015b; Jaffe, 1996)

In 1967, Charles Kelman developed the phacoemulsification technique for cataract removal that uses a tip driven by ultrasounds (Figure 37).(Kelman, 1969; Kelman, 1967)

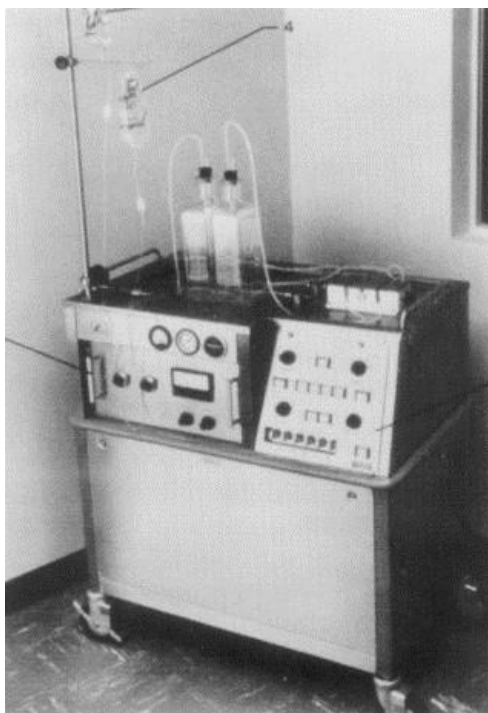


Figure 37 – First phacoemulsification machine.(Ming, 2013)

After prolapsing the cataract into the anterior chamber through a circular opening in the anterior capsule, the phaco tip was used to fragment and emulsify the nucleus of the cataract. After this step, the remaining cortical material was removed by using an aspiration system.(Kelman, 1979; Kelman, 1970) Compared to extracapsular extraction, this surgical approach presented several advantages, including the smaller size of the corneal incision, lesser wound-related complications, and faster visual rehabilitation. Since phacoemulsification is performed in a closed anterior chamber, the incidence of complications associated with the posterior segment tended to occur in a less number.(Nieves-Moreno *et al.*, 2015b; Jaffe, 1996) Corneal endothelium damage was a common issue described in the early stages of phacoemulsification and was attributed to the small distance between the posterior surface of the cornea and the phaco tip. With the advent of ophthalmic viscosurgical devices, there was a reduction in the incidence of this complication.(Nieves-Moreno *et al.*, 2015b; Jaffe, 1996) Moreover, the management of harder cataract was correlated with more surgical manipulation and greater energy dissipation from the phaco tip, which might contribute to endothelial injury.(Nieves-Moreno *et al.*, 2015b; Jaffe, 1996) As mentioned before, the main goal of cataract surgery is to restore the transparency of ocular media, to improve visual acuity and contrast sensitivity. In

such a way to functionally replace the crystalline lens, an intraocular lens is inserted in the eye after the nucleus and cortex aspiration. In 1949, Harold Ridley introduced the concept of intraocular lens (IOL) implantation. He noticed that adding this surgical step would allow more efficient and faster visual rehabilitation after cataract surgery. At that point, the corneal incision was enlarged to 5-mm to 7-mm to insert an anterior chamber or a posterior chamber IOLs, which were made of polymethylmethacrylate. (Ridley, 1956; Ridley, 1953; Ridley, 1952) After the implantation, a suture was needed to close the corneal incision. In the early 1980s, Thomas R. Mazzocco presented the first foldable IOL made of silicone, also known as the “Mazzocco taco”. Subsequently, other foldable IOLs made of silicone or acrylic became available. By permitting to keep a small incision (1.8 mm – 3.2 mm), the implantation of a foldable IOL is currently considered the state-of-the-art procedure. (Colvard *et al.*, 1983; Kratz *et al.*, 1981; Mazzocco *et al.*, 1981) Figure 38 illustrates the current technique for cataract extraction: phacoemulsification combined with IOL implantation by clear corneal incision.

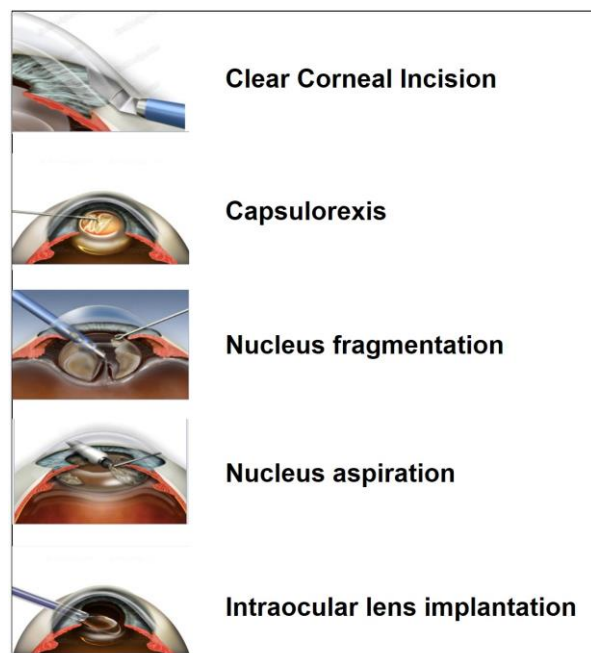


Figure 38 – Cataract extraction by phacoemulsification combined with IOL implantation.

Currently, cataract surgery is the most performed surgical procedure worldwide (approximately 22 million interventions per year). In Portugal, about 75,000 cataract surgeries are performed each year. Due to the technological and safety evolution of this procedure associated with the aging of the population, it is

estimated that the number of surgeries will increase in the next decades.(Mertens, 2015)

### 3.2 – Nucleus management techniques in phacoemulsification

Over the past decades, distinct nucleus management approaches were described, including the “divide and conquer” technique and several “chopping” techniques.(Park *et al.*, 2013; Mierzejewski *et al.*, 2004; Friedman *et al.*, 2002; Vasavada & Desai, 1996; Koch & Katzen, 1994; Gimbel, 1991; Shepherd, 1990) Concerning the latter, the “stop and chop” technique will be described considering the purpose of the present thesis. They are designated by chopping techniques, since they are similar to chopping wood by a lumberjack. This concept can be applied to the crystalline lens, because it has its cleavage planes, which follows the direction of the lens fibers from equator to equator through the center of the lens nucleus. These techniques use the phaco tip to stabilize the nucleus, and a second surgical instrument (designated by chopper) to fracture and pull apart fragments of the cataract.(Chang, 1999; Vasavada & Singh, 1998)

“Stop and chop” (Figure 39) is a derived from the “horizontal chop” technique, in which the nucleus is divided into two fragments before chopping begins. In a similar pattern as in the initial step of the “divide and conquer”, a central groove is created through the lens nucleus with the phaco tip.(Koch & Katzen, 1994)

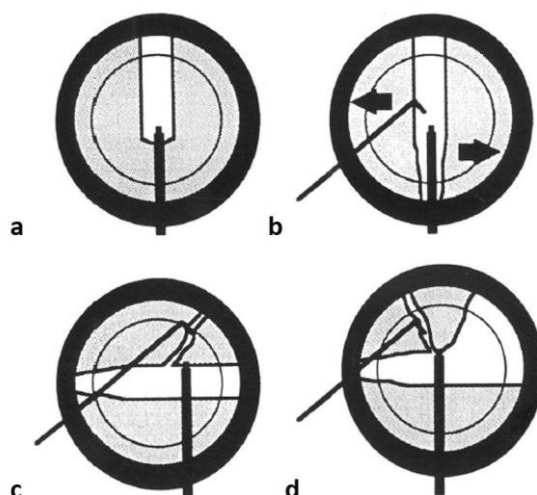


Figure 39 – “Stop and Chop” Technique: a) Sculpting a central groove in the middle of the cataract; b) After sculpting is complete, the nucleus is fractured into halves with the phaco tip and the chopper; c) The phaco tip is driven into the nuclear half about a third of the way across from the right to left. The chopper is buried in the periphery of the nucleus and pulled toward the phaco tip. When the instruments are close to each other, they are separated, and a small segment of nucleus is chopped off and emulsified. d) This sequence is repeated for the remaining nucleus.

(Koch & Katzen, 1994)

This first step provides space for later manipulation. The chopper and phaco tip are placed together in the deep groove and then separated to fracture the nucleus into two halves. Each half is then held in position with the phaco tip, by using relatively high vacuum. Subsequently, the chopper is passed under the distal edge of the anterior capsulotomy and around the lens equator. The tip of the chopper is then drawn through the lens nucleus toward the phaco tip in the horizontal plane. The phaco tip and chopper are then separated laterally, fracturing the fragment into smaller pieces. The nucleus is then rotated 90 degrees, and the same procedure is performed on each of the lens halves. The nucleus is broken into four or more pieces, depending on the density of the lens, and are emulsified and aspirated by the phaco tip.(Koch & Katzen, 1994) Compared to other chopping techniques, “stop and chop” likely will use more ultrasound (US) energy.(Park *et al.*, 2013) Nevertheless, “stop and chop” technique provides more maneuvering room, which is essential to remove the first nuclear fragment in easier way. As the outward force on the capsular bag is also reduced, this approach is considered a safe technique.(Mierzejewski *et al.*, 2004; Park *et al.*, 2013; Storr-Paulsen *et al.*, 2008)

### **3.3 – Scheimpflug-based lens densitometry and its relationship with phacodynamics**

Previous research studies described the correlation between Scheimpflug-based lens densitometry and phacodynamics parameters, such as US energy delivered or cumulative dissipative energy (CDE).(Kim *et al.*, 2009; Lim *et al.*, 2014; Nixon, 2010; Gupta *et al.*, 2013) As the LOCS III system, the Scheimpflug-based densitometry also proved to be a predictor of intraoperative complications, such as posterior capsule rupture.(Gupta *et al.*, 2011; Davison & Chylack, 2003) Different phacoemulsification techniques and densitometric evaluation modes used in previous studies compromise the extrapolation of results and conclusions for clinical application.(Weiner *et al.*, 2014) As the hardness of the lens opacity is correlated with a higher ultrasonic energy used during surgery, the selection of the most appropriate densitometry mode and parameter might be essential for a more accurate preoperative evaluation and planning.

#### **4 - Purposes**

1 - To test correlations between Scheimpflug optical densitometry and ocular HOAs in patients with mild nuclear cataract.

2 - To describe the Dysfunctional Lens Index (DLI) from ray-tracing aberrometry and to test its relationship with corrected distance visual acuity (CDVA) and lens grading based on the LOCS III and the Scheimpflug-based lens density.

3 - To evaluate the correlations between preoperative Scheimpflug-based lens densitometry metrics and phacodynamics.

4 – To analyze the relationship between objective metrics for quantifying crystalline lens dysfunction with visual impairment and phacodynamics parameters in patients with age-related nuclear cataract.



## **CHAPTER II**

RELATIONSHIP BETWEEN SCHEIMPFLUG OPTICAL  
DENSITOMETRY AND OCULAR HOAS IN PATIENTS  
WITH MILD NUCLEAR CATARACT



ARTICLE

# Scheimpflug lens densitometry and ocular wavefront aberrations in patients with mild nuclear cataract



Fernando Faria-Correia, MD, Bernardo Lopes, MD, Tiago Monteiro, MD,  
Nuno Franqueira, MD, Renato Ambrósio Jr, MD, PhD

**PURPOSE:** To test correlations between Scheimpflug optical densitometry and ocular higher-order aberrations (HOAs) in patients with mild nuclear cataract.

**SETTING:** Cornea and Refractive Surgery Department, Hospital de Braga, Braga, Portugal.

**DESIGN:** Retrospective single-center study.

**METHODS:** In eyes with mild nuclear cataract, lens densitometry was evaluated by Scheimpflug imaging (Pentacam HR), which provided an objective quantification (mean density and maximum density) and grading (nuclear staging score) of the crystalline lens. A visual function analyzer that combines ray-tracing aberrometry and Placido disk-based topography (iTrace) was used to evaluate the total ocular and internal HOAs.

**RESULTS:** The study comprised 40 eyes of 30 patients. The mean density of the lens nucleus was  $8.99\% \pm 0.76\%$  (SD) (range 7.5% to 10.8%), and the mean maximum density was  $27.96\% \pm 6.97\%$  (range 16.9% to 56.1%). Regarding the score of nuclear staging of the Scheimpflug device, 28 eyes had level 0 and 12 eyes had level 1. Significant positive correlations were found between the mean density and maximum density parameters and the internal HOAs ( $\rho = 0.661$ ,  $P < .001$  and  $\rho = 0.570$ ,  $P < .001$ , respectively).

**CONCLUSIONS:** There were significant correlations between the quantification parameters derived from Scheimpflug lens densitometry and ocular HOAs. The integration of these technologies can help in clinical decision making and in understanding the subjective symptoms of patients with mild nuclear cataracts.

**Financial Disclosure:** Dr. Ambrósio is a consultant to Oculus Optikgeräte GmbH, Alcon Surgical, Inc., and Carl Zeiss Meditec AG. None of the other authors has a financial or proprietary interest in any material or method mentioned.

*J Cataract Refract Surg* 2016; 42:405–411 © 2016 ASCRS and ESCRS

Opacification of the crystalline lens is a commonly observed age-related process that contributes to the degradation of visual acuity and contrast sensitivity.<sup>1,2</sup> The clinical method most commonly used to assess crystalline lens opacification is the Lens Opacities Classification System III (LOCS III).<sup>3</sup> This score system is based on slitlamp biomicroscopy and was validated in 1993.<sup>4,5</sup> Scheimpflug systems objectively measure lens density and might assist phacodynamics in cataract surgery.<sup>6–9</sup> Various methods for the measurement of lens optical densitometry have been

used; however, there is still no consensus regarding this topic.<sup>10</sup>

Other diagnostic devices, such as wavefront analyzers, can objectively assess higher-order aberrations (HOAs) of the optical system.<sup>2,11,12</sup> This technology also has shown to be useful for the evaluation of patients with different grades of cataract because HOAs play an essential role in the reduction in optical performance in these patients.<sup>13–15</sup> The present study evaluated the relationship between Scheimpflug lens densitometry and ocular

HOAs in patients with mild grades of nuclear cataract.

## PATIENTS AND METHODS

This retrospective single-center study evaluated patients who were recruited for a clinical visit in the Cornea and Refractive Surgery Department, Hospital de Braga, Braga, Portugal, from October 2014 to February 2015. The study was approved by the institutional review board and complied with the tenets of the Declaration of Helsinki of the World Medical Association.

No patient had a history of ocular disease, ocular surgery, or general disorders affecting vision, such as diabetic retinopathy or uveitis. Exclusion criteria included poor mydriasis, corneal opacities, LOCS III nuclear cataract grade greater than 4.0, and cortical opacities.

All patients had a complete ophthalmic examination that included logMAR corrected distance visual acuity (CDVA), noncontact tonometry, slitlamp biomicroscopy, and dilated fundus evaluation. The nuclear sclerotic grade was classified according to the LOCS III.<sup>3</sup> The same ophthalmologist examined all patients using a slitlamp microscope after pupil dilation attained using a combination of topical tropicamide 1.0% and phenylephrine 10.0%. The LOCS III nuclear opacity was graded on a scale of 0.1 to 6.9 by comparing a digital photograph of each lens with standard color photographic transparencies of nuclear opalescence (NO).

## Scheimpflug System Measurement

The Pentacam HR (Oculus Optikgeräte GmbH) is a Scheimpflug-based device that generates a 3-dimensional representation of the anterior segment of the eye. In fewer than 2 seconds, the rotating camera captures up to 25 slit images of the anterior segment, collecting 25 000 true elevation datapoints. Three measurements of each eye were taken in a dark room. The nuclear staging software of the Scheimpflug device permits the determination of objective crystalline lens densitometry. The software measures the optical density inside a cylindrical template volume of the lens (Figure 1). The template volume used for the cataract analysis was the standardized model provided by the automatic mode (diameter 4.0 mm, height 3.0 mm, front curvature 8.0 mm, back curvature 6.0 mm), which corresponds to 34.9 mm<sup>3</sup> for

densitometric analysis. It enables objective quantification of lens opacities inside the template (mean density and maximum density parameters) on a continuous scale from 0% to 100%. The software also provides a lens opacity grade (nuclear staging score of the Scheimpflug device) on a scale from 0 to 5.

## Wavefront Measurement

The iTrace device (Tracey Technologies) was used for the wavefront analysis. Three measurements of each eye were taken in a dark room. This wavefront analyzer integrates an aberrometer with corneal topography. The aberrometer uses the ray-tracing principle, which sequentially projects 256 near-infrared laser beams into the eye in a specific scanning pattern. Topographies were captured using the Placido-based corneal topographer (Eyesys Vision, Inc.) mounted on the same device. The corneal aberrations were calculated based on topography data, and the internal aberrations were calculated by subtracting the corneal aberrations from those of the entire eye measured by the ray-tracing aberrometer using the built-in program.

## Data and Statistical Analysis

An experienced rater reviewed the Scheimpflug and wavefront analyzer scans. The best-quality scan of the 3 measurements from each device was selected for further analysis. Regarding the lens assessment by Scheimpflug imaging, scans with artifacts that would interfere with the densitometry results (eg, the presence of cortical shadowing artifacts or misplacement of the reference template) were excluded. The mean density and maximum density values were registered. The nuclear staging score of the Scheimpflug device was also noted. The wavefront scans were checked regarding the centration of the measurement with the visual axis of the eye. For statistical analysis, the examiner selected only eyes in which the total wavefront map showed greater resemblance to the internal optics map. The wavefront was measured in a 6.0 mm optical zone set by the software. The following data of the total ocular and internal optics were registered: coma, spherical aberration, trefoil, and the root mean square (RMS) of HOAs from 3rd- to 5th-order Zernike coefficients.

All results were analyzed using Medcalc statistical software (version 14.12.0, Medcalc Software). Values are presented as the mean  $\pm$  SD. Data normality was assessed using the Kolmogorov-Smirnov test. Statistically significant correlations were evaluated using Pearson or Spearman correlation coefficients according to the normality of data. A *P* value of 0.05 or less was considered statistically significant. However, because of the large number of comparisons (32 for both wavefront and cataract grading methods), the Bonferroni adjustment was used to lower the possibility of a statistically significant difference based on chance alone. The significance level was divided by the number of comparisons (32) using the Bonferroni adjustment. Thus, the *P* value had to be less than 0.0016 to be considered statistically significant.

## RESULTS

Forty eyes of 30 patients (17 women, 13 men) were enrolled in the analysis. Table 1 shows the patients' characteristics.

The RMS HOAs in the internal optics were higher than those in the entire eye. Coma was the

Submitted: March 31, 2015.

Final revision submitted: October 4, 2015.

Accepted: October 7, 2015.

From the Cornea and Refractive Surgery Department (Faria-Correia, Monteiro, Franqueira), Hospital de Braga, and the Life and Health Sciences Research Institute (ICVS) (Faria-Correia, Monteiro), School of Health Sciences, University of Minho, Braga, and the ICVS/3B's-PT Government Associate Laboratory (Faria-Correia), Braga/Guimarães, Portugal; the Rio de Janeiro Corneal Tomography and Biomechanics Study Group (Faria-Correia, Lopes, Ambrósio), Instituto de Olhos Renato Ambrósio (Lopes, Ambrósio), and VisareRio (Ambrósio), Rio de Janeiro, and the Federal University of São Paulo (Ambrósio), São Paulo, Brazil.

Corresponding author: Fernando Faria-Correia, MD, Avenida de Bessa, Edifício Boapor II, 216, 7° Frente, 4100-012 Porto, Portugal. E-mail: f.faria.correia@gmail.com.

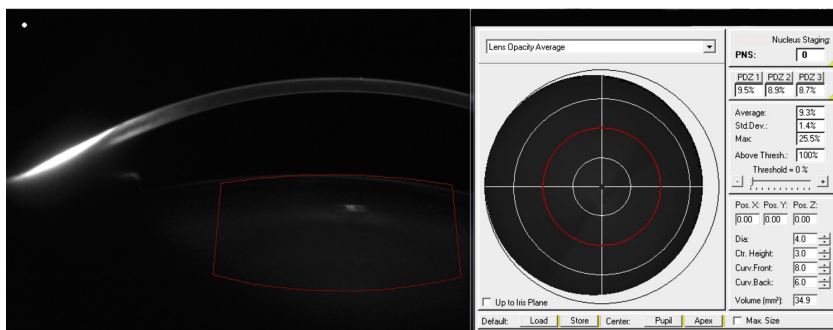


**Figure 1.** The nuclear staging software of the Scheimpflug device measures the lens optical density inside a cylindrical template. Although the grading system has a 0 score, the mean density is 9.3% and the maximum density is 25.5%.

predominant HOA in the total ocular and internal optics. Table 2 shows the mean total ocular and internal HOA values with a 6.0 mm optical zone.

Age was positively correlated with the LOCS III NO score ( $\rho = 0.364, P = .023$ ), nuclear staging of the Scheimpflug device ( $\rho = 0.518, P = .001$ ), mean density ( $r = 0.767, P < .001$ ), and maximum density ( $r = 0.401, P = .010$ ).

The CDVA was correlated with the LOCS III NO score ( $\rho = 0.339, P = .034$ ) and with the nuclear staging of the Scheimpflug device ( $\rho = 0.453, P = .005$ ). Regarding the densitometric variables, the CDVA had a stronger relationship with the mean density ( $r = 0.744, P < .001$ ) than the maximum density ( $r = 0.408, P = .003$ ).

Table 3 shows the correlation coefficients between wavefront data and the different methods of cataract assessment. As shown in Figure 2, the internal RMS HOAs had a positive linear correlation with mean density ( $\rho = 0.661, P < .001$ ) and with maximum density ( $\rho = 0.570, P < .001$ ). Figure 3 shows the relationship of the average density and maximum density variables with the individual HOAs in the internal optics. Only trefoil had a statistically significant correlation with the average density ( $r = 0.657, P < .001$ ). Coma ( $r = 0.649, P < .001$ ) and trefoil aberrations ( $r = 0.536, P = .001$ ) had a statistically significant correlation with the maximum density.

**DISCUSSION**

In this study, ocular wavefront and lens densitometry were analyzed in eyes with mild nuclear cataract. Although the LOCS III is the most widely used grading system, there are concerns about its reproducibility.<sup>16-18</sup> Objective cataract quantification is essential for patient education and to predict phacodynamics.<sup>6,7,9</sup> Scheimpflug imaging enables objective lens densitometry evaluation that is not susceptible to observer variability and is considered to be a more sensitive and repeatable approach.<sup>8,10</sup> Wavefront analysis objectively evaluates the visual deterioration by quantifying the HOAs of the ocular optical system. In our study, we used a ray-tracing aberrometer (iTrace) that has known advantages over Hartmann-Shack and other types of wavefront sensors.<sup>19</sup>

Previous studies<sup>17,20</sup> showed that nuclear sclerosis is an age-related process, contributing to vision deterioration and lens optical densitometry changes. Our results are in accordance with these findings because the subjective (LOCS III NO score) and objective (Scheimpflug [Pentacam] nuclear staging score, mean density, and maximum density) lens evaluations yielded the same relationship with age and CDVA.

Concerning wavefront analysis, we focused on the main HOAs, including coma, spherical aberration,

**Table 1.** Demographic data.

Parameter	Mean ± SD	Range
Age (y)	65.65 ± 11.60	44, 86
CDVA (logMAR)	0.15 ± 0.13	0.0, 0.4
LOCS III NO score	2.42 ± 0.61	1, 3
NS score	0.30 ± 0.47	0, 1
Average density (%)	8.99 ± 0.76	7.5, 10.8
Maximum density (%)	22.96 ± 6.97	16.9, 56.1

CDVA = corrected distance visual acuity; LOCS III NO = Lens Opacities Classification System III nuclear opalescence; NS = nuclear staging of the Scheimpflug device

**Table 2.** Root mean square of HOAs, coma, trefoil, and spherical aberration.

Parameter (µm)	Mean ± SD	Range
Total ocular HOAs	0.23 ± 0.11	0.09, 0.55
Total ocular spherical aberration	0.04 ± 0.10	-0.36, 0.19
Total ocular coma	0.13 ± 0.08	0.03, 0.40
Total ocular trefoil	0.12 ± 0.09	0.02, 0.38
Internal HOAs	0.25 ± 0.15	0.07, 0.63
Internal spherical aberration	-0.02 ± 0.10	-0.38, 0.20
Internal coma	0.12 ± 0.10	0.01, 0.40
Internal trefoil	0.10 ± 0.09	0.01, 0.34

HOAs = higher-order aberrations

**Table 3.** Correlation coefficients between the total ocular and internal aberrations and between the LOCS III NO score and the 3-dimensional densitometric parameters.

Parameter	Nuclear Opalescence		NS		Average Densitometry		Maximum Densitometry	
	Correlation Coefficient*	P Value	Correlation Coefficient*	P Value	Correlation Coefficient	P Value	Correlation Coefficient	P Value
Total ocular HOAs	0.427	.008	0.383	.017	0.582*	.001	0.626*	<.001
Total ocular spherical aberration	-0.131	.413	-0.175	.275	-0.327	.040	-0.325	.041
Total ocular coma	0.236	.141	0.279	.082	0.481	.002	0.607	<.001
Total ocular trefoil	0.359	.025	0.267	.095	0.491	.001	0.626	<.001
Internal HOAs	0.454	.005	0.421	.009	0.661*	<.001	0.570*	<.001
Internal spherical aberration	-0.239	.136	-0.300	.061	-0.398	.011	-0.412	.008
Internal coma	0.153	.341	0.054	.734	0.352	.026	0.649	<.001
Internal trefoil	0.513	.001	0.418	.009	0.657	<.001	0.536	.001

HOAs = higher-order aberrations; NS = nuclear staging of the Scheimpflug device  
\*Spearman

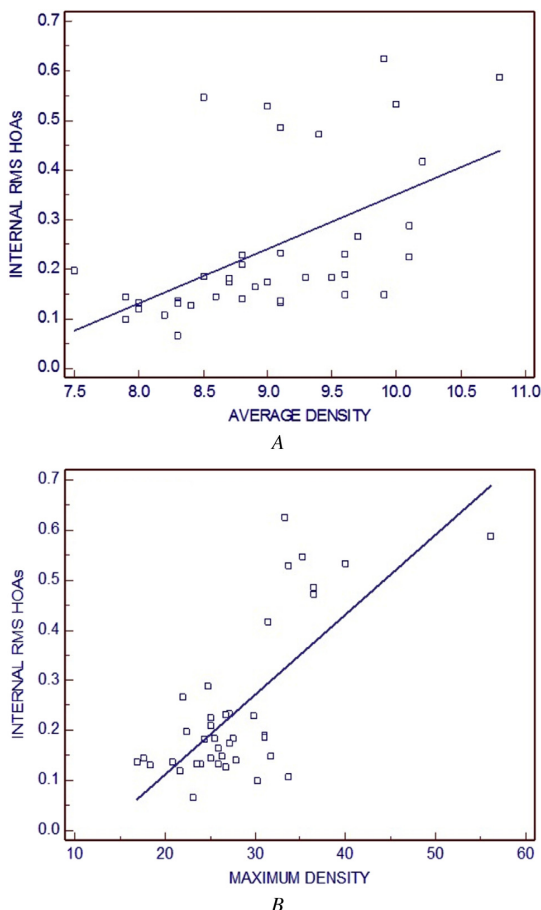


**Figure 2.** Relationships between internal RMS HOAs and mean (average) density (A) and internal RMS HOAs and maximum density (B).

and trefoil. Applegate et al.<sup>21,22</sup> reported that aberrations located in the central and upper areas of the Zernike pyramid tend to cause greater visual quality distortion. We included the internal HOAs because the crystalline lens is responsible for the increase in ocular aberrations that occurs with aging.<sup>1,11,23</sup> In our study, the RMS HOAs in the entire eye were lower than in the internal optics, indicating the presence of nuclear sclerosis. Coma was the most predominant HOA in our study. Using the same wavefront technology, Lee et al.<sup>24</sup> also found that comatic aberrations are increased in eyes with nuclear cataract.

Our results showed a relationship between the increase in internal HOAs and the nuclear sclerosis process. Similar findings were reported in previous studies. Sachdev et al.<sup>15</sup> reported an increase in HOAs in patients with nuclear and cortical opacification. Lim et al.<sup>25</sup> found a positive linear correlation between ocular scatter index (measured by a double-pass system) and the Scheimpflug-derived lens density. In our study, the internal HOAs were significantly correlated with the quantification parameters derived from Scheimpflug lens densitometry, such as mean density ( $\rho = 0.661, P < .001$ ) and maximum density ( $\rho = 0.570, P < .001$ ).

Using the same wavefront analysis technology, a previous study<sup>24</sup> showed a negative correlation between internal spherical aberration and the grade of nuclear cataract. This finding was attributed to the wavefront delay in the pupillary area caused by the increase in the nuclear refractive index.<sup>26</sup> Although not statistically significant, the internal spherical aberration had a negative relationship with the different methods of cataract grading. Interestingly, Lee et al.<sup>24</sup> reported that the internal RMS HOAs, coma, and trefoil had no significant correlation with the

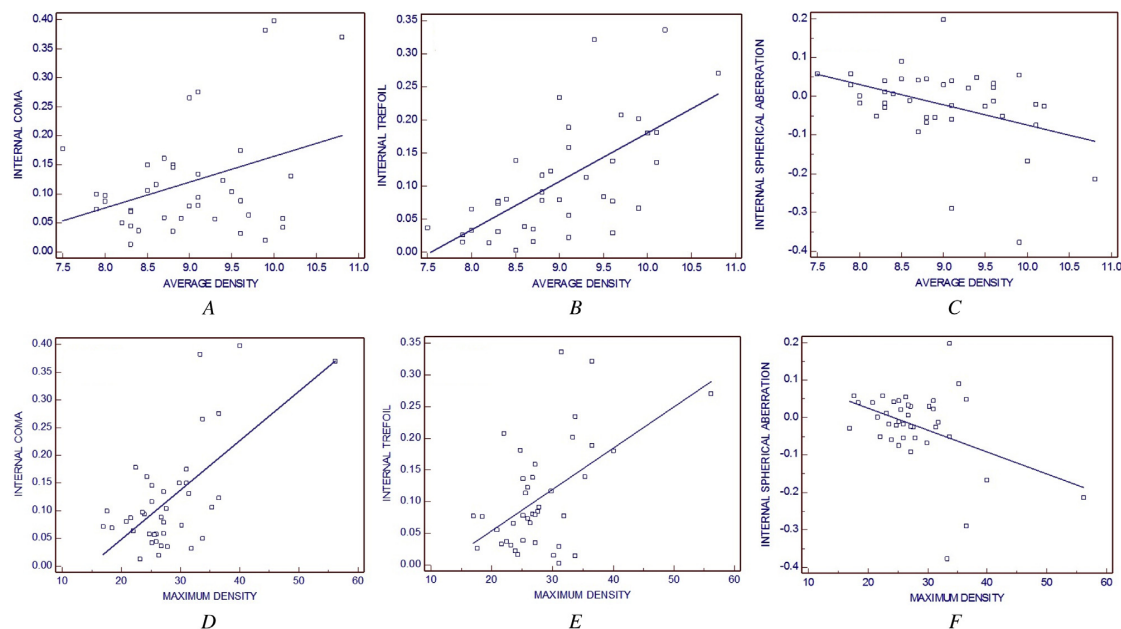


**Figure 3.** Relationships between internal coma and mean (average) density (A), internal trefoil and mean density (B), internal spherical aberration and mean density (C), internal coma and maximum density (D), internal trefoil and maximum density (E), and internal spherical aberration and maximum density (F).

LOCS III NO score. In the present study, the quantification parameters derived from Scheimpflug lens densitometry were significantly correlated with the same wavefront variables. This means that lens densitometry parameters are useful in identifying early nuclear sclerosis and might explain early visual problems reported by patients with nuclear cataract.

Regarding Scheimpflug-based densitometry, there are limitations. There is no consensus regarding which method and variable are the most representative of the true optical status of the lens nucleus.<sup>10</sup> In a previous study,<sup>17</sup> the maximum value assessed at a single point was found to be most likely representative of the nucleus because the nuclear cataract is regarded as a homogenous structure. Another issue is the presence of reflex artifacts in front or within the lens. This is a problem inherent in this technology that could lead to higher and false maximum values.<sup>10</sup> Careful analysis of previously published studies also showed the same limitation. In the present study, we used the automatic densitometry method. Despite being a repeatable method compared with others, such as peak and linear modes, the automatic densitometry method also analyzes an anterior cortical area of the lens. Because this is the main region with scattering changes in a large percentage of cases, this finding influences the real assessment of the nucleus optical density.<sup>10,17</sup>

Customization of the cylindrical template might help overcome this limitation. Improvements in the Scheimpflug camera would be useful for a more detailed and specific assessment of the nucleus. Previous studies have pointed out that the nuclear staging classification of the Pentacam device is a good tool for preoperative planning of cataract surgery, presenting a positive correlation with ultrasound energy and fluid consumption.<sup>6</sup> Concerning the wavefront analysis, this score showed a lower correlation than other quantitative parameters derived from lens densitometry. Thus, we can infer that the Pentacam nuclear staging score system is not really representative of the functional state of the lens. Another advantage of quantification variables is their presentation on a continuous scale, allowing better and more precise densitometric assessment of the lens.

Other limitations of this study are the small number of cases and the absence of age-matched controls. A study with a larger number of patients with normal age-matched controls would be appropriate. In our series, we include only nuclear cataract with opalescence less than 4 on the LOCS III scale. Less precise and repeatable measurements of Scheimpflug densitometry are more likely to occur in eyes with high-grade nuclear cataract.<sup>10,17</sup>

The demand for premium cataract surgery has increased. Cataract surgery is being performed earlier,

as soon as the first signs of opacification appear, because patients ask for a better quality of vision and to reduce or avoid the need for spectacles. Integrating these technologies in clinical practice might help in preoperative counseling and patient education to optimize the results and overall patient satisfaction.<sup>27,28</sup>

To our knowledge, this is the first study to establish a relationship between Scheimpflug lens densitometry and ray-tracing aberrometry. Our findings indicate that the quantification parameters derived from Scheimpflug densitometry has a stronger relationship with the functional status of the crystalline lens in eyes with mild nuclear cataract. The integration of these objective parameters might be useful for clinical and research purposes. Although there is no consensus on the densitometric parameters, a combination of these variables or new metrics might be useful for better evaluation of these patients.

#### WHAT WAS KNOWN

- Internal HOAs, such as coma and trefoil measured by ray tracing, are not correlated with the LOCS III grade of nuclear cataract.
- Internal spherical aberration has a negative correlation with the grade of nuclear cataract.

#### WHAT THIS PAPER ADDS

- Quantification parameters derived from the Scheimpflug lens densitometry showed a relationship with aging, CDVA decrease, and NO.
- Scheimpflug densitometry of mild grade nuclear cataracts showed a positive correlation with internal HOAs measured by ray-tracing aberrometry.

#### REFERENCES

1. Alió JL, Schimchak P, Negri HP, Montés-Micó R. Crystalline lens optical dysfunction through aging. *Ophthalmology* 2005; 112:2022–2029
2. Kuroda T, Fujikado T, Ninomiya S, Maeda N, Hirohara Y, Mihashi T. Effect of aging on ocular light scatter and higher order aberrations. *J Refract Surg* 2002; 18:S598–S602
3. Chylack LT Jr, Wolfe JK, Singer DM, Leske MC, Bullimore MA, Bailey IL, Friend J, McCarthy D, Wu S-Y; for the Longitudinal Study of Cataract Study Group. The Lens Opacities Classification System III. *Arch Ophthalmol* 1993; 111:831–836; erratum 1506. Available at: [http://www.chylackinc.com/LOCS\\_III/LOCS\\_III\\_Certification\\_files/LOCS\\_III\\_Reprint\\_pdf.pdf](http://www.chylackinc.com/LOCS_III/LOCS_III_Certification_files/LOCS_III_Reprint_pdf.pdf). Accessed December 4, 2015
4. Chylack LT Jr, Wolfe JK, Friend J, Khu PM, Singer DM, McCarthy D, del Carmen J, Rosner B. Quantitating cataract and nuclear brunescence; the Harvard and LOCS systems. *Optom Vis Sci* 1993; 70:886–895
5. Karbassi M, Khu PM, Singer DM, Chylack LT Jr. Evaluation of lens opacities classification system III applied at the slitlamp. *Optom Vis Sci* 1993; 70:923–928
6. Nixon DR. Preoperative cataract grading by Scheimpflug imaging and effect on operative fluidics and phacoemulsification energy. *J Cataract Refract Surg* 2010; 36:242–246
7. Kim J-S, Chung S-H, Joo C-K. Clinical application of a Scheimpflug system for lens density measurements in phacoemulsification. *J Cataract Refract Surg* 2009; 35:1204–1209; erratum, 1483
8. Grewal DS, Grewal SPS. Clinical applications of Scheimpflug imaging in cataract surgery. *Saudi J Ophthalmol* 2012; 26:25–32. Available at: <http://www.ncbi.nlm.nih.gov/pmc/articles/PMC3729842/pdf/main.pdf>. Accessed December 4, 2015
9. Gupta M, Ram J, Jain A, Sukhija J, Chaudhary M. Correlation of nuclear density using the Lens Opacity Classification System III versus Scheimpflug imaging with phacoemulsification parameters. *J Cataract Refract Surg* 2013; 39:1818–1823
10. Weiner X, Baumeister M, Kohnen T, Bühren J. Repeatability of lens densitometry using Scheimpflug imaging. *J Cataract Refract Surg* 2014; 40:756–763
11. Guirao A, González C, Redondo M, Geraghty E, Norrby S, Artal P. Average optical performance of the human eye as a function of age in a normal population. *Invest Ophthalmol Vis Sci* 1999; 40:203–213. Available at: <http://iovs.arvojournals.org/article.aspx?articleid=2162102>. Accessed December 4, 2015
12. Packer M, Fine IH, Hoffman RS. Wavefront technology in cataract surgery. *Curr Opin Ophthalmol* 2004; 15:56–60
13. Rocha KM, Nosé W, Bottós K, Bottós J, Morimoto L, Soriano E. Higher-order aberrations of age-related cataract. *J Cataract Refract Surg* 2007; 33:1442–1446
14. Donnelly WJ III, Pesudovs K, Marsack JD, Sarver EJ, Applegate RA. Quantifying scatter in Shack-Hartmann images to evaluate nuclear cataract. *J Refract Surg* 2004; 20:S515–S522
15. Sachdev N, Ormonde SE, Sherwin T, McGhee CNJ. Higher-order aberrations of lenticular opacities. *J Cataract Refract Surg* 2004; 30:1642–1648
16. Magno BV, Freidlin V, Datiles MB III. Reproducibility of the NEI Scheimpflug Cataract Imaging System. *Invest Ophthalmol Vis Sci* 1994; 35:3078–3084. Available at: <http://iovs.arvojournals.org/article.aspx?articleid=2179797>. Accessed December 4, 2015
17. Grewal DS, Brar GS, Grewal SPS. Correlation of nuclear cataract lens density using Scheimpflug images with Lens Opacities Classification System III and visual function. *Ophthalmology* 2009; 116:1436–1443
18. Kirkwood BJ, Hendicott PL, Read SA, Pesudovs K. Repeatability and validity of lens densitometry measured with Scheimpflug imaging. *J Cataract Refract Surg* 2009; 35:1210–1215
19. Bartsch D-UG, Bessho K, Gomez L, Freeman WR. Comparison of laser ray-tracing and skiascopic ocular wavefront-sensing devices. *Eye* 2008; 22:1384–1390. Available at: <http://www.nature.com/eye/journal/v22/n11/pdf/6702901a.pdf>. Accessed December 4, 2015
20. Pei X, Bao Y, Chen Y, Li X. Correlation of lens density measured using the Pentacam Scheimpflug system with the Lens Opacities Classification System III grading score and visual acuity in age-related nuclear cataract. *Br J Ophthalmol* 2008; 92:1471–1475
21. Applegate RA, Marsack JD, Ramos R, Sarver EJ. Interaction between aberrations to improve or reduce visual performance. *J Cataract Refract Surg* 2003; 29:1487–1495



22. Applegate RA, Sarver EJ, Khemsara V. Are all aberrations equal? *J Refract Surg* 2002; 18:S556–S562
23. Artal P, Berrio E, Guirao A, Piers P. Contribution of the cornea and internal surfaces to the change of ocular aberrations with age. *J Opt Soc Am A Opt Image Sci Vis* 2002; 19:137–143
24. Lee J, Kim MJ, Tchah H. Higher-order aberrations induced by nuclear cataract. *J Cataract Refract Surg* 2008; 34:2104–2109; erratum, 2009; 35:4
25. Lim SA, Hwang J, Hwang K-Y, Chung S-H. Objective assessment of nuclear cataract: comparison of double-pass and Scheimpflug systems. *J Cataract Refract Surg* 2014; 40:716–721
26. Kuroda T, Fujikado T, Maeda N, Oshika T, Hirohara Y, Mihashi T. Wavefront analysis in eyes with nuclear or cortical cataract. *Am J Ophthalmol* 2002; 134:1–9
27. Market Scope. 2013 Annual Cataract Surgeon Survey. St. Louis, MO, Market Scope LLC, 2013
28. Braga-Mele R, Chang D, Dewey S, Foster G, Henderson BA, Hill W, Hoffman R, Little B, Mamalis N, Oetting T, Serafano D, Talley-Rostov A, Vasavada A, Yoo S; for the ASCRS Cataract Clinical Committee. Multifocal intraocular lenses: relative indications and contraindications for implantation. *J Cataract Refract Surg* 2014; 40:313–322



First author:  
Fernando Faria-Correia, MD  
*Hospital de Braga, Braga, Portugal*



## **CHAPTER III**

RELATIONSHIP BETWEEN THE DLI WITH LENS  
GRADING BASED ON THE LOCS III AND THE  
SCHEIMPFLUG-BASED LENS DENSITOMETRY



# Comparison of Dysfunctional Lens Index and Scheimpflug Lens Densitometry in the Evaluation of Age-Related Nuclear Cataracts

Fernando Faria-Correia, MD; Isaac Ramos, MD; Bernardo Lopes, MD; Tiago Monteiro, MD; Nuno Franqueira, MD; Renato Ambrósio, Jr., MD, PhD

## ABSTRACT

**PURPOSE:** To describe the Dysfunctional Lens Index (DLI) from ray-tracing aberrometry and to test its correlations with logMAR corrected distance visual acuity (CDVA) and lens grading based on the Lens Opacities Classification System III (LOCS III) and the Scheimpflug-based lens density.

**METHODS:** The DLI was calculated by the i-Trace Visual Functional Analyzer (Tracey Technologies, Houston, TX). Forty eyes of 30 patients with mild to moderate age-related nuclear cataract were included retrospectively. Nuclear opalescence grading was obtained by slit lamp using the LOCS III, and objective lens densitometry was evaluated by Scheimpflug imaging (Pentacam HR; Oculus Optikgeräte GmbH, Wetzlar, Germany). The average density parameter obtained by Scheimpflug imaging of the nucleus lens was considered.

**RESULTS:** The DLI showed a high negative linear correlation with the LOCS III nuclear opalescence score ( $r = -0.662$ ;  $P < .01$ ). The average density of the lens nucleus was positively correlated with the LOCS III nuclear opalescence score ( $r = 0.682$ ;  $P < .01$ ). The CDVA had a stronger relationship with the DLI parameter ( $r = -0.702$ ,  $P < .01$ ) compared to the average density values ( $r = 0.630$ ,  $P < .01$ ).

**CONCLUSIONS:** The DLI was correlated with the LOCS III nuclear opalescence score and the Scheimpflug-based lens density. The DLI had a stronger correlation with CDVA compared to the LOCS III classification or the Scheimpflug-based lens density. The DLI may improve the preoperative evaluation of nuclear cataract and the monitoring of its progression.

[*J Refract Surg.* 2016;32(4):244-248.]

**A**s an age-related process, the molecular changes that occur in the crystalline lens induce a gradual loss of ocular transparency in the human eye and an increase of the lens density.<sup>1-3</sup> There is currently an increasing demand for premium cataract surgery. Cataract surgery is being performed earlier because patients ask for a better quality of vision and wish to reduce or avoid the need for glasses.<sup>4,5</sup>

Clinically, the methods used for cataract evaluation can be divided into two types: subjective and objective. The method most commonly used to assess crystalline lens opacification is the Lens Opacities Classification System III (LOCS III). It is a grading system based on slit-lamp biomicroscopy, which is widely used for clinical purposes and for research.<sup>6-8</sup> The group of objective evaluation methods includes different ancillary devices. For example, Scheimpflug imaging systems objectively measure lens density and may assist phacodynamics in cataract surgery.<sup>9-15</sup> Wavefront sensors have also proved to be useful for the evaluation of patients with different grades of cataract because higher order aberrations (HOAs) play an essential role in the reduction of optical performance in patients with age-related cataract.<sup>16-21</sup> The iTrace Visual Function Analyzer (Tracey Technologies, Houston, TX) is a ray-tracing aberrometry system that provides several parameters, including the Dysfunctional Lens Index (DLI). The DLI is

*From the Ophthalmology Department, Hospital de Braga, Braga, Portugal (FF-C, TM, NF); the Refractive Surgery Department, Instituto CUF, Porto, Portugal (FF-C, TM); Life and Health Sciences Research Institute (ICVS), School of Health Sciences, University of Minho, Braga, Portugal (FF-C, TM); ICVS/3B's-PT Government Associate Laboratory, Braga/Guimarães, Portugal (FF-C); Rio de Janeiro Corneal Tomography and Biomechanics Study Group, Rio de Janeiro, Brazil (FF-C, IR, BL, RA); Instituto de Olhos Renato Ambrósio, Rio de Janeiro, Brazil; VisareRio (Ambrósio), Rio de Janeiro, Brazil (BL, RA); and Federal University of São Paulo, São Paulo, Brazil (RA).*

*Submitted: October 20, 2015; Accepted: December 9, 2015*

*Dr. Ambrósio is a consultant for Oculus Optikgeräte GmbH (Wetzlar, Germany), Alcon Laboratories, Inc. (Fort Worth, Texas), and Carl Zeiss Meditec (Jena, Germany). The remaining authors have no financial or proprietary interest in the materials presented herein.*

*Correspondence: Fernando Faria-Correia, MD, Avenida de Bessa, Edifício Boapor II, 216, 7<sup>o</sup> Frente, 4100-012 Porto, Portugal. E-mail: f.faria.correia@gmail.com*

*doi:10.3928/1081597X-20160209-01*



**Figure 1.** (A) Scheimpflug-based lens density and (B) Dysfunctional Lens Index (DLI) of a patient with age-related nuclear cataract. The average density is 9.2 and the DLI is 6.20.

an objective lens performance metric derived from internal HOAs, pupil size, and contrast sensitivity data.

The purpose of the current study was to investigate the relationship between the DLI and the Scheimpflug-based lens density and LOCS III grading score in age-related nuclear cataracts.

#### PATIENTS AND METHODS

This retrospective single-center study was conducted with patients who were recruited for a clinical visit in the Cornea and Refractive Surgery Department, Hospital de Braga (Portugal) from June 2015 to September 2015. The study was approved by the institutional review board and complied with the tenets of the Declaration of Helsinki. No patient had a history of ocular disease, ocular surgery, or general disorders affecting vision, such as diabetic retinopathy or uveitis. All patients underwent a complete ophthalmic examination, which included corrected distance visual acuity measurement (CDVA; recorded in logMAR units), noncontact tonometry, slit-lamp biomicroscopy, and dilated fundus examination. The nuclear sclerotic grade was classified according to the LOCS III.<sup>6</sup> The same ophthalmologist examined all patients using a slit-lamp microscope after pupil dilation with a combination of topical 1.0% tropicamide and 10% phenylephrine. LOCS III nuclear opalescence was graded on a scale of 0.1 to 6.9 by comparing a digital photograph of each lens to standard color photographic transparencies of nuclear opalescence. Exclusion criteria were: eyes with poor mydriasis, eyes with any corneal opacities, and eyes with a LOCS III nuclear opalescence grade greater than 4, cortical opacities, or anterior/posterior subcapsular cataract.

#### SCHEIMPFLUG SYSTEM MEASUREMENT

The Pentacam HR (Oculus Optikgeräte GmbH, Wetzlar, Germany) is a Scheimpflug-based device that generates a three-dimensional representation of the

anterior segment of the eye. In less than 2 seconds, the rotating camera captures up to 25 slit-images of the anterior segment, collecting 25,000 true elevation data points. Three measurements of each eye were taken in a dark room. The Pentacam Nuclear Staging software permits the determination of objective crystalline lens densitometry. The software automatically generates a cylindrical template for the density measurement (Oculus Optikgeräte GmbH). The template volume used for the study had the following features: 4-mm diameter, 2.4-mm height, 8.3-mm front curvature, and 4.8-mm back curvature. The three-dimensional template was placed in the center of the nucleus, excluding the anterior and posterior cortex, permitting objective quantification of lens opacities inside the template (average density and maximum density parameters) on a continuous scale from 0 to 100 points.

#### WAVEFRONT MEASUREMENT

The i-Trace was used for wavefront analysis. Three measurements of each eye were also taken in a dark room. This device integrates an aberrometer with a corneal topographer. The aberrometer uses the ray-tracing principle, which sequentially projects 256 near-infrared laser beams into the eye in a specific scanning pattern. Topographies were captured using the Placido-based corneal topographer (EyeSys Vision, Houston, TX) mounted on the same device. The corneal aberrations were calculated based on topography data, and the internal aberrations were calculated by subtracting the corneal aberrations from those of the entire eye measured by the ray-tracing aberrometer using the built-in program. The DLI is an objective lens performance parameter provided by this wavefront sensor and is calculated based on the internal HOAs, pupil size, and contrast sensitivity data (**Figure 1**). This objective index ranks overall lens performance from 0 (very poor) to 10 (excellent) points.

Age-Related Nuclear Cataracts/Faria-Correia et al

TABLE 1  
Cataract Evaluation by the Different Methods

Parameter	Range	Mean ± SD
LOCS III NO score	1.0 to 3.0	2.13 ± 0.56
Average density (based on Scheimpflug system)	7.1 to 11.0	8.21 ± 0.80
DLI (based on ray-tracing system)	2.01 to 10.0	7.54 ± 2.56

SD = standard deviation; LOCS III NO = Lens Opacities Classification System III nuclear opalescence; DLI = Dysfunctional Lens Index

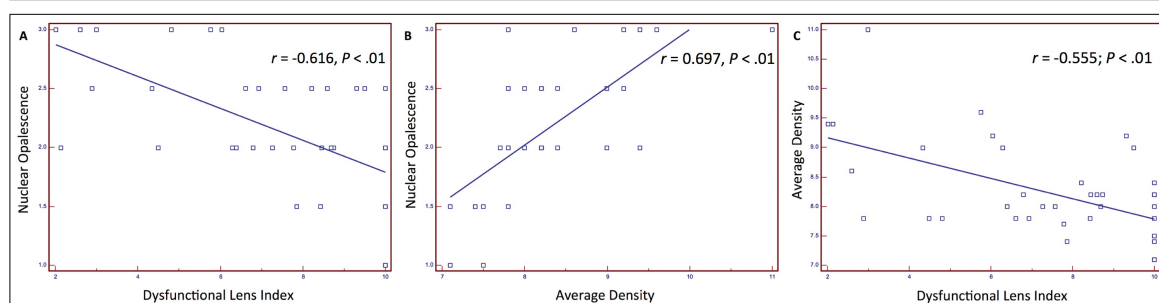


Figure 2. Relationships between (A) nuclear opalescence (Lens Opacities Classification System III score) and Dysfunctional Lens Index, (B) nuclear opalescence and average density, and (C) average density and Dysfunctional Lens Index.

DATA AND STATISTICAL ANALYSIS

An experienced rater (FF-C) reviewed the Pentacam and i-Trace scans. The best-quality scan of the three measurements with each device was selected for further analysis. We excluded Scheimpflug scans with artifacts that would interfere with the densitometry results (ie, presence of cortical shadowing artifacts or misplacement of the reference template). The average density value was registered. The wavefront scans were checked regarding the centration of the measurement with the visual axis of the eye. The wavefront was measured in a 4-mm optical zone set by the software, and the DLI was registered for each eye included in the study.

All results were analyzed using MedCalc software (version 14.12.02; MedCalc, Ostend, Belgium). Values are presented as means ± standard deviations. Data normality was assessed using the Kolmogorov–Smirnov test. Significant correlations were evaluated using Pearson or Spearman correlation coefficients according to data normality. A P value of .05 or less was considered to be statistically significant.

RESULTS

Forty eyes of 30 patients were included in the study. The study population consisted of 15 women and 15 men. Mean age was 67.53 ± 10.70 years (range: 46 to 90 years) and mean CDVA in logMAR units was 0.15 ± 0.13 (range: 0 to 0.4). Table 1 shows the patients' cataract evaluation scores obtained with the different methods.

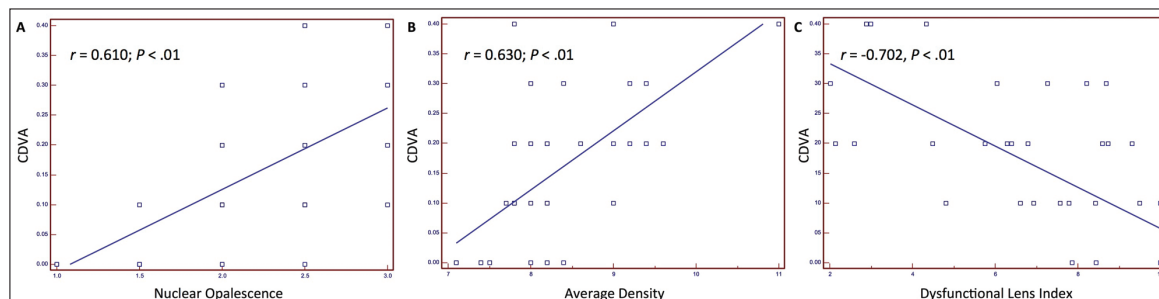
The DLI showed a high negative linear correlation with the LOCS III nuclear opalescence score ( $r = -0.616$ ,  $P < .01$ ). The average nuclear density was positively correlated with the LOCS III nuclear opalescence score ( $r = 0.697$ ,  $P < .01$ ). As shown in Figure 2, the Scheimpflug-based average density parameter was negatively correlated with the DLI ( $r = -0.555$ ; both  $P < .01$ ).

Figure 3 displays the relationship between the CDVA and the different methods of cataract grading. The CDVA was correlated with the LOCS III nuclear opalescence score ( $r = 0.610$ ; both  $P < .01$ ) and with the average density values ( $r = 0.630$ ; both  $P < .01$ ). However, the CDVA had a stronger relationship with the DLI parameter ( $r = -0.702$ ,  $P < .01$ ) compared to the other methods of cataract evaluation (Figure 2).

DISCUSSION

In the current study, we found that the DLI parameter provided by the iTrace Visual Function Analyzer was negative and significantly correlated with the Scheimpflug-based lens densitometry in eyes with age-related nuclear cataract. The DLI was also negatively correlated with the nuclear opalescence score of the LOCS III grading system and the CDVA. Because this new parameter reflects the performance of the crystalline lens, it may be clinically useful for objective quantification of age-related nuclear cataracts.

Although the LOCS III is the most widely used grading system, there are concerns regarding its reproduc-



**Figure 3.** Relationships between (A) corrected distance visual acuity (CDVA) and nuclear opalescence (Lens Opacities Classification System III score), (B) CDVA and average density, and (C) CDVA and Dysfunctional Lens Index.

ibility.<sup>22,23</sup> To avoid these drawbacks, Scheimpflug imaging is an option that allows objective lens densitometry evaluation and is not susceptible to observer variability. Precise cataract quantification is essential for patient education and for predicting phacodynamics.<sup>11-13</sup> Compared to the LOCS III grading system, Scheimpflug-based densitometry is considered to be a more sensitive and repeatable approach.<sup>12,23</sup> Wavefront analysis demonstrated that the increase of internal HOAs leads to visual deterioration of the ocular optical system.<sup>17,19,20</sup> A ray-tracing aberrometer was the selected device because it has known advantages over the Hartmann-Shack and other types of wavefront sensors.<sup>24,25</sup>

Previous studies have shown that nuclear sclerosis is an age-related process, contributing to vision deterioration and lens optical densitometry changes.<sup>11,12</sup> Sachdev et al. reported an increase of HOAs in patients with nuclear and cortical opacification.<sup>26</sup> Alió et al. described a positive linear correlation in eyes with clear lenses between age and ocular HOAs and spherical-like aberrations.<sup>1</sup> Lee et al. also reported an increase of HOAs in nuclear cataracts using ray-tracing wavefront technology.<sup>21</sup>

The Optical Quality Analysis System (Visiometrics, Terrasa, Spain) is a clinical device that evaluates the combined effect of optical aberrations and light scattering derived from the loss of ocular transparency in the human eye.<sup>27</sup> This double-pass system provides the objective scatter index (OSI) that represents the degree of objective scattering caused by deterioration of ocular transparency. Previous studies have shown that this parameter is useful for the quantification of nuclear cataracts. Artal et al. described a significant correlation between the OSI and the LOCS III nuclear opalescence score.<sup>28</sup> Lim et al. reported a positive linear correlation between the OSI with the Scheimpflug-derived lens density and phacodynamics.<sup>29</sup>

The DLI based on the ray-tracing system was also significantly correlated with the LOCS III nuclear

opalescence score and the Scheimpflug-derived lens densitometry. The usefulness of the DLI as a metric to objectively evaluate the severity of age-related nuclear sclerosis is suggested by its correspondence with lens density. In this study, we found reduction of the CDVA with the DLI, LOCS III nuclear opalescence score, and Scheimpflug-measured lens density ( $P < .01$ ). The CDVA showed a stronger correlation with the DLI ( $r = -0.702$ ) than with the LOCS III nuclear opalescence score ( $r = 0.610$ ) and average density ( $r = 0.630$ ). These results suggest that the DLI parameter is more closely related to the patient's visual symptoms regarding optical quality than the LOCS III classification or Scheimpflug-based lens density.

The current study has some limitations. Concerning the Scheimpflug-based densitometry, there is no consensus regarding which method or variable is the most representative of the true optical status of the lens nucleus.<sup>22,23</sup> We used the automatic densitometry method because it is considered the most repeatable method. Another issue is the presence of reflex artifacts in front of or within the lens, which is an inherent limitation of this technology. The presence of these findings may lead to higher and false maximum values.<sup>23</sup> For this reason, we decided not to include the maximum lens density parameter in the analysis. Other limitations of this study are the small number of cases and the absence of age-matched controls. We only included nuclear cataracts with opalescence of less than 4 on the LOCS III, because less precise and repeatable measurements of Scheimpflug densitometry are more prone to occur in high-grade nuclear cataracts.<sup>12,23</sup> "Nucleus color" evaluation was not considered in the methodology because previous studies have reported that lens density had a stronger correlation with nuclear opalescence.<sup>12,15</sup>

Because the demand for premium cataract surgery has been recently increasing, objective and sensitive methods of lens performance assessment are useful in



## Age-Related Nuclear Cataracts/Faria-Correia et al

clinical practice.<sup>4,5</sup> Integrating these new concepts may be of help in preoperative counseling and patient education to optimize the results and overall satisfaction.

The DLI based on the ray-tracing system was useful for the quantification of age-related nuclear cataracts. This parameter was also correlated with the subjective LOCS III score and with the objective Scheimpflug-based lens density. Regarding visual performance, the DLI showed a stronger correlation with CDVA compared to the LOCS III classification or the Scheimpflug-based lens density. Thus, the DLI may be considered as an auxiliary metric for objective lens opacity evaluation and monitoring of cataract progression. Further studies are needed to assess its usefulness in predicting phacodynamics in cataract surgery.

## AUTHOR CONTRIBUTIONS

Study concept and design (FF-C); data collection (FF-C, IR, BL, TM, NF, RA); analysis and interpretation of data (FF-C, RA); writing the manuscript (FF-C); critical revision of the manuscript (FF-C, IR, BL, TM, NF, RA)

## REFERENCES

- Alió JL, Schimchak P, Negri HP, Montés-Micó R. Crystalline lens optical dysfunction through aging. *Ophthalmology*. 2005;112:2022-2029.
- Brunette I, Bueno JM, Parent M, Hamam H, Simonet P. Monochromatic aberrations as a function of age, from childhood to advanced age. *Invest Ophthalmol Vis Sci*. 2003;44:5438-5446.
- Guirao A, Gonzalez C, Redondo M, Geraghty E, Norrby S, Artal P. Average optical performance of the human eye as a function of age in a normal population. *Invest Ophthalmol Vis Sci*. 1999;40:203-213.
- Braga-Mele R, Chang D, Dewey S, et al. Multifocal intraocular lenses: relative indications and contraindications for implantation. *J Cataract Refract Surg*. 2014;40:313-322.
- Market Scope. 2013 Annual Cataract Surgeon Survey. St. Louis: Market Scope LLC.
- Chylack LT, Wolfe JK, Singer DM, et al. The Lens Opacities Classification System III. The Longitudinal Study of Cataract Study Group. *Arch Ophthalmol*. 1993;111:831-836.
- Chylack LT Jr, Wolfe JK, Friend J, et al. Quantitating cataract and nuclear brunescence, the Harvard and LOCS systems. *Optom Vis Sci*. 1993;70:886-895.
- Karbassi M, Khu PM, Singer DM, Chylack LT Jr. Evaluation of lens opacities classification system III applied at the slitlamp. *Optom Vis Sci*. 1993;70:923-928.
- Magno BV, Freidlin V, Datiles MB. Reproducibility of the NEI Scheimpflug Cataract Imaging System. *Invest Ophthalmol Vis Sci*. 1994;35:3078-3084.
- Datiles MB, Magno BV, Freidlin V. Study of nuclear cataract progression using the National Eye Institute Scheimpflug system. *Br J Ophthalmol*. 1995;79:527-534.
- Pei X, Bao Y, Chen Y, Li X. Correlation of lens density measured using the Pentacam Scheimpflug system with the Lens Opacities Classification System III grading score and visual acuity in age-related nuclear cataract. *Br J Ophthalmol*. 2008;92:1471-1475.
- Grewal DS, Brar GS, Grewal SP. Correlation of nuclear cataract lens density using Scheimpflug images with Lens Opacities Classification System III and visual function. *Ophthalmology*. 2009;116:1436-1443.
- Kim JS, Chung SH, Joo CK. Clinical application of a Scheimpflug system for lens density measurements in phacoemulsification. *J Cataract Refract Surg*. 2009;35:1204-1209. Erratum in: *J Cataract Refract Surg*. 2009;35:1483.
- Magalhães FP, Costa EF, Cariello AJ, Rodrigues EB, Hofling-Lima AL. Comparative analysis of the nuclear lens opalescence by the Lens Opacities Classification System III with nuclear density values provided by Oculus Pentacam: a cross-section study using Pentacam Nucleus Staging software. *Arq Bras Oftalmol*. 2011;74:110-113.
- Gupta M, Ram J, Jain A, Sukhija J, Chaudhary M. Correlation of nuclear density using the Lens Opacity Classification System III versus Scheimpflug imaging with phacoemulsification parameters. *J Cataract Refract Surg*. 2013;39:1818-1823.
- Kuroda T, Fujikado T, Maeda N, Oshika T, Hirohara Y, Mihashi T. Wavefront analysis of higher-order aberrations in patients with cataract. *J Cataract Refract Surg*. 2002;28:438-444.
- Applegate RA, Marsack JD, Ramos R, Sarver EJ. Interaction between aberrations to improve or reduce visual performance. *J Cataract Refract Surg*. 2003;29:1487-1495.
- Donnelly WJ, Pesudovs K, Marsack JD, Sarver EJ, Applegate RA. Quantifying scatter in Shack-Hartmann images to evaluate nuclear cataract. *J Refract Surg*. 2004;20:S515-S522.
- Packer M, Fine IH, Hoffman RS. Wavefront technology in cataract surgery. *Curr Opin Ophthalmol*. 2004;15:56-60.
- Rocha KM, Nosé W, Bottós K, Bottós J, Morimoto L, Soriano E. Higher-order aberrations of age-related cataract. *J Cataract Refract Surg*. 2007;33:1442-1446.
- Lee J, Kim MJ, Tchah H. Higher-order aberrations induced by nuclear cataract. *J Cataract Refract Surg*. 2008;34:2104-2109. Erratum in: *J Cataract Refract Surg*. 2009;35:4.
- Kirkwood BJ, Hendicott PL, Read SA, Pesudovs K. Repeatability and validity of lens densitometry measured with Scheimpflug imaging. *J Cataract Refract Surg*. 2009;35:1210-1215.
- Weiner X, Baumeister M, Kohnen T, Bühren J. Repeatability of lens densitometry using Scheimpflug imaging. *J Cataract Refract Surg*. 2014;40:756-763.
- Bartsch DU, Bessho K, Gomez L, Freeman WR. Comparison of laser ray-tracing and skiascopic ocular wavefront-sensing devices. *Eye (Lond)*. 2008;22:1384-1390.
- Piñero DP, Sánchez-Pérez PJ, Alió JL. Repeatability of measurements obtained with a ray tracing aberrometer. *Optom Vis Sci*. 2011;88:1099-1105.
- Sachdev N, Ormonde SE, Sherwin T, McGhee CN. Higher-order aberrations of lenticular opacities. *J Cataract Refract Surg*. 2004;30:1642-1648.
- Cabot F, Saad A, McAlinden C, Haddad NM, Grise-Dulac A, Gatinel D. Objective assessment of crystalline lens opacity level by measuring ocular light scattering with a double-pass system. *Am J Ophthalmol*. 2013;155:629-635.
- Artal P, Benito A, Perez GM, et al. An objective scatter index based on double-pass retinal images of a point source to classify cataracts. *PLoS One*. 2011;6:e16823.
- Lim SA, Hwang J, Hwang KY, Chung SH. Objective assessment of nuclear cataract: comparison of double-pass and Scheimpflug systems. *J Cataract Refract Surg*. 2014;40:716-721.



# **CHAPTER IV**

RELATIONSHIP BETWEEN PREOPERATIVE  
SCHEIMPFLUG-BASED LENS DENSITOMETRY  
METRICS AND PHACODYNAMICS



# Application of different Scheimpflug-based lens densitometry methods in phacodynamics prediction

Fernando Faria-Correia<sup>1-5</sup>  
Bernardo T Lopes<sup>5,6</sup>  
Isaac C Ramos<sup>5,6</sup>  
Tiago Monteiro<sup>1,2</sup>  
Nuno Franqueira<sup>1</sup>  
Renato Ambrósio Jr<sup>5-8</sup>

<sup>1</sup>Ophthalmology Department, Hospital de Braga, Braga, Portugal; <sup>2</sup>Life and Health Sciences Research Institute (ICVS), School of Health Sciences, University of Minho, Braga, Portugal; <sup>3</sup>ICVS/3B's - PT Government Associate Laboratory, Braga, Portugal; <sup>4</sup>ICVS/3B's - PT Government Associate Laboratory, Guimarães, Portugal; <sup>5</sup>Rio de Janeiro Corneal Tomography and Biomechanics Study Group, Rio de Janeiro, Brazil; <sup>6</sup>Instituto de Olhos Renato Ambrósio, Rio de Janeiro, Brazil; <sup>7</sup>VisareRio, Rio de Janeiro, Brazil; <sup>8</sup>Department of Ophthalmology and Visual Sciences, Federal University of São Paulo, São Paulo, Brazil

**Purpose:** To evaluate the correlations between preoperative Scheimpflug-based lens densitometry metrics and phacodynamics.

**Methods:** The Lens Opacities Classification System III (LOCS III) was used to grade nuclear opalescence (NO), along with different methods of lens densitometry evaluation (absolute scale from 0% to 100%): three-dimensional (3D), linear, and region of interest (ROI) modes. Cumulative dissipated energy (CDE) and total ultrasound (US) time were recorded and correlated with the different methods of cataract grading. Significant correlations were evaluated using Pearson or Spearman correlation coefficients according to data normality.

**Results:** A positive correlation was detected between the NO score and the average density and the maximum density derived from the 3D mode ( $r=0.624$ ,  $P<0.001$ ;  $r=0.619$ ,  $P<0.001$ , respectively) and the ROI mode ( $r=0.600$ ,  $P<0.001$ ;  $r=0.642$ ,  $P<0.001$ , respectively). Regarding the linear mode, only the average density parameter presented a significant relationship with the NO score ( $r=0.569$ ,  $P<0.001$ ). The 3D-derived average density and maximum density were positively correlated with CDE ( $\rho=0.682$ ,  $P<0.001$ ;  $\rho=0.683$ ,  $P<0.001$ , respectively) and total US time ( $\rho=0.631$  and  $\rho=0.668$ , respectively). There was a linear relationship between the average density and maximum density of the ROI mode and CDE ( $\rho=0.686$ ,  $P<0.001$ ;  $\rho=0.598$ ,  $P<0.001$ , respectively) and total US time ( $\rho=0.642$  and  $\rho=0.644$ , respectively). The average density was the only parameter derived from the linear mode that showed a significant correlation with CDE ( $\rho=0.522$ ,  $P<0.001$ ) and total US time ( $\rho=0.450$ ,  $P<0.001$ ).

**Conclusion:** Specific Scheimpflug-derived densitometric parameters of the nucleus correlated with phacoemulsification parameters. The use of the appropriate densitometry approach can predict more efficiently the phacodynamics.

**Keywords:** cataract, phacoemulsification, scheimpflug, densitometry

## Introduction

Detailed evaluation of cataract density is essential in surgery planning in order to improve visual outcomes and to avoid possible intraoperative and postoperative complications. The Lens Opacities Classification System III (LOCS III) is a subjective evaluation method based on slit-lamp examination.<sup>1</sup> Although this is a cost-effective grading system, interobserver and intraobserver variations influence the reproducibility of the evaluations.<sup>2,3</sup>

Anterior segment imaging has become progressively attractive with the advent of Scheimpflug-based systems, such as the Pentacam (OCULUS Optikgeräte GmbH, Wetzlar, Germany). Previous studies have enabled objective measurements of lens density, providing more precise and reliable assessments compared to the LOCS III grading system.<sup>4-7</sup> Different approaches have been described to quantify cataract density from the Scheimpflug images, and some correlated better with lens grading and

Correspondence: Fernando Faria-Correia  
Life and Health Sciences Research  
Institute (ICVS), Universidade do Minho,  
Campus de Gualtar, 4710-057 Braga,  
Portugal  
Email f.faria.correia@gmail.com



visual performance than others.<sup>8–10</sup> This technology has also provided the opportunity to analyze the relationship between the densitometric measurements and the phacoemulsification parameters.<sup>9,11–14</sup> Concerning this topic, the variety of the evaluation and surgical methods described in the literature affects the conclusions of scientific studies. In this context, we intended to perform a comprehensive assessment of all lens densitometry methods available in Pentacam by checking their relationship with the LOCS III classification and phacodynamics in age-related nuclear cataracts.

## Methods

This retrospective study was performed at Hospital de Braga, Braga, Portugal, from June to October 2014. The study enrolled patients with age-related nuclear cataract who had uneventful phacoemulsification during this period. Written informed consent was obtained from each patient before the surgical procedure. The study was approved by the Institutional Review Board (Hospital de Braga) and complied with the Declaration of Helsinki of the World Medical Association. No patient had a history of ocular disease, ocular surgery, or general disorders affecting vision, such as diabetic retinopathy or uveitis. All patients were submitted to a complete ophthalmic examination that included uncorrected and corrected visual acuity measurements, noncontact tonometry, slit-lamp biomicroscopy, and dilated fundus examination. Nuclear opalescence (NO) was assessed according to the LOCS III scale (range: 0.0 to 6.9) by using a slit-lamp microscope after pupil dilation with 1% topical tropicamide and 10% phenylephrine. The same ophthalmologist (FFC) performed the LOCS III evaluation. Patients with poor mydriasis, corneal opacities, cataracts with NO score exceeding 4.1, and cortical opacities were excluded from the study. Preoperative examinations also included optical biometry (ALLEGRO BioGraph; Wavelight AG, Erlangen, Germany) and Scheimpflug-based anterior segment tomography (Pentacam HR; OCULUS Optikgeräte GmbH). In the Pentacam HR examination, the camera rotates around the eye from 0 to 180 degrees and captures 25 single slit images in less than 2 seconds. The scan collects 25,000 true elevation data points, which are processed to generate a three-dimensional (3D) representation of the anterior segment of the eye. It also provides an image of the whole crystalline lens, permitting an objective measurement of lens density. After pupil mydriasis, three consecutive scans of each eye were taken in a dark room. Regarding the lens assessment by Scheimpflug imaging, we excluded scans with artifacts that would interfere with the densitometry results, such as the presence of cortical shadowing artifacts or blinking during the scan.

We selected the Scheimpflug images on the vertical plane (90 to 270 degrees for the right eye and 270 to 90 degrees for the left eye). Three different densitometric analyses were performed to measure lens optical density on a continuous scale (Figure 1): two manual modes, ie, the linear and region of interest (ROI) modes, and one 3D mode. These densitometric methods have been described in previous studies.<sup>7,11</sup> The software measures the lens optical density on a scale from 0% to 100% (0=no cloudiness; 100=completely opaque lens). The linear mode evaluates the density of a vertical line manually drawn along the axial length of the crystalline lens. The ROI mode provides a density assessment for a specific area drawn on an individual Scheimpflug image. In this study, we manually drew an elliptical ROI centered on the lens nucleus on the Scheimpflug image, excluding its anterior and posterior cortex. For the 3D mode, the software of the Pentacam system (PNS [Pentacam Nuclear Staging] software) automatically generates a cylindrical template for the density measurement. The template volume used for the study had the following features: 4.0 mm diameter, 2.4 mm height, 8.3 mm front curvature, and 4.8 mm back curvature. The 3D template was placed in the center of the nucleus, excluding the anterior and posterior cortex. For each densitometric mode, the average density and maximum density parameters were observed. All patients received clear corneal phacoemulsification and posterior chamber intraocular lens implantation by the same surgeon (FFC) under local anesthesia. The stop-and-chop phacoemulsification technique was performed with a Kelman microtip 0.9 mm 45-degree using the Infiniti System (Alcon Laboratories, Inc., Fort Worth, TX, USA). At the end of the nucleus management, the following phacoemulsification parameters were observed: cumulative dissipated energy (CDE) and total ultrasound (US) time. No intraoperative complications occurred.

All results were analyzed using Medcalc software (version 14.12.0; Ostend, Belgium) and values are reported as mean  $\pm$  standard deviation. Data normality was assessed using the Kolmogorov–Smirnov test. Significant correlations were evaluated using Pearson or Spearman correlation coefficients according to data normality. A *P*-value of 0.05 or less was considered statistically significant. However, because of the large number of comparisons (14 for both phacoemulsification parameters and cataract grading methods), the Bonferroni adjustment was used to reduce the possibility of a statistically significant difference based on chance alone. The level of significance was divided by the number of comparisons (14) using the Bonferroni adjustment. Thus, the *P*-value must be less than 0.004 to be considered statistically significant.

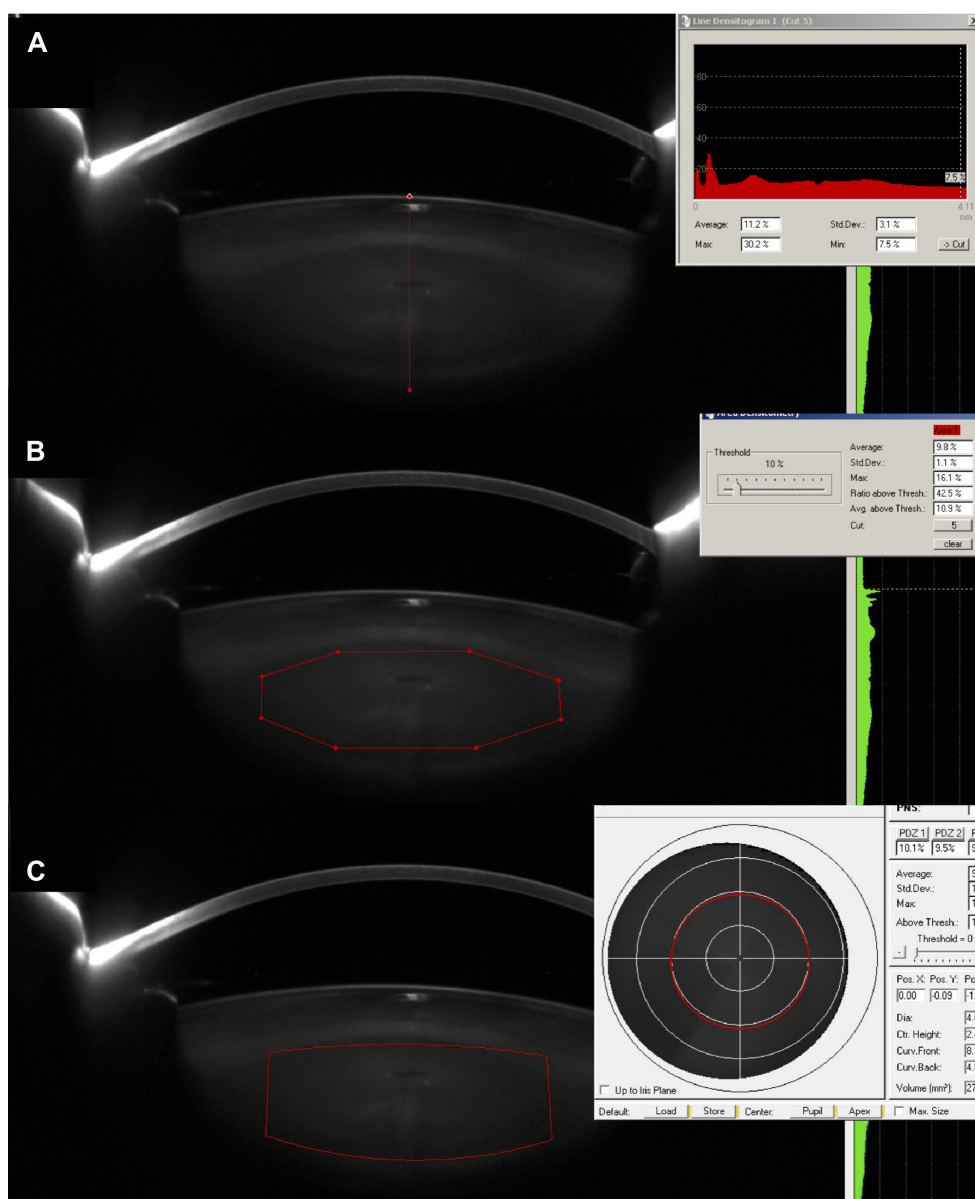


**Figure 1** Densitometric analysis modes.

**Notes:** (A) Linear mode evaluates the density of a vertical line manually drawn along the axial length of the crystalline lens (red line). (B) Region of interest mode provides a density assessment inside an elliptical area manually drawn and centered on the lens nucleus (red lines). (C) Three-dimensional (3D) mode automatically generates a cylindrical template for the density measurement (red lines). The 3D template was placed in the center of the nucleus, excluding the anterior and posterior cortex.

**Abbreviation:** PNS, Pentacam Nuclear Staging.

## Results

A stop-and-chop technique was performed in 50 eyes of 50 patients (30 women, 20 men) with age-related nuclear cataract. No intraoperative complications occurred. The mean age of the patients was  $71.52 \pm 7.71$  years (range: 57 to 75 years). The mean NO grade was  $2.88 \pm 1.02$  (range: 1.0 to 4.0). There were four eyes with grade 1, 15 eyes with

grade 2, 15 eyes with grade 3, and 16 eyes with grade 4. Table 1 displays the cataract evaluation by the LOCS III classification and the different Scheimpflug densitometric modes.

Table 2 shows the correlation coefficients between the LOCS III NO score and the quantification variables obtained from the different densitometric modes. There was a positive correlation between the NO score and the average

**Table 1** Densitometric data provided by the different evaluation methods

Cataract evaluation	Range	Mean ± SD
Nuclear opalescence (score)	1.0–4.0	2.88±1.02
Linear average density (%)	7.9–11.9	9.69±0.96
Linear maximum density (%)	9.8–29.8	17.61±4.90
ROI average density (%)	6.3–11.4	8.44±0.87
ROI maximum density (%)	6.2–19.2	12.11±2.63
3D average density (%)	6.3–11.4	8.46±0.90
3D maximum density (%)	6.2–18.0	11.97±2.23

**Abbreviations:** ROI, region of interest; 3D, three-dimensional; SD, standard deviation.

density and the maximum density derived from the 3D mode ( $r=0.624, P<0.001$ ;  $r=0.619, P<0.001$ , respectively) and the ROI mode ( $r=0.600, P<0.001$ ;  $r=0.642, P<0.001$ , respectively). Regarding the linear mode, only the average density parameter presented a significant relationship with the NO score ( $r=0.569, P<0.001$ ).

The mean CDE was  $7.22\pm 3.38$  %/s (range: 1.78 to 20.19 %/s) and the mean total US time was  $40.61\pm 19.26$  s (range: 12.90 to 102.70 s). Table 3 shows the correlation coefficients between the phacoemulsification parameters and the different evaluation methods. The densitometric parameters derived from the 3D and ROI modes showed the highest correlation coefficients with the phacoemulsification parameters ( $P<0.001$ ). The NO score showed only significant correlation with total US time ( $\rho=0.481, P<0.001$ ; Figure 2). The average density was the only parameter derived from the linear mode that showed a significant correlation with CDE ( $\rho=0.522, P<0.001$ ) and total US time ( $\rho=0.450, P<0.001$ ). As shown in Figure 3, the 3D-derived average density and maximum density were positively correlated with CDE ( $\rho=0.682$  and  $\rho=0.683$ , respectively) and total US time ( $\rho=0.631$  and  $\rho=0.668$ , respectively). Figure 4 displays the linear relationship between average density and maximum density of the ROI mode and CDE

**Table 2** Correlation coefficients between nuclear opalescence and the quantification parameters derived from the different densitometry methods

Cataract evaluation	Nuclear opalescence	
	Correlation coefficient	P-value
Linear average density	0.569	<0.001
Linear maximum density	0.045*	0.766
ROI average density	0.600	<0.001
ROI maximum density	0.642	<0.001
3D average density	0.624	<0.001
3D maximum density	0.619	<0.001

**Note:** \*Spearman correlation coefficient.

**Abbreviations:** ROI, region of interest; 3D, three-dimensional.

**Table 3** Spearman correlation coefficients between the phacoemulsification parameters and the different evaluation methods

Cataract evaluation	CDE		Total US time	
	Correlation coefficient	P-value	Correlation coefficient	P-value
Nuclear opalescence	0.414	0.004	0.481	<0.001
Linear average density	0.522	<0.001	0.450	<0.001
Linear maximum density	0.024	0.871	0.044	0.722
ROI average density	0.686	<0.001	0.642	<0.001
ROI maximum density	0.598	<0.001	0.644	<0.001
3D average density	0.682	<0.001	0.631	<0.001
3D maximum density	0.683	<0.001	0.668	<0.001

**Abbreviations:** CDE, cumulative dissipated energy; US, ultrasound; ROI, region of interest; 3D, three-dimensional.

( $\rho=0.686$  and  $\rho=0.598$ , respectively) and total US time ( $\rho=0.642$  and  $\rho=0.644$ , respectively).

**Discussion**

The aim of this study was to evaluate the relationship of the different lens densitometric modes available in the Pentacam system with their clinical applicability. Concerning this topic, factors that compromise the comparison of results and conclusions of previous studies are the different densitometric evaluation methods (such as PNS score, peak mode, ROI mode, and external software) and the use of different phacoemulsification techniques (such as phaco-chop and stop-and-chop).<sup>11–13,15</sup> Although the LOCS III classification is a validated cataract grading system, there are some issues regarding interobserver and intraobserver variability.<sup>1,16</sup> The Pentacam is a noncontact Scheimpflug system for objective imaging of the anterior segment of the eye, which provides highly reproducible measurements. This device allows objective measurements of the lens nuclear density, representing an acceptable option to the LOCS III grading system.<sup>8,12</sup>

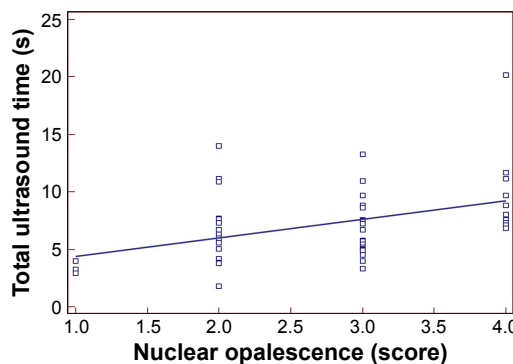


**Figure 2** Relationship between total ultrasound time and nuclear opalescence.



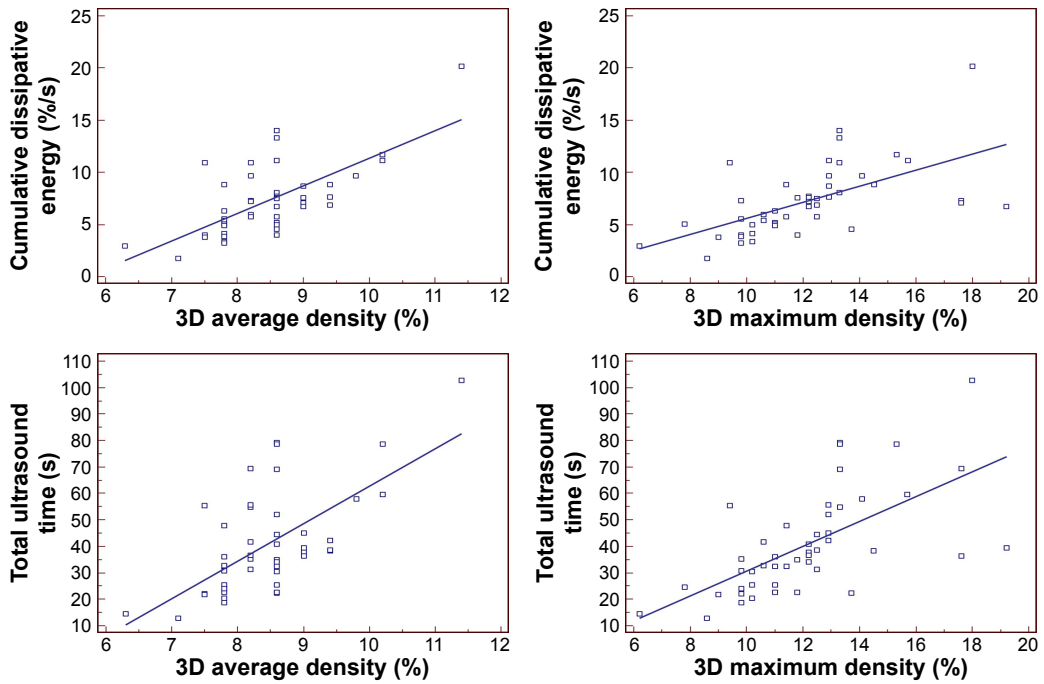


Figure 3 Relationship of average density and maximum density derived from the three-dimensional mode with cumulative dissipated energy and total ultrasound time. Abbreviation: 3D, three-dimensional.

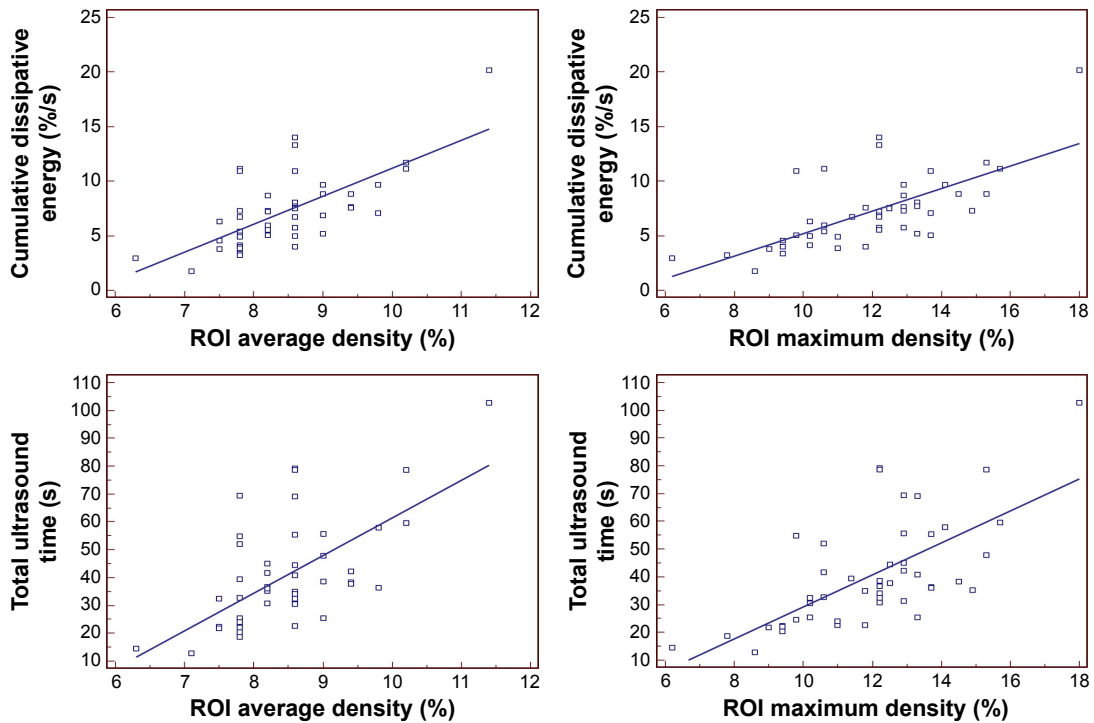


Figure 4 Relationship of average density and maximum density derived from the region of interest mode with cumulative dissipated energy and total ultrasound time. Abbreviation: ROI, region of interest.

We need to comment about certain aspects of the methodology of the present study. Regarding the LOCS III classification, we did not consider the “nucleus color” evaluation since previous studies have reported that lens density has a stronger correlation with NO.<sup>10,12</sup> Nuclear cataracts with an NO score higher than 4.1 were not included in the present study group. In these specific cases, the lens density is too high to allow light to pass through the nucleus and may induce erroneous densitometric values.<sup>7</sup> Regarding the densitometry evaluation, we selected the linear, ROI, and 3D modes for analysis, which are available in the same imaging device. Compared to the PNS grading score, these methods are displayed on a continuous scale, allowing a more precise measurement of lens density.<sup>4,7,12,15</sup> Although the peak mode is a method used in previous studies, we did not consider it based on repeatability reports.<sup>7</sup> After a careful literature review, we noticed that the value provided by the peak mode basically corresponds to the maximum lens density of the linear mode used in the present study.

We found a positive correlation between the NO score and most of the nuclear density metrics, excluding the maximum density of the linear mode ( $P=0.766$ ). We presume that this result was due to the inclusion of the anterior cortical area of the lens in the densitometric analysis of the cited mode, which is the main region of opacification in most eyes.<sup>7,12</sup> Another issue might be the presence of reflex artifacts in front of or within the lens.<sup>7</sup> It is an inherent problem in this technology that may lead to higher and false maximum values.

Concerning the ROI and 3D modes, the maximum density achieved similar correlation coefficients with the NO score ( $\rho=0.642$  and  $\rho=0.619$ , respectively) compared to the average density metric ( $\rho=0.600$  and  $\rho=0.624$ , respectively).

In order to increase the validity of the study, the same surgeon (FFC) performed all surgeries. “Stop-and-chop” was the selected surgical technique, since the US energy consumption for the central groove creation at the beginning of the procedure is closely related to the nuclear density. Since harder nuclei require more energy, the US energy consumption is representative of the nucleus hardness. A greater correlation was found with the metrics derived from the 3D and ROI modes. These findings suggest that proper selection and placement of the densitometric template may help predict phacodynamics in nuclear cataracts. We did not include the estimated balanced salt solution used in the analysis since this parameter was not correlated with Scheimpflug-measured lens density or the LOCS III score in previous studies.<sup>11,16</sup>

There are some limitations related to Scheimpflug imaging, since it is challenging to assess the posterior part of the crystalline lens, even in full mydriasis.<sup>8,10</sup> Further studies with new anterior segment imaging modalities, such as anterior segment optical coherence tomography, may provide new insights into lens density measurement, allowing more precise evaluation of the opacification in specific areas.<sup>17</sup> Other limitations of this study are the small number of cases and the exclusion of cortical and nuclear cataracts with NO score higher than 4.1 on the LOCS III classification.

## Conclusion

Although having different analysis algorithms (area versus volume), the metrics of the ROI and the 3D modes presented similar correlations with LOCS III classification and phacodynamics. The present study also alerts to the fact that proper selection and placement of the densitometric template are essential for correct evaluation of nuclear cataracts. Further studies for densitometric template and metrics optimization are required.

## Disclosure

Dr Ambrósio is a consultant for OCULUS Optikgeräte GmbH (Wetzlar, Germany), Alcon (Fort Worth, TX, USA), and Carl Zeiss Meditec (Jena, Germany). The other authors report no conflicts of interest in this work.

## References

- Chylack LT Jr, Wolfe JK, Singer DM, et al. The Lens Opacities Classification System III. The Longitudinal Study of Cataract Study Group. *Arch Ophthalmol*. 1993;111:831–836.
- Karbassi M, Khu PM, Singer DM, Chylack LT Jr. Evaluation of lens opacities classification system III applied at the slitlamp. *Optom Vis Sci*. 1993;70:923–928.
- Chylack LT Jr, Wolfe JK, Friend J, et al. Validation of methods for the assessment of cataract progression in the Roche European-American Anticataract Trial (REACT). *Ophthalmic Epidemiol*. 1995;2:59–75.
- Kirkwood BJ, Hendicott PL, Read SA, Pesudovs K. Repeatability and validity of lens densitometry measured with Scheimpflug imaging. *J Cataract Refract Surg*. 2009;35:1210–1215.
- Datiles MB 3rd, Magno BV, Freidlin V. Study of nuclear cataract progression using the National Eye Institute Scheimpflug system. *Br J Ophthalmol*. 1995;79:527–534.
- Magno BV, Freidlin V, Datiles MB 3rd. Reproducibility of the NEI Scheimpflug Cataract Imaging System. *Invest Ophthalmol Vis Sci*. 1994;35:3078–3084.
- Weiner X, Baumeister M, Kohnen T, Bühren J. Repeatability of lens densitometry using Scheimpflug imaging. *J Cataract Refract Surg*. 2014;40:756–763.
- Pei X, Bao Y, Chen Y, Li X. Correlation of lens density measured using the Pentacam Scheimpflug system with the Lens Opacities Classification System III grading score and visual acuity in age-related nuclear cataract. *Br J Ophthalmol*. 2008;92:1471–1475.
- Ortiz D, Alio JL, Ruiz-Colecha J, Oser U. Grading nuclear cataract opacity by densitometry and objective optical analysis. *J Cataract Refract Surg*. 2008;34:1345–1352.

10. Grewal DS, Brar GS, Grewal SP. Correlation of nuclear cataract lens density using Scheimpflug images with Lens Opacities Classification System III and visual function. *Ophthalmology*. 2009;116:1436–1443.
11. Kim JS, Chung SH, Joo CK. Clinical application of a Scheimpflug system for lens density measurements in phacoemulsification. *J Cataract Refract Surg*. 2009;35:1204–1209.
12. Gupta M, Ram J, Jain A, Sukhija J, Chaudhary M. Correlation of nuclear density using the Lens Opacity Classification System III versus Scheimpflug imaging with phacoemulsification parameters. *J Cataract Refract Surg*. 2013;39:1818–1823.
13. Lim SA, Hwang J, Hwang KY, Chung SH. Objective assessment of nuclear cataract: comparison of double-pass and Scheimpflug systems. *J Cataract Refract Surg*. 2014;40:716–721.
14. Magalhaes FP, Costa EF, Cariello AJ, Rodrigues EB, Hoffing-Lima AL. Comparative analysis of the nuclear lens opalescence by the Lens Opacities Classification System III with nuclear density values provided by Oculus Pentacam: a cross-section study using Pentacam Nucleus Staging software. *Arq Bras Oftalmol*. 2011;74:110–113.
15. Nixon DR. Preoperative cataract grading by Scheimpflug imaging and effect on operative fluidics and phacoemulsification energy. *J Cataract Refract Surg*. 2010;36:242–246.
16. Davison JA, Chylack LT. Clinical application of the lens opacities classification system III in the performance of phacoemulsification. *J Cataract Refract Surg*. 2003;29:138–145.
17. Wong AL, Leung CK, Weinreb RN, et al. Quantitative assessment of lens opacities with anterior segment optical coherence tomography. *Br J Ophthalmol*. 2009;93:61–65.

### Clinical Ophthalmology

#### Publish your work in this journal

Clinical Ophthalmology is an international, peer-reviewed journal covering all subspecialties within ophthalmology. Key topics include: Optometry; Visual science; Pharmacology and drug therapy in eye diseases; Basic Sciences; Primary and Secondary eye care; Patient Safety and Quality of Care Improvements. This journal is indexed on

Submit your manuscript here: <http://www.dovepress.com/clinical-ophthalmology-journal>

PubMed Central and CAS, and is the official journal of The Society of Clinical Ophthalmology (SCO). The manuscript management system is completely online and includes a very quick and fair peer-review system, which is all easy to use. Visit <http://www.dovepress.com/testimonials.php> to read real quotes from published authors.

Dovepress



# **CHAPTER V**

RELATIONSHIP BETWEEN OBJECTIVE METRICS FOR  
QUANTIFYING CRYSTALLINE LENS DYSFUNCTION WITH  
VISUAL IMPAIRMENT AND PHACODYNAMICS PARAMETERS IN  
PATIENTS WITH AGE-RELATED NUCLEAR CATARACT



ORIGINAL ARTICLE

## Correlations of Objective Metrics for Quantifying Dysfunctional Lens Syndrome With Visual Acuity and Phacodynamics

Fernando Faria-Correia, MD; Isaac Ramos, MD; Bernardo Lopes, MD; Tiago Monteiro, MD; Nuno Franqueira, MD; Renato Ambrósio, Jr., MD, PhD

### ABSTRACT

**PURPOSE:** To study the relationship between objective metrics for quantifying crystalline lens dysfunction with visual impairment and phacodynamics parameters in age-related nuclear cataracts.

**METHODS:** A total of 51 eyes (34 patients) with age-related nuclear cataract had phacoemulsification. The Dysfunctional Lens Index (0 to 10 points) was measured by a ray-tracing aberrometry (iTrace Visual Function Analyzer; Tracey Technologies, Houston, TX). The average lens density (0 to 100) was evaluated using a rotating Scheimpflug system (Pentacam HR; Oculus Optikgeräte GmbH, Wetzlar, Germany), and the nuclear opalescence score was subjectively assessed using the Lens Opacities Classification System III (LOCS III). The different parameters for evaluating crystalline lens dysfunction were correlated with preoperative corrected distance visual acuity (CDVA) and cumulative dissipated energy (CDE).

**RESULTS:** There was a negative linear correlation between the Dysfunctional Lens Index and the LOCS III nuclear opalescence and Scheimpflug-measured average density ( $r = -0.728$  and  $r = -0.771$ , respectively; both  $P < .01$ ). The preoperative CDVA was correlated with the Scheimpflug-measured lens nuclear density value ( $r = 0.612$ ,  $P < .01$ ) and Dysfunctional Lens Index score A ( $r = -0.670$ ,  $P < .01$ ). The CDE was more strongly correlated with Dysfunctional Lens Index and Scheimpflug-derived average density ( $r = -0.744$  and  $r = 0.700$ , respectively; both  $P < .01$ ) than with LOCS III nuclear opalescence ( $r = 0.646$ ,  $P < .01$ ).

**CONCLUSIONS:** The Dysfunctional Lens Index was correlated with the Scheimpflug-measured average density, subjective lens grading, and preoperative CDVA. This metric also presented the highest correlation with phacodynamics. Correlation with other clinical measures related to visual quality and impairment are still needed.

[*J Refract Surg.* 2017;33(2):79-83.]

**A**ppropriate assessment of dysfunctional lens and cataract is essential for documenting the condition and deciding whether to proceed with refractive cataract surgery. Objective measurements are also fundamental for assessing the outcomes, determining strategies for improving the results, and minimizing intraoperative and postoperative complications. The Lens Opacities Classification System III (LOCS III) is an accepted subjective and cost-effective grading method based on slit-lamp examination.<sup>1,2</sup> Previous studies have shown that the issues of the reproducibility of this classification are essentially related to interobserver and intraobserver variations.<sup>3</sup>

Scheimpflug imaging provides more precise and reliable lens densitometry measurements compared to the LOCS III grading system.<sup>4-7</sup> Different methods have been described to quantify cataract density from the Scheimpflug images, and some were found to be better with lens grading and visual performance than others.<sup>8-10</sup> Scheimpflug imaging also enabled us to analyze the relationship between lens densitometry and phacodynamics.<sup>11-15</sup>

Wavefront sensors are useful tools for the evaluation of patients with different grades of cataract because higher order aberrations play an essential role in the reduction of optical performance in patients with age-related cataract.<sup>16-18</sup> The

From Hospital de Braga, Braga, Portugal (FF-C, TM, NF); Life and Health Sciences Research Institute (ICVS), School of Health Sciences, University of Minho, Braga, Portugal (FF-C, TM); ICVS/3B's - PT Government Associate Laboratory, Braga/Guimarães, Portugal (FF-C, TM); Rio de Janeiro Corneal Tomography and Biomechanics Study Group, Rio de Janeiro, Brazil (FF-C, IR, BL, RA); Instituto de Olhos Renato Ambrósio (BL, RA), Rio de Janeiro, Brazil; VisareRio, Rio de Janeiro, Brazil (RA); Federal University of São Paulo, São Paulo, Brazil (RA); and Hospital de Olhos Santa Luzia, Maceió, Brazil (IR).

Submitted: June 27, 2016; Accepted: November 16, 2016

Dr. Ambrósio is a consultant for Oculus (Wetzlar, Germany), Alcon (Fort Worth, Texas), and Carl Zeiss Meditec (Jena, Germany). The remaining authors have no financial or proprietary interest in the materials presented herein.

Correspondence: Fernando Faria-Correia, MD, Avenida de Bessa, Edifício Boapor II, 216, 7ª Frente, 4100-012 Porto-Portugal. E-mail: f.faria.correia@gmail.com

doi:10.3928/1081597X-20161206-05

## Quantifying Dysfunctional Lens Syndrome/Faria-Correia et al

iTrace Visual Function Analyzer (Tracey Technologies, Houston, TX) is a ray-tracing aberrometry system that provides several parameters, including the Dysfunctional Lens Index (DLI). A previous study demonstrated a relationship between the DLI and other methods of cataract assessment, such as Scheimpflug-based lens density and the LOCS III grading score.<sup>19</sup>

The aim of the current study was to investigate the relationship between the different lens evaluation methods, including DLI and Scheimpflug densitometry, and phacodynamics in age-related nuclear cataracts.

### PATIENTS AND METHODS

This retrospective single-center study included patients who were recruited for a clinical visit in the Cornea and Refractive Surgery Department, Hospital de Braga (Portugal) from September 2015 to May 2016. The study was approved by the institutional review board and complied with the tenets of the Declaration of Helsinki. No patient had a history of ocular disease, ocular surgery, or general disorders affecting vision, such as macular disease, diabetic retinopathy, or uveitis. All patients underwent a complete ophthalmic examination, which included corrected distance visual acuity measurement (CDVA; recorded in logMAR units), noncontact tonometry, slit-lamp biomicroscopy, and dilated fundus examination. The nuclear sclerotic grade was classified according to the LOCS III.<sup>2</sup> The same ophthalmologist examined all patients using a slit-lamp microscope after pupil dilation with a combination of topical 1.0% tropicamide and 10% phenylephrine. LOCS III nuclear opacity was graded on a scale of 0.1 to 6.9 by comparing a digital photograph of each lens to standard color photographic transparencies of nuclear opalescence. Exclusion criteria were: eyes with poor mydriasis, any corneal opacities, a LOCS III nuclear cataract grade greater than 5.1, and any cortical opacities.

### SCHEIMPFLUG SYSTEM MEASUREMENT

The Pentacam HR (Oculus Optikgeräte GmbH, Wetzlar, Germany) is a Scheimpflug-based device that generates a three-dimensional representation of the anterior segment of the eye. In less than 2 seconds, the rotating camera captures up to 25 slit-images of the anterior segment, collecting 25,000 true elevation data points. For this study, we excluded scans with artifacts that would interfere with the densitometry results (ie, presence of cortical shadowing artifacts or misplacement of the reference template). The Pentacam Nuclear Staging software allows the measurement of objective crystalline lens densitometry. The software automatically generates a cylindrical template for the density measurement (Figure A, available in the online version of this article).

The template volume used for the study had the following features: 4-mm diameter, 2.4-mm height, 8.3-mm front curvature, and 4.8-mm back curvature. The three-dimensional template was placed in the center of the nucleus, excluding the anterior and posterior cortex, to permit objective quantification of lens opacities inside the template (average density and maximum density parameters) on a continuous scale from 0 to 100 points. For the study purpose, the average density parameter was recorded.

### WAVEFRONT MEASUREMENT

The i-Trace (Tracey Technologies, Houston, TX), which combines a ray-tracing aberrometer with a Placido-disc topographer, was used for wavefront analysis. Three measurements of each eye were also taken in a dark room. The wavefront was measured in a 4-mm optical zone set by the software, and the DLI was recorded for each eye included in the study. This parameter is an objective lens performance parameter provided by the wavefront sensor and calculated based on the internal higher order aberrations, pupil size, and contrast sensitivity data (Figure 1). This objective index ranks overall lens performance from 0 (very poor) to 10 (excellent) points.

### SURGICAL TECHNIQUE

All patients received clear corneal phacoemulsification and posterior chamber intraocular lens implantation by the same surgeon (FF-C) under local anesthesia. The stop-and-chop phacoemulsification technique was performed with a Kelman micro-tip (0.9 mm, 45°) using the Infiniti System (Alcon Laboratories, Inc., Fort Worth, TX). At the end of the nucleus management, the cumulative dissipated energy (CDE) parameter was recorded. No intraoperative complications occurred.

### DATA AND STATISTICAL ANALYSIS

All results were analyzed using MedCalc software (version 14.12.02; MedCalc, Ostend, Belgium). Values are presented as means  $\pm$  standard deviations. Data normality was assessed using the Kolmogorov-Smirnov test. Significant correlations were evaluated using Pearson or Spearman correlation coefficients according to data normality. A *P* value of .05 or less was considered to be statistically significant.

### RESULTS

A total of 51 eyes of 34 patients were included in the study. The study population consisted of 20 women and 14 men. Mean age was 70.77  $\pm$  9.19 years (range: 52 to 90 years) and mean preoperative CDVA was 0.24  $\pm$  0.16



Quantifying Dysfunctional Lens Syndrome/Faria-Correia et al

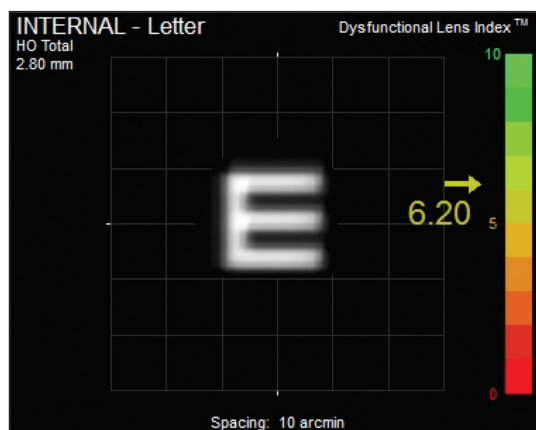


**Figure 1.** Dysfunctional Lens Index measured by ray-tracing aberrometry of a patient with age-related nuclear cataract.

TABLE 1  
**Cataract Evaluation by the Different Methods**

Parameter	Range	Mean ± SD
LOCS III NO score	1.0 to 5.0	2.75 ± 1.19
Average density <sup>a</sup>	6.3 to 11.0	8.22 ± 1.16
DLI <sup>b</sup>	1.2 to 10.0	5.93 ± 2.49

SD = standard deviation; LOCS III = Lens Opacities Classification System III; NO = nuclear opalescence; DLI = Dysfunctional Lens Index  
<sup>a</sup>Based on the Scheimpflug system.  
<sup>b</sup>Based on the ray-tracing system.

density ( $r = -0.744$  and  $r = 0.700$ , respectively; both  $P < .01$ ) than with LOCS III nuclear opalescence score ( $r = 0.646$ ,  $P < .01$ ).

**DISCUSSION**

The aim of this study was to evaluate the relationship of the different cataract evaluation methods with phacodynamics. Because the demand for refractive cataract surgery has increased, objective lens evaluation methods are useful in clinical practice.<sup>20,21</sup> Integrating new concepts may help in preoperative counseling and patient education.

Similar to a previous study, we also found that the DLI measured by ray-tracing aberrometry was correlated with Scheimpflug-derived nuclear density in eyes with age-related nuclear cataract.<sup>19</sup> This metric also presented a significant relationship with preoperative CDVA and phacodynamics.

Although the LOCS III classification is a validated cataract grading system, there are some issues regarding interobserver and intraobserver variability.<sup>3,7</sup> To avoid these limitations, Scheimpflug imaging enables objective and repeatable lens densitometry measurements.<sup>9,10</sup> In previous studies, this technology presented a stronger relationship with CDE compared to LOCS III grading scores.<sup>11-13</sup>

(range: 0 to 0.7). **Table 1** shows the patients' cataract evaluation scores obtained with the different methods.

The DLI showed a high negative linear correlation with the LOCS III nuclear opalescence score ( $r = -0.728$ ,  $P < .01$ ). The average nuclear density was positively correlated with the LOCS III nuclear opalescence score ( $r = 0.680$ ,  $P < .01$ ).

The preoperative CDVA was correlated with the LOCS III nuclear opalescence score ( $r = 0.564$ ,  $P < .01$ ) and with the Scheimpflug-measured lens nuclear density value ( $r = 0.612$ ,  $P < .01$ ). However, the DLI score presented the strongest correlation with CDVA ( $r = -0.670$ ,  $P < .01$ ) compared to the other evaluation methods (**Figure 2**).

The mean CDE was  $8.92 \pm 6.70$  (range: 0.05 to 21.42). **Table 2** and **Figure 3** show the relationships between the CDE and the following parameters: LOCS III nuclear opalescence score, Scheimpflug-measured average density, and DLI. The CDE had stronger relationships with the DLI and Scheimpflug-measured lens nuclear

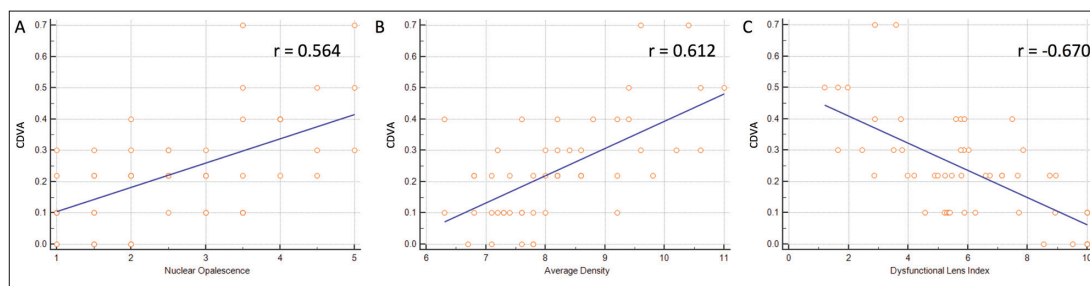


**Figure 2.** Relationships between corrected distance visual acuity (CDVA) and (A) nuclear opalescence, (B) average density, and (C) Dysfunctional Lens Index.

Quantifying Dysfunctional Lens Syndrome/Faria-Correia et al

TABLE 2  
Relationships Between CDE and LOCS III NO Score, Average Density, and DLI

Parameter	CDE	
	R	P
LOCS III NO score	0.646	< .01
Average density <sup>a</sup>	0.700	< .01
DLI <sup>b</sup>	-0.744	< .01

CDE = cumulative dissipated energy; LOCS III = Lens Opacities Classification System III; NO = nuclear opalescence; DLI = Dysfunctional Lens Index

<sup>a</sup>Based on the Scheimpflug system.

<sup>b</sup>Based on the ray-tracing system.

Wavefront analysis objectively evaluates the visual deterioration by quantifying the higher order aberrations of the ocular optical system. Nuclear sclerosis is an age-related process that contributes to vision deterioration and lens optical densitometry changes.<sup>16</sup> Previous reports demonstrated a relationship between internal higher order aberrations and nuclear cataracts.<sup>17,18,22</sup>

Other available wavefront sensors may also provide an objective lens score, such as the Optical Quality Analysis System (Visiometrics, Terrasa, Spain). This double-pass system measures the Objective Scatter Index that represents the degree of objective scattering caused by deterioration of ocular transparency.<sup>23</sup> Literature review shows that the Objective Scatter Index metric is useful for the quantification of nuclear cataracts.<sup>14,23-25</sup> Lim et al. described a significant relationship between the Objective Scatter Index with the Scheimpflug-derived lens density and phacodynamics.<sup>14</sup> The DLI based on a ray-tracing aberrometry system was significantly correlated with the LOCS III nuclear opalescence score and the Scheimpflug-derived lens densitometry. In this study, we also found a correlation between the visual performance with the

LOCS III nuclear opalescence score, Scheimpflug-measured lens, and DLI. The preoperative CDVA showed a higher correlation with the DLI than with the LOCS III nuclear opalescence score and average density. A previous study reported similar findings regarding the correlations between these variables and CDVA.<sup>19</sup> The differences found in the correlation coefficients may be justified by the distinct inclusion criteria because we enrolled eyes with nuclear opalescence scores higher than 3 in the LOCS III grading system.

Concerning phacodynamics, the same surgeon (FF-C) performed all surgeries to guarantee the validity of the study. Because harder nuclei require more energy, the CDE metric is representative of the nucleus hardness. In the current study, the CDE presented a stronger correlation with the DLI compared to Scheimpflug-derived lens density and LOCS III nuclear opalescence score. These findings suggest the applicability of using this objective parameter to predict phacodynamics.

This study has some limitations. There is no consensus regarding the most representative Scheimpflug-based densitometry method and variable of the lens nucleus. The automatic densitometry method was selected because it is considered to be the most repeatable one.<sup>9</sup> Another inherent limitation of this technology is the presence of reflex artifacts in front of or within the lens. The presence of these findings may lead to higher and false maximum values. For this reason, the maximum lens density parameter was not included in the analysis.<sup>9,10</sup>

Other limitations of this study are the small number of cases and the absence of age-matched controls. "Nucleus color" evaluation was not considered in the methodology because previous studies have reported that lens density had a stronger correlation with nuclear opalescence.<sup>5,12</sup>

The DLI based on the ray-tracing aberrometry system was useful for the objective assessment and phacodynamics prediction in eyes with age-related nuclear

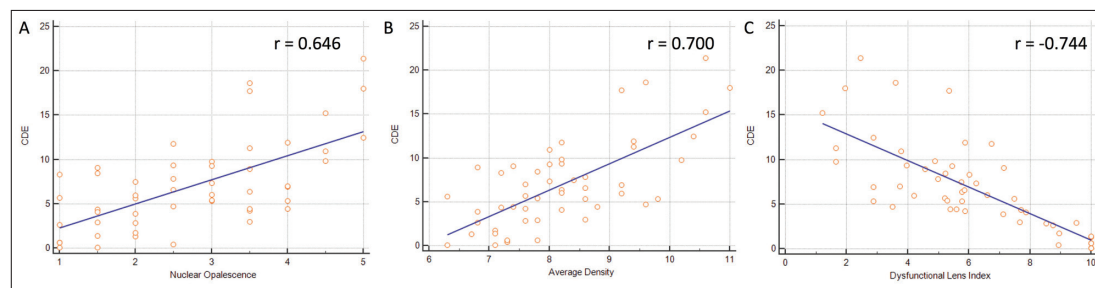


Figure 3. Relationships between cumulative dissipated energy (CDE) and (A) nuclear opalescence, (B) average density, and (C) Dysfunctional Lens Index.

Quantifying Dysfunctional Lens Syndrome/Faria-Correia et al

cataracts. This parameter was also correlated with other cataract evaluation methods, such as the LOCS III grading system and the Scheimpflug-based lens density. To our knowledge, this study is the first to study the relationship between the DLI and cataract surgery. The DLI parameter may indicate the functional status of the lens nucleus and can help predict phacodynamics in cataract surgery.

**AUTHOR CONTRIBUTIONS**

Study concept and design (FF-C); data collection (FF-C, IR, BL, TM, NF, RA); analysis and interpretation of data (FF-C, RA); writing the manuscript (FF-C); critical revision of the manuscript (FF-C, IR, BL, TM, NF, RA)

**REFERENCES**

- Chylack LT Jr, Wolfe JK, Friend J, et al. Quantitating cataract and nuclear brunescence, the Harvard and LOCS systems. *Optom Vis Sci.* 1993;70:886-895.
- Chylack LT, Wolfe JK, Singer DM, et al. The Lens Opacities Classification System III. The Longitudinal Study of Cataract Study Group. *Arch Ophthalmol.* 1993;111:831-836.
- Karbassi M, Khu PM, Singer DM, Chylack LT Jr. Evaluation of lens opacities classification system III applied at the slitlamp. *Optom Vis Sci.* 1993;70:923-928.
- Datiles MB 3rd, Magno BV, Freidlin V. Study of nuclear cataract progression using the National Eye Institute Scheimpflug system. *Br J Ophthalmol.* 1995;79:527-534.
- Grewal DS, Brar GS, Grewal SP. Correlation of nuclear cataract lens density using Scheimpflug images with Lens Opacities Classification System III and visual function. *Ophthalmology.* 2009;116:1436-1443.
- Magalhães FP, Costa EF, Cariello AJ, Rodrigues EB, Hofling-Lima AL. Comparative analysis of the nuclear lens opalescence by the Lens Opacities Classification System III with nuclear density values provided by Oculus Pentacam: a cross-section study using Pentacam Nucleus Staging software. *Arq Bras Ophthalmol.* 2011;74:110-113.
- Pei X, Bao Y, Chen Y, Li X. Correlation of lens density measured using the Pentacam Scheimpflug system with the Lens Opacities Classification System III grading score and visual acuity in age-related nuclear cataract. *Br J Ophthalmol.* 2008;92:1471-1475.
- Ullrich K, Pesudovs K. Comprehensive assessment of nuclear and cortical backscatter metrics derived from rotating Scheimpflug images. *J Cataract Refract Surg.* 2012;38:2100-2107.
- Weiner X, Baumeister M, Kohnen T, Bühren J. Repeatability of lens densitometry using Scheimpflug imaging. *J Cataract Refract Surg.* 2014;40:756-763.
- Kirkwood BJ, Hendicott PL, Read SA, Pesudovs K. Repeatability and validity of lens densitometry measured with Scheimpflug imaging. *J Cataract Refract Surg.* 2009;35:1210-1215.
- Faria-Correia F, Lopes BT, Ramos IC, Monteiro T, Franqueira N, Ambrósio R Jr. Application of different Scheimpflug-based lens densitometry methods in phacodynamics prediction. *Clin Ophthalmol.* 2016;10:609-615.
- Gupta M, Ram J, Jain A, Sukhija J, Chaudhary M. Correlation of nuclear density using the Lens Opacity Classification System III versus Scheimpflug imaging with phacoemulsification parameters. *J Cataract Refract Surg.* 2013;39:1818-1823.
- Kim JS, Chung SH, Joo CK. Clinical application of a Scheimpflug system for lens density measurements in phacoemulsification. *J Cataract Refract Surg.* 2009;35:1204-1209.
- Lim SA, Hwang J, Hwang KY, Chung SH. Objective assessment of nuclear cataract: comparison of double-pass and Scheimpflug systems. *J Cataract Refract Surg.* 2014;40:716-721.
- Nixon DR. Preoperative cataract grading by Scheimpflug imaging and effect on operative fluidics and phacoemulsification energy. *J Cataract Refract Surg.* 2010;36:242-246.
- Alió JL, Schimchak P, Negri HP, Montés-Micó R. Crystalline lens optical dysfunction through aging. *Ophthalmology.* 2005;112:2022-2029.
- Rocha KM, Nosé W, Bottós K, Bottós J, Morimoto L, Soriano E. Higher-order aberrations of age-related cataract. *J Cataract Refract Surg.* 2007;33:1442-1446.
- Faria-Correia F, Lopes B, Monteiro T, Franqueira N, Ambrósio R Jr. Scheimpflug lens densitometry and ocular wavefront aberrations in patients with mild nuclear cataract. *J Cataract Refract Surg.* 2016;42:405-411.
- Faria-Correia F, Ramos I, Lopes B, Monteiro T, Franqueira N, Ambrósio R Jr. Comparison of dysfunctional lens index and Scheimpflug lens densitometry in the evaluation of age-related nuclear cataracts. *J Refract Surg.* 2016;32:244-248.
- Braga-Mele R, Chang D, Dewey S, et al. Multifocal intraocular lenses: relative indications and contraindications for implantation. *J Cataract Refract Surg.* 2014;40:313-322.
- Market Scope. *2013 Annual Cataract Surgeon Survey.* St. Louis: Market Scope LLC.
- Sachdev N, Ormonde SE, Sherwin T, McGhee CN. Higher-order aberrations of lenticular opacities. *J Cataract Refract Surg.* 2004;30:1642-1648.
- Guirao A, González C, Redondo M, Geraghty E, Norrby S, Artal P. Average optical performance of the human eye as a function of age in a normal population. *Invest Ophthalmol Vis Sci.* 1999;40:203-213.
- Artal P, Benito A, Perez GM, et al. An objective scatter index based on double-pass retinal images of a point source to classify cataracts. *PLoS One.* 2011;6:e16823.
- Cabot F, Saad A, McAlinden C, Haddad NM, Grise-Dulac A, Gatinel D. Objective assessment of crystalline lens opacity level by measuring ocular light scattering with a double-pass system. *Am J Ophthalmol.* 2013;155:629-635.

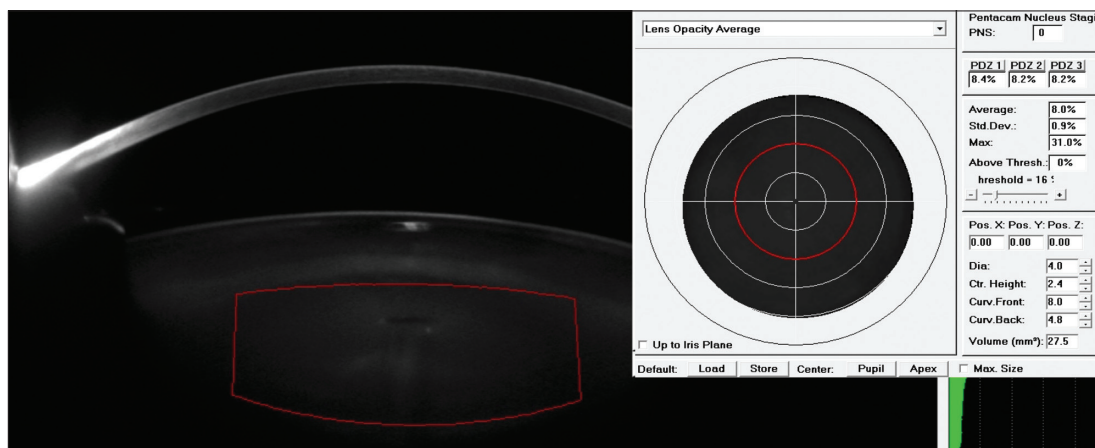


Figure A. Scheimpflug-based lens density of a patient with age-related nuclear cataract.

# **CHAPTER VI**

## DISCUSSION



## CHAPTER VI – DISCUSSION

Cataract is defined as an age-related opacity of the crystalline lens at the slit lamp and is usually associated with visual acuity reduction.(Beebe, 2011; Hockwin, 1994; Sasaki *et al.*, 1989) Epidemiological data related to this disease is undefined. WHO described cataract as the leading cause of blindness and the second most frequent cause of visual impairment worldwide.(World Health Organisation, 2013; World Health Organisation, 2016; World Health Organisation, 2016) Due to the aging of the population, the prevalence of cataracts is expected to increase in the following decades. Interestingly, this condition has an inherent social and financial impact, as it can affect the daily activities of the elderly due to low vision. Appropriate diagnosis and management are needed for national health programs, as this condition may interfere with economic and social aspects. After cataract removal, previous reports described that patients were more able to perform productive activities and there was an improvement of the quality of life.(Frick & Foster, 2003; Smith & Smith, 1996) Currently, cataract surgery is also being performed earlier, as soon as the first signs of lens opacification appear, because patients demand a better quality of vision and spectacles independence.(Braga-Mele *et al.*, 2014) Such clinical points reinforce the demand for objective methods that can measure a cataract's impact on vision, to improve our sensitivity in identifying those patients whose quality of life can be markedly improved with cataract surgery.

Standardized classification of the type of cataract is essential because it determines specific complaints, loss of functional vision, and surgical decision.(Chua *et al.*, 2004) The distinct assessment methods need to be integrated with clinical data, such as visual function and functional impairment tests, to clarify the impact of the cataract on patient's visual status or functional ability.(Pan *et al.*, 2015; Rosenberg & Sperazza, 2008; D'Ambrósio, 1999) Visual acuity is the standard measurement of visual function in cataract patients. Nevertheless, cataract patients may present relatively good visual acuity but still complain of poor vision. It has been suggested that visual acuity provides an inaccurate assessment of vision in these patients and other tests should be used to clarify the status of the crystalline lens.(Stifter *et al.*, 2005)

It is worthwhile to note that direct comparison of results and conclusions between different studies involving this ocular condition are limited by the diversity of classification systems, which use distinct evaluation methods. Slit lamp evaluation is routinely used in ophthalmological consultation. Distinct classification systems based on slit lamp findings have been developed and used to measure the type and severity of cataracts including the LOCS, Wisconsin Cataract Grading System, Age-Related Eye Disease Study Grading System or Oxford Clinical Cataract Classification System.(Chylack *et al.*, 1993; Hall *et al.*, 1997; Wong *et al.*, 2013) In 1993, Chylack *et al.* presented the LOCS III grading scale and it is the most common and standardized method used in routine practice. This method classifies the type and severity of age-related cataract and was derived from the LOCS II, that was presented in 1989.(Chylack *et al.*, 1993) It overcomes some drawbacks inherent to the previous classification scale: classification scales were quite coarse; early stages of nuclear change were not well characterized; criteria for brunescant cataracts were difficult to apply; there was no objective validation of the scaling intervals.(Chylack *et al.*, 1993) Despite the LOCS III grading system presented significant correlations with visual acuity and quality deterioration, the results also showed an intra and inter-variability among physicians.(Tan *et al.*, 2008)

The development of anterior segment imaging systems allowed the evaluation of lens density in eyes with different types of cataract. For example, Scheimpflug imaging enables objective lens densitometry evaluation that is not susceptible to observer variability, and is considered to be a more sensitive and reproducible approach.(Kirkwood *et al.*, 2009; Weiner *et al.*, 2014) The literature review demonstrates that Scheimpflug-based lens densitometry presents a significant correlation with visual acuity and LOCS III classification in age-related nuclear cataracts.(Datiles *et al.*, 1995; Grewal *et al.*, 2009; Gupta *et al.*, 2013; Pei *et al.*, 2008; Magno, Freidlin, *et al.*, 1994; Magno, Lasa, *et al.*, 1994) Although the usefulness of this technology for the preoperative evaluation of nuclear cataracts has been demonstrated, the use of different densitometric evaluation parameters and modes hampered the extrapolation of results and conclusions for clinical application.(Weiner *et al.*, 2014; Kirkwood *et al.*, 2009) Interestingly, there is a limited number of research studies regarding the relationship between the wavefront analysis and Scheimpflug-based lens densitometry. As the wavefront



analysis proved to detect changes in the crystalline lens even before a noticeable reduction in visual acuity, the study of its relationship with lens densitometry might be interesting for the detection of early forms of cataract by Scheimpflug-based densitometry, and may help to understand the application of this technology as a functional assessment tool of the crystalline lens. In this context, we selected the Scheimpflug-based lens densitometry and ray-tracing aberrometry. (**Chapters II and III**) Previous reports illustrated the advantages of the ray-tracing analysis compared to other wavefront sensors. For example, there is no confusion in the analysis of the sequential 256 points on the pupil entrance with the reflected location on the retina because of its high-speed capture. (Bartsch *et al.*, 2008; Molebny *et al.*, 2000; Rozema *et al.*, 2005)

Our results also suggest that nuclear sclerosis is an age-related process and contributes for the degradation of visual acuity. For instance, the subjective (LOCS III NO score) and the objective (PNS score, average density, and maximum density) lens evaluations presented similar relationships with age and CDVA. Thus, these findings validate the concept that an automated density analysis of nuclear sclerosis can provide comparable information to a clinician's evaluation of the lens. (**Chapter II**) We also focused on the internal HOAs measured by ray tracing wavefront analysis, since the crystalline lens is responsible for the age-related increase of ocular aberrations. (Alió *et al.*, 2005; Artal *et al.*, 2002) The RMS HOAs of the whole eye was lower than the RMS HOAs of the internal optics, which indicates the presence of nuclear sclerosis. Our results demonstrated that the comatic aberration was the most predominant HOA. (**Chapter II**) Lee *et al.* also described that comatic aberrations are increased in nuclear cataracts by using the ray tracing aberrometry. (Lee *et al.*, 2008) We present a methodological advantage compared to this study with the inclusion of Scheimpflug-based lens densitometry, as the authors classified nuclear cataracts with the LOCS III grading system. Interestingly, Lee *et al.* also described the absence of a significant relationship between the internal RMS HOAs, coma, and trefoil with the LOCS III NO score. (Lee *et al.*, 2008) Our data demonstrated that Scheimpflug-based lens densitometry data (average density and maximum density) was significantly correlated with the same wavefront variables. (**Chapter II**) In addition to confirm a relationship between the internal HOAs and the age-

related nuclear sclerosis, these results prove that lens densitometry parameters can be useful in identifying early nuclear cataract.

A previous study concluded that the PNS score is a very good parameter for preoperative planning of cataract surgery, since it presented a positive correlation with ultrasonic energy and fluid consumption.(Nixon, 2010) Our data suggests that the PNS score is not representative of the functional status of the crystalline lens compared to other quantitative parameters derived from Scheimpflug lens densitometry.(**Chapter II**) Another advantage of these quantification variables (average density and maximum density) is their presentation on a continuous scale (0-100%), allowing a more precise densitometric evaluation. In conclusion, this is the first study to describe a relationship between Scheimpflug-based lens densitometry and ray tracing wavefront analysis. Our results indicate that quantification parameters derived from Scheimpflug densitometry had a stronger relationship with the functional status of the crystalline lens in eyes with age-related nuclear cataract.

In another study we included the DLI variable based on ray tracing wavefront analysis in order to analyze its relationship with Scheimpflug-based lens densitometry.(**Chapter III**) Besides the internal HOAs, the DLI also integrates pupillometry and contrast sensitivity data, providing a more detailed overview of the internal optics performance. This variable is based on the DLS concept that was presented in 2013. (Waring IV, 2013) As mentioned before, the DLS is characterized by three sequential stages that included the age-related changes of the crystalline lens: loss of accommodation, reduction of crystalline lens transparency and change of the internal aberrations profile. (Waring IV, 2013; Waring IV, 2014) Recently, the i-Trace Visual Function Analyzer developed the DLI parameter, which ranks overall crystalline lens performance from 0 (very poor) to 10 (excellent) points and was designed specifically to measure the early age-related changes in the crystalline lens.

The findings presented in **Chapter III** demonstrated a significant relationship between the Scheimpflug-based lens densitometry and the DLI, suggesting the former as an essential tool to assess the functional state of age-related nuclear cataracts. Interestingly, our results indicate that the functional status of the crystalline lens based on CDVA evaluation is more correlated with the DLI parameter compared to LOCS III NO score and Scheimpflug-derived average

density variables. Other available wavefront sensors also provide other parameters of optical performance, such as the Optical Quality Analysis System (OQAS; Visiometrics, Terrasa, Spain). This double-pass system measures the objective scatter index (OSI) that represents the degree of scattering caused by deterioration of ocular transparency.(Guirao *et al.*, 1999) Like the results presented in **Chapter III**, previous studies also demonstrated a significant correlation between the OSI and the LOCS III NO score and Scheimpflug-based lens density in nuclear cataracts.(Artal *et al.*, 2011; Cabot *et al.*, 2013; Guirao *et al.*, 1999; Lim *et al.*, 2014) The wavefront analyzer used in this PhD thesis integrates a ray tracing aberrometer with corneal topography. By using a built-in program, the internal aberrations are measured by subtracting the corneal aberrations (calculated based on topographic data) from those of the entire eye that are acquired by the ray tracing aberrometer. Therefore, the total aberrations and HOAs derived from the crystalline lens can be measured (Figure 30).(Rozema *et al.*, 2005; Bartsch *et al.*, 2008) With the OQAS device, the OSI parameter is representative of the overall ocular system, and it does not provide a clear differentiation regarding the source of ocular scattering (cornea versus crystalline lens). Regarding the methodology presented in **Chapters II and III**, some features should be highlighted. In the study presented in **Chapter III**, we only selected the average density derived from the 3D mode, and the densitometric template was further customized and centered in the nucleus, excluding the anterior and posterior cortex. By selecting this approach, we likely avoid the anterior hyperreflective artifacts that may interfere with the densitometric readings. (Weiner *et al.*, 2014) In resume, the Scheimpflug-based lens densitometry demonstrated a significant correlation with the DLI parameter, proving that it can be considered a representative tool of the functional state of the crystalline lens. Integrating these distinct assessment methods in clinical practice should be considered as they may improve preoperative counseling, patient education and surgery indication.

Currently, the anterior segment tomography by Scheimpflug imaging is widely used in the preoperative planning of cataract surgery, especially in candidates for toric or multifocal IOLs implantation.(Maeda, 2011) The application of Scheimpflug-based lens densitometry in phacodynamics prediction was addressed in **Chapters IV and V**. The role of this technology in the prediction of

ultrasonic energy consumption during phacoemulsification has been the topic in several studies. (Gupta *et al.*, 2013; Kim *et al.*, 2009; Nixon, 2010; Weiner *et al.*, 2014; Lim *et al.*, 2014) Nevertheless, literature review also demonstrates the absence of studies that evaluate the relationship between the different lens densitometry modes with phacodynamics. The use of distinct densitometric evaluation methods (such as, PNS score, peak mode, ROI mode, external software) and different phacoemulsification techniques (such as, phaco-chop and stop-and-chop) hampers the comparison of results and conclusions of published data.(Lim *et al.*, 2014; Gupta *et al.*, 2013; Kim *et al.*, 2009; Nixon, 2010) Regarding the methodology of the study presented in **Chapter IV**, we should remark certain features. We did not include the LOCS III NC score since previous studies determined a stronger correlation between the NO with the nucleus lens densitometry and phacodynamics.(Grewal *et al.*, 2009; Gupta *et al.*, 2013; Davison & Chylack, 2003) The linear, ROI and 3D modes were selected for the nucleus densitometry analysis, since they are available in the Scheimpflug imaging system used for the study and were also described in previous studies.(Kim *et al.*, 2009; Ortiz *et al.*, 2008; Kirkwood *et al.*, 2009; Weiner *et al.*, 2014) As mention before, these methods are displayed on a continuous scale, allowing a more precise measurement of the lens density.(Weiner *et al.*, 2014; Kirkwood *et al.*, 2009; Gupta *et al.*, 2013; Nixon, 2010) Despite being a method used in previous studies, we do not consider the peak mode based on repeatability reports.(Weiner *et al.*, 2014) After a careful literature review, we noticed that the value derived from the peak mode corresponds to the maximum lens density of the linear mode. Our results demonstrated a positive correlation between the LOCS III NO score and the nuclear density metrics, except of the maximum density derived from the linear mode. We presume that this finding was due to the inclusion of the anterior cortical area of the lens in this densitometric analysis mode, which may present hyperreflective artifacts and consequently providing erroneous maximum values.(Weiner *et al.*, 2014; Gupta *et al.*, 2013) To ensure methodological validity, the same surgeon performed a “stop-and-chop” surgical technique in all procedures. We preferred to use this technique, as the US energy consumption for the central groove creation at the beginning of the surgery is closely related to the nuclear density. As harder nuclei require more energy, the US energy consumption is representative of the nucleus hardness.

We used the Infiniti System (Alcon Laboratories, Inc., Fort Worth, TX, USA) phacoemulsification platform that provides the CDE and the total US time variables. Despite having different analysis algorithms (area versus volume), the density variables derived from the ROI and 3D modes presented similar relationship with phacodynamics. The presented data also warns that proper selection and placement of the densitometry template are essential for correct evaluation in nuclear cataracts. No data is available regarding the repeatability of the ROI mode in the literature. Further studies are required to address this point. In this sequence, the relationship between objective metrics for quantifying crystalline lens dysfunction (DLI and 3D lens densitometry) and CDE in patients with age-related nuclear cataract was also evaluated (**Chapter V**). As described above, the results presented in **Chapter V** show a significant correlation between the LOCS III grading system and CDVA with the objective metrics for quantifying crystalline lens dysfunction, such as the DLI based on a ray tracing aberrometry and the Scheimpflug-derived lens densitometry. These findings are similar to those presented in **Chapter III**. The differences found in the correlation coefficients may be justified by the distinct inclusion criteria, because we enrolled eyes with NO score higher than 3.0 in the LOCS III grading system in the study presented in **Chapter V**. As mention above, the same surgeon and the “stop-and-chop” surgical technique was performed in all surgeries. In this context, the CDE is representative of the nucleus hardness. Our results demonstrated the CDE presented a stronger and significant correlation with the objective metrics (DLI and Scheimpflug-derived lens density) compared to the LOCS III NO score. Other authors described similar results. For example, Lim *et al.* also reported that OSI and Scheimpflug lens density presented a significant relationship with the CDVA and CDE.(Lim *et al.*, 2014) The differences presented in the correlation coefficients between these studies result from the distinct methodological criteria. For example, Lim *et al.* selected the maximum density parameter and the cataract surgery was performed with a different technique (phaco prechooper was used to divide the nucleus in half).(Lim *et al.*, 2014) Concerning the densitometric analysis, we selected the average density based on the 3D analysis mode and Lim *et al.* used the point of maximum density along the nucleus. Therefore, the comparison of the results derived from these studies should be carried out with precaution. In conclusion, the findings presented in **Chapter V** revealed that

Scheimpflug-derived lens densitometry and DLI based on the ray tracing aberrometry were useful for the objective assessment and phacodynamics prediction in eyes with age-related nuclear cataracts. Both objective methods were also correlated with the LOCS III grading system and may integrate the preoperative visit consultation and may help phacodynamics prediction.

Indeed, we should highlight that the CDE parameter is not available in all phacoemulsification devices and is exclusive to Alcon Laboratories, Inc. platforms. Fine *et al.* postulated the “Effective Phacoemulsification Time” parameter to compare phacoemulsification platforms.(Fine *et al.*, 2004) Further standardization of phacodynamic parameters is required for scientific and clinical purposes. Future studies including similar lens densitometry analysis methods and standardized phacodynamics variables, such as Effective Phacoemulsification Time, are also needed, to avoid incongruities between the results and conclusions.

Femtosecond lasers have been successfully implemented in anterior segment surgery, especially in refractive laser surgery for the creation of corneal lamellar flaps.(Kim *et al.*, 2011; Ratkay-Traub *et al.*, 2001) Since this technology combines the accuracy and the lowest likelihood of tissue damage, it can deliver these gains to cataract surgery with improvements in reproducibility and safety. Recently, femtosecond lasers may assist or replace several steps of cataract surgery, including the creation of clear corneal incisions, anterior capsulotomy, and lens nucleus fragmentation.(He *et al.*, 2011) When femtosecond laser is applied to the nucleus, it softens the lens and helps to reduce the overall US energy and surgical time required compared to a standard phacoemulsification procedure.(Nagy *et al.*, 2009) Preoperative Scheimpflug-based lens densitometry might be useful to improve and refine the laser settings of the femtosecond platform. Future clinical and research studies may clarify this concept in order to improve surgical outcomes and safety for the intraocular structures.

Despite the widespread acceptance of Scheimpflug imaging in the area of anterior segment surgery, we have to highlight some limitations inherent to this technology regarding the crystalline lens assessment. The drawbacks of this imaging technology are partially inherent to the optically based Scheimpflug principle. Due to the light scattering, the resolution of the densitometry tool is

influenced by the transparency of the cornea and anterior chamber, or by opacities located in the anterior region of the crystalline lens.(Kirkwood *et al.*, 2009; Weiner *et al.*, 2014) As mentioned before, the presence of reflective artifacts in front of or within the lens may also interfere with the densitometry readings.(Kirkwood *et al.*, 2009; Weiner *et al.*, 2014) By using a customized densitometry mode with proper placement in the nucleus, we likely enhance the density analysis. Another limitation is the challenging study of the posterior part of the crystalline lens, even in full mydriasis. In this PhD thesis, we only selected eyes with age-related nuclear cataracts, since this type of lens opacity is the most prevalent.(Klein *et al.*, 1998) Additionally, Scheimpflug-based lens densitometry has been found to be less reproducible in studies of the anterior cortex, posterior cortex, and posterior subcapsular opacities. These types of cataracts should be evaluated by using retroillumination cameras.(Kirkwood *et al.*, 2009; Weiner *et al.*, 2014)

Anterior segment imaging is considered to be a clinical and research area in constant evolution. Rotational Scheimpflug imaging enables tomographic analysis of the anterior segment of the eye, providing objective data from the anterior surface of the cornea to the posterior surface of the crystalline lens. Standardized slit lamp biomicroscopy is not going to be replaced by this imaging technology, but Scheimpflug imaging may supplement ophthalmic research and clinical evaluation, especially in the cataract area. Nevertheless, Scheimpflug imaging proved to be a more sensitive and reproducible approach for crystalline lens assessment. Our findings suggest that Scheimpflug-based lens densitometry is useful in the preoperative evaluation of patients with age-related nuclear cataracts. This tool demonstrated to be representative of the functional status of the crystalline lens. Scheimpflug-based densitometry also showed to be useful regarding phacodynamics prediction, in order to reduce the US energy delivery and resulting endothelial damage. The data presented in this PhD thesis warns for the proper use of the lens densitometry software, concerning selection and placement of the densitometry template, as well as the density metric adopted. Further studies are needed to optimize the analysis algorithms and parameters. Combination with other parameters derived from other technology, such as the DLI, may enhance the preoperative evaluation of eyes with age-related nuclear cataract.





# **CHAPTER VII**

## CONCLUSIONS



## CHAPTER VII – CONCLUSIONS

The discussion that we have just make allows us to present the following conclusions:

### **1 – Relationship between Scheimpflug optical densitometry and ocular HOAs in patients with mild nuclear cataract:**

- Quantification parameters derived from the Scheimpflug lens densitometry (average density and maximum density) demonstrated a relationship with aging, CDVA decrease and NO.
- Scheimpflug densitometry of mild grade nuclear cataracts showed a positive correlation with total HOAs measured by ray-tracing aberrometry.
- Internal HOAs, including coma and trefoil aberrations, also demonstrated a relationship with Scheimpflug-based lens density variables.
- Despite not being statistically significant, internal spherical aberration presented a negative correlation with the densitometric parameters

### **2 – Relationship between the DLI with lens grading based on the LOCS III and the Scheimpflug-based lens Densitometry**

- Our results indicate that the functional status based on CDVA assessment is more correlated with the DLI parameter compared to LOCS III NO score and Scheimpflug-derived average density variables.
- A relationship between the DLI and the Scheimpflug-based lens densitometry was described, suggesting the usefulness of the lens densitometry based on Scheimpflug imaging as an essential tool to assess objectively the severity of mild forms of age-related nuclear cataracts, as well as for deducing the functional state of the crystalline lens.

### **3 – Relationship between preoperative Scheimpflug-based lens densitometry metrics and phacodynamics:**

- The maximum density derived from the linear mode did not revealed a significant correlation with the LOCS III NO score. Caution should be taken when using this variable for lens densitometry assessment.

- Regarding the ROI and 3D modes, both average density and maximum density parameters presented a significant relationship with the LOCS III NO score.
- Specific Scheimpflug-derived densitometric parameters of the nucleus correlated with phacoemulsification parameters, such as the average density and maximum density variables derived from the ROI and 3D modes.
- The presented data also suggests that proper selection and placement of the densitometry template are essential for correct preoperative evaluation in nuclear cataracts.

#### **4 – Relationship between objective metrics for quantifying crystalline lens dysfunction with visual impairment and phacodynamics parameters in patients with age-related nuclear cataract.**

- The Scheimpflug-derived lens densitometry and the DLI were correlated with the LOCS III grading system and the CDVA, providing useful data regarding the functional status of the crystalline lens.
- Both objective metrics were useful to predict phacodynamics in eyes with age-related nuclear cataracts.

Regarding future perspectives, new imaging technologies are currently available in the market, such as swept-source optical coherence tomography and very-high frequency US.(Wong *et al.*, 2009; Reinstein *et al.*, 2009) The measurement principles are distinct compared to Scheimpflug imaging. Research studies are needed to compare these technologies with Scheimpflug imaging and to analyze their role in the preoperative evaluation and surgical planning. Further widespread of femtosecond-assisted cataract surgery may enhance the concept for an adequate and objective preoperative assessment of the cataract density. Scheimpflug-based lens density might help in the improvement of the laser parameters settings, to promote safety for the intraocular structures and to avoid surgical complications. Research studies are testing new therapeutic options for treating age-related cataracts, especially focusing on restoring lens transparency. In this context, a recent drug based on lanosterol was developed. The concept to test the effectiveness of this naturally-occurring steroid on cataracts resulted from

the evaluation of two Chinese children with an inherited congenital cataract.(Makley *et al.*, 2015) Interestingly, these siblings presented a similar mutation that stopped the production of lanosterol, which their parents lacked and consequently did not present cataracts. The researchers proposed that lanosterol might stabilize the Alpha crystallin proteins and restore the protein solubility in age-related cataracts.(Kong *et al.*, 2015) In a laboratory setting, a lanosterol-based eye drop was produced and tested on mice and synthetic human cataracts.(Makley *et al.*, 2015) This solution demonstrated to reduce the lens opacity significantly in all study groups. Interestingly, another Chinese research group presented a technique of generating a new transparent and accommodating crystalline lens following cataract removal in rabbits, macaques and in a series of 24 eyes of paediatric patients.(Lin *et al.*, 2016) This procedure involved the opaque lens removal through a 1.5 mm anterior capsulorhexis and leaving intact the lens epithelial cells on the periphery of the capsular bag. During the follow-up, the anterior capsular openings healed within one month after surgery and by three months a regenerated transparent biconvex crystalline lens was present.(Lin *et al.*, 2016) The role of Scheimpflug imaging is undoubtful in clinical trials for testing the effectiveness of new therapeutic approaches, as this technology can objectively report density changes in the crystalline lens.



## **REFERENCES**





**REFERENCES**

- Adamsons I, Rubin GS, Vitale S, Taylor HR, Stark WJ. The effect of early cataracts on glare and contrast sensitivity. A pilot study. *Arch Ophthalmol* 1992;110:1081-6.
- Agarwal S, Agarwal A, Apple DJ, Buratto L, Alio JL, Pandey SK, Agarwal A. *Textbook of Ophthalmology*. 1 ed. New Dehli - India: Jaypee Brothers Medical Publishers; 2002.
- Ahuja RP, Borchman D, Dean WL, Paterson CA, Zeng J, Zhang Z, Ferguson-Yankey S, Yappert MC. Effect of oxidation on Ca<sup>2+</sup> -ATPase activity and membrane lipids in lens epithelial microsomes. *Free Radic Biol Med* 1999;27:177-85.
- al-Ghoul KJ, Costello MJ. Fiber cell morphology and cytoplasmic texture in cataractous and normal human lens nuclei. *Curr Eye Res* 1996;15:533-42.
- Alió JL, Schimchak P, Negri HP, Montés-Micó R. Crystalline lens optical dysfunction through aging. *Ophthalmology* 2005;112:2022-9
- Ambrósio R, Jr., Belin MW. Imaging of the cornea: topography vs tomography. *J Refract Surg* 2010;26:847-9.
- Ambrósio R, Jr., Caiado AL, Guerra FP, Louzada R, Roy AS, Luz A, Dupps WJ, Belin MW. Novel pachymetric parameters based on corneal tomography for diagnosing keratoconus. *J Refract Surg* 2011;27:753-8.
- Ambrósio R, Jr., Chalita MR, Netto MV, Schor P, Chamon W, Fontes BM. *Wavefront & Topografia, Tomografia e Biomecânica da Córnea - Propedêutica Complementar em Cirurgia Refrativa*. 1 ed. Rio de Janeiro - Brasil: Cultura Médica; 2012.
- Ambrósio R, Jr., Klyce SD, Wilson SE. Corneal topographic and pachymetric screening of keratorefractive patients. *J Refract Surg* 2003;19:24-9.
- Ambrósio R, Jr., Nogueira LP, Caldas DL, Fontes BM, Luz A, Casal JO, Alves MR, Belin MW. Evaluation of corneal shape and biomechanics before LASIK. *Int Ophthalmol Clin* 2011;51:11-38.
- Ambrósio R, Jr., Valbon BF, Faria-Correia F, Ramos I, Luz A. Scheimpflug imaging for laser refractive surgery. *Curr Opin Ophthalmol* 2013;24:310-20.

- Applegate R, Atchison D, Bradley A, Bruce A, Collins M, Marsack J, Read S, Thibos LN, Yoon G. Wavefront refraction and correction. *Optom Vis Sci* 2014;91:1154-5.
- Applegate RA, Ballentine C, Gross H, Sarver EJ, Sarver CA. Visual acuity as a function of Zernike mode and level of root mean square error. *Optom Vis Sci* 2003;80:97-105.
- Applegate RA, Hilmantel G, Howland HC, Tu EY, Starck T, Zayac EJ. Corneal first surface optical aberrations and visual performance. *J Refract Surg* 2000;16:507-14.
- Applegate RA, Howland HC. Refractive surgery, optical aberrations, and visual performance. *J Refract Surg* 1997;13:295-9.
- Applegate RA, Marsack JD, Ramos R, Sarver EJ. Interaction between aberrations to improve or reduce visual performance. *J Cataract Refract Surg* 2003;29:1487-95.
- Applegate RA, Sarver EJ, Khemsara V. Are all aberrations equal? *J Refract Surg* 2002;18:S556-62.
- Archer SM. Monocular diplopia due to spherocylindrical refractive errors (an American Ophthalmological Society thesis). *Trans Am Ophthalmol Soc* 2007;105:252-71.
- Artal P, Benito A, Perez GM, Alcon E, De Casas A, Pujol J, Marin JM. An objective scatter index based on double-pass retinal images of a point source to classify cataracts. *PLoS One* 2011;6:e16823.
- Artal P, Berrio E, Guirao A, Piers P. Contribution of the cornea and internal surfaces to the change of ocular aberrations with age. *J Opt Soc Am A Opt Image Sci Vis* 2002;19:137-43.
- Audette DS, Scheiblin DA, Duncan MK. The molecular mechanisms underlying lens fiber elongation. *Exp Eye Res* 2016.
- Balaram M, Tung WH, Kuszak JR, Ayaki M, Shinohara T, Chylack LT, Jr. Noncontact specular microscopy of human lens epithelium. *Invest Ophthalmol Vis Sci* 2000;41:474-81.
- Bartsch DU, Bessho K, Gomez L, Freeman WR. Comparison of laser ray-tracing and skiascopic ocular wavefront-sensing devices. *Eye (Lond)* 2008;22:1384-90.

- Bassnett S. Mitochondrial dynamics in differentiating fiber cells of the mammalian lens. *Curr Eye Res* 1992;11:1227-32.
- Bassnett S. The fate of the Golgi apparatus and the endoplasmic reticulum during lens fiber cell differentiation. *Invest Ophthalmol Vis Sci* 1995;36:1793-803.
- Bassnett S, Beebe DC. Coincident loss of mitochondria and nuclei during lens fiber cell differentiation. *Dev Dyn* 1992;194:85-93.
- Bassnett S, Costello MJ. The cause and consequence of fiber cell compaction in the vertebrate lens. *Exp Eye Res* 2016.
- Bassnett S, Kuszak JR, Reinisch L, Brown HG, Beebe DC. Intercellular communication between epithelial and fiber cells of the eye lens. *J Cell Sci* 1994;107 ( Pt 4):799-811.
- Bassnett S, Missey H, Vucemilo I. Molecular architecture of the lens fiber cell basal membrane complex. *J Cell Sci* 1999;112 ( Pt 13):2155-65.
- Beebe DC. The lens, in *Adler's Physiology of the Eye*, 11<sup>th</sup> ed. (Philadelphia: Elsevier Saunders, 2011), 131 - 63.
- Bencic G, Zoric-Geber M, Saric D, Corak M, Mandic Z. Clinical importance of the lens opacities classification system III (LOCS III) in phacoemulsification. *Coll Antropol* 2005;29 Suppl 1:91-4.
- Berthoud VM, Beyer EC. Oxidative stress, lens gap junctions, and cataracts. *Antioxid Redox Signal* 2009;11:339-53.
- Bhuyan KC, Bhuyan DK. Superoxide dismutase of the eye: relative functions of superoxide dismutase and catalase in protecting the ocular lens from oxidative damage. *Biochim Biophys Acta* 1978;542:28-38.
- Bloemendal H, de Jong W, Jaenicke R, Lubsen NH, Slingsby C, Tardieu A. Ageing and vision: structure, stability and function of lens crystallins. *Prog Biophys Mol Biol* 2004;86:407-85.
- Bobrow JC, Beardsley TL, Jick SL, Rosenberg LF, Wiggins MN, Reich J, Isbey EK. 2014 - 2015 Basic and Clinical Science Course, Section 11: Lens and Cataract ed.: American Academy of Ophthalmology; 2014.
- Boileau TW, Bray TM, Bomser JA. Ultraviolet radiation modulates nuclear factor kappa B activation in human lens epithelial cells. *J Biochem Mol Toxicol* 2003;17:108-13.
- Borchman D, Paterson CA, Delamere NA. Ca<sup>2+</sup>-ATPase activity in the human lens. *Curr Eye Res* 1989;8:1049-54.

- Braccio L, Camparini M, Graziosi P, Baratta G, Ferrigno L, Williams SL, Rosmini F, Sperduto RD, Maraini G. An independent evaluation of the Age-Related Eye Disease Study (AREDS) cataract grading system. *Curr Eye Res* 1998;17:53-9.
- Braga-Mele R, Chang D, Dewey S, Foster G, Henderson BA, Hill W, Hoffman R, Little B, Mamalis N, Oetting T, Serafino D, Talley-Rostov A, Vasavada A, Yoo S, Committee ACC. Multifocal intraocular lenses: relative indications and contraindications for implantation. *J Cataract Refract Surg* 2014;40:313-22.
- Brennan LA, McGreal RS, Kantorow M. Oxidative stress defense and repair systems of the ocular lens. *Front Biosci (Elite Ed)* 2012;4:141-55.
- Brown N. Quantitative slit-image photography of the anterior chamber. *Trans Ophthalmol Soc U K* 1973a;93:277-86.
- Brown N. Slit-image photography and measurement of the eye. *Med Biol Illus* 1973b;23:192-203.
- Buscemi P. Clinical applications of the OPD-Scan wavefront aberrometer/corneal topographer. *J Refract Surg* 2002;18:S385-8.
- Bye LA. Anatomy, in *Basic Sciences for Ophthalmology*, 1st ed. (Oxford: Oxford University Press; 2013) 1-57.
- Cabot F, Saad A, McAlinden C, Haddad NM, Grise-Dulac A, Gatinel D. Objective assessment of crystalline lens opacity level by measuring ocular light scattering with a double-pass system. *Am J Ophthalmol* 2013;155:629-35, 35 e1-2.
- Callahan A. Direct zonulolysis with stripper for cataract extraction. *Am J Ophthalmol* 1967;63:316-9.
- Canals M, Costa-Vila J, Potau JM, Merindano MD, Ruano D. Scanning electron microscopy of the human zonule of the lens (Zonula ciliaris). *Acta Anat (Basel)* 1996;157:309-14.
- Carpentier J. Improvements in Enlarging or like Cameras. GB Patent 1901;1139.
- Cervino A, Hosking SL, Montes-Mico R, Bates K. Clinical ocular wavefront analyzers. *J Refract Surg* 2007;23:603-16.
- Chang DF. Converting to phaco chop: why and how. *Ophthalmic Practice* 1999;22:526-29.

- Cheng C, Xia CH, Li L, White TW, Niimi J, Gong X. Gap junction communication influences intercellular protein distribution in the lens. *Exp Eye Res* 2008;86:966-74.
- Cheng HM, Fagerholm P, Chylack LT, Jr. Response of the lens to oxidative-osmotic stress. *Exp Eye Res* 1983;37:11-21.
- Cheng X, Thibos LN, Bradley A. Estimating visual quality from wavefront aberration measurements. *J Refract Surg* 2003;19:S579-84.
- Chua BE, Mitchell P, Cumming RG. Effects of cataract type and location on visual function: the Blue Mountains Eye Study. *Eye (Lond)* 2004;18:765-72.
- Chylack LT, Jr. Mechanisms of senile cataract formation. *Ophthalmology* 1984;91:596-602.
- Chylack LT, Wolfe JK, Singer DM, Leske MC, Bullimore MA, Bailey IL, Friend J, McCarthy D, Wu SY. The Lens Opacities Classification System III. The Longitudinal Study of Cataract Study Group. *Arch Ophthalmol* 1993;111:831-6.
- Colvard DM, Mazzocco TR, Davidson B, Kratz RP, Johnson SH. Technique for implanting secondary posterior chamber intraocular lenses. *J Am Intraocul Implant Soc* 1983;9:463-5.
- Cotlier E. Cataract Image Analysis System. *Eye (Lond)* 1999;13 ( Pt 3b):457-63.
- Courville CB, Smolek MK, Klyce SD. Contribution of the ocular surface to visual optics. *Exp Eye Res* 2004;78:417-25.
- D'Ambrósio FA, Jr. Assessing disability in the patient with cataracts. *Curr Opin Ophthalmol* 1999;10:42-5.
- Danysh BP, Duncan MK. The lens capsule. *Exp Eye Res* 2009;88:151-64.
- Datiles MB, Magno BV, Freidlin V. Study of nuclear cataract progression using the National Eye Institute Scheimpflug system. *Br J Ophthalmol* 1995;79:527-34.
- Daviel J. On a new method to cure cataract by extraction of the lens. *Br J Ophthalmol* 1967;51:449-58.
- Davison JA, Chylack LT. Clinical application of the lens opacities classification system III in the performance of phacoemulsification. *J Cataract Refract Surg* 2003;29:138-45.

- Dicarlo CD, Roach WP, Gagliano DA, Boppart SA, Hammer DX, Cox AB, Fujimoto JG. Comparison of optical coherence tomography imaging of cataracts with histopathology. *J Biomed Opt* 1999;4:450-8.
- Direção Geral da Saúde. Programa Nacional para a Saúde da Visão. Lisboa (Portugal). 2005. [Accessed 30<sup>th</sup> October, 2016]. Available at <https://www.dgs.pt/documentos-e-publicacoes/programa-nacional-para-a-saude-da-visao.aspx>
- Direção Geral da Saúde. Rede de Referência de Oftalmologia. Lisboa (Portugal). 2007. [Accessed 30<sup>th</sup> October, 2016]. Available at <http://www.acss.min-saude.pt/Portals/0/Oftalmologia.pdf>.
- Dudek EJ, Shang F, Taylor A. H(2)O(2)-mediated oxidative stress activates NF-kappa B in lens epithelial cells. *Free Radic Biol Med* 2001;31:651-8.
- Duncan G. Cation movements across lens membranes. *Exp Eye Res* 1969a;8:233.
- Duncan G. Relative permeabilities of the lens membranes to sodium and potassium. *Exp Eye Res* 1969b;8:315-25.
- Duncan G, Wormstone IM, Davies PD. The aging human lens: structure, growth, and physiological behaviour. *Br J Ophthalmol* 1997;81:818-23.
- Eckerskorn U, Hockwin O, Muller-Breitenkamp R, Chen TT, Knowles W, Dobbs RE. Evaluation of cataract-related risk factors using detailed classification systems and multivariate statistical methods. *Dev Ophthalmol* 1987;15:82-91.
- Fagerholm PP, Philipson BT. Human lens epithelium in normal and cataractous lenses. *Invest Ophthalmol Vis Sci* 1981;21:408-14.
- Fagerholm PP, Philipson BT, Lindstrom B. Normal human lens - the distribution of protein. *Exp Eye Res* 1981;33:615-20.
- Fang L, Wang Y, He X. Effect of pupil size on residual wavefront aberration with transition zone after customized laser refractive surgery. *Opt Express* 2013;21:1404-16.
- Ferrer JV, Gasco E, Sastre J, Pallardo FV, Asensi M, Vina J. Age-related changes in glutathione synthesis in the eye lens. *Biochem J* 1990;269:531-4.
- Fine IH, Packer M, Hoffman RS. Power modulations in new phacoemulsification technology: improved outcomes. *J Cataract Refract Surg* 2004;30:1014-9.

- Fischbarg J, Diecke FP, Kuang K, Yu B, Kang F, Iserovich P, Li Y, Rosskoth H, Koniarek JP. Transport of fluid by lens epithelium. *Am J Physiol* 1999;276:C548-57.
- Fisher RF, Pettet BE. The postnatal growth of the capsule of the human crystalline lens. *J Anat* 1972;112:207-14.
- Foster CS, Sainz de la Maza M. *The Sclera*. ed.: 1<sup>st</sup>. New York: Springer-Verlag: 1994.
- Fotiadis D, Hasler L, Muller DJ, Stahlberg H, Kistler J, Engel A. Surface tongue-and-groove contours on lens MIP facilitate cell-to-cell adherence. *J Mol Biol* 2000;300:779-89.
- Frick KD, Foster A. The magnitude and cost of global blindness: an increasing problem that can be alleviated. *Am J Ophthalmol* 2003;135:471-6.
- Friedman NJ, Kohlen T, Koch DD. Phaco chop: making the transition. *Dev Ophthalmol* 2002;34:74-8.
- Fujikado T, Kuroda T, Maeda N, Ninomiya S, Goto H, Tano Y, Oshika T, Hirohara Y, Mihashi T. Light scattering and optical aberrations as objective parameters to predict visual deterioration in eyes with cataracts. *J Cataract Refract Surg* 2004;30:1198-208.
- Gao J, Sun X, Martinez-Wittinghan FJ, Gong X, White TW, Mathias RT. Connections between connexins, calcium, and cataracts in the lens. *J Gen Physiol* 2004;124:289-300.
- Gao J, Wang H, Sun X, Varadaraj K, Li L, White TW, Mathias RT. The effects of age on lens transport. *Invest Ophthalmol Vis Sci* 2013;54:7174-87.
- Garland DL, Duglas-Tabor Y, Jimenez-Asensio J, Datiles MB, Magno B. The nucleus of the human lens: demonstration of a highly characteristic protein pattern by two-dimensional electrophoresis and introduction of a new method of lens dissection. *Exp Eye Res* 1996;62:285-91.
- Garner MH, Kong Y. Lens epithelium and fiber Na,K-ATPases: distribution and localization by immunocytochemistry. *Invest Ophthalmol Vis Sci* 1999;40:2291-8.
- Gilroy AM, MacPherson BR, Ross LR. *Atlas of Anatomy*. ed.: 2nd. New York: Thieme Medical Publishers, Inc.; 2009.
- Gimbel HV. Divide and conquer nucleofractis phacoemulsification: development and variations. *J Cataract Refract Surg* 1991;17:281-91.

- Gomez AC, del Rey AV, Bautista CP, Ferrandiz AE, Gonzales DC, Burgos SC. Principles and Clinical Applications of Ray-Tracing aberrometry (Part I). *J Emmetropia* 2012;96-110.
- Grewal DS, Brar GS, Grewal SP. Correlation of nuclear cataract lens density using Scheimpflug images with Lens Opacities Classification System III and visual function. *Ophthalmology* 2009;116:1436-43.
- Guirao A, Gonzalez C, Redondo M, Geraghty E, Norrby S, Artal P. Average optical performance of the human eye as a function of age in a normal population. *Invest Ophthalmol Vis Sci* 1999;40:203-13.
- Gupta A, Singh J, Dhillon B. Cataract classification system for risk stratification in surgery. *J Cataract Refract Surg* 2011;37:1363-4.
- Gupta M, Ram J, Jain A, Sukhija J, Chaudhary M. Correlation of nuclear density using the Lens Opacity Classification System III versus Scheimpflug imaging with phacoemulsification parameters. *J Cataract Refract Surg* 2013;39:1818-23.
- Hall AB, Thompson JR, Deane JS, Rosenthal AR. LOCS III versus the Oxford Clinical Cataract Classification and Grading System for the assessment of nuclear, cortical and posterior subcapsular cataract. *Ophthalmic Epidemiol* 1997;4:179-94.
- Handzel DM, Meyer CH, Wegener A. [Possibilities for use of Scheimpflug technology in cataract surgery]. *Ophthalmologe* 2014;111:927-34.
- Hanssen E, Franc S, Garrone R. Fibrillin-rich microfibrils: structural modifications during ageing in normal human zonule. *J Submicrosc Cytol Pathol* 1998;30:365-9.
- He L, Sheehy K, Culbertson W. Femtosecond laser-assisted cataract surgery. *Curr Opin Ophthalmol* 2011;22:43-52.
- Hejtmancik JF, Riazuddin SA, McGreal R, Liu W, Cvekl A, Shiels A. Lens Biology and Biochemistry. *Prog Mol Biol Transl Sci* 2015;134:169-201.
- Hejtmancik JF, Shiels A. Overview of the Lens. *Prog Mol Biol Transl Sci* 2015;134:119-27.
- Hockwin O. Cataract classification. *Doc Ophthalmol* 1994;88:263-75.
- Holden BA. Blindness and poverty: a tragic combination. *Clin Exp Optom* 2007;90:401-3.
- Jaffe NS. History of cataract surgery. *Ophthalmology* 1996;103:S5-16.



- Jahngen-Hodge J, Taylor A, Shang F, Huang LL, Mura C. Oxidative stress to lens crystallins. *Methods Enzymol* 1994;233:512-22.
- Javitt J, Venkataswamy G, Sommer A, Henkind P. The economic and social aspect of restoring sight. . In: J.P. Lippincott. ACTA: 24th International Congress of Ophthalmology pp 1308-1312. ed. New York: 1983.
- Kaemmerer M, Mrochen M, Mierdel P, Krinke HE, Seiler T. Clinical experience with the Tscherning aberrometer. *J Refract Surg* 2000;16:S584-7.
- Kamei A. Glutathione levels of the human crystalline lens in aging and its antioxidant effect against the oxidation of lens proteins. *Biol Pharm Bull* 1993;16:870-5.
- Karbassi M, Khu PM, Singer DM, Chylack LT, Jr. Evaluation of lens opacities classification system III applied at the slitlamp. *Optom Vis Sci* 1993;70:923-8.
- Kelley PB, Sado Y, Duncan MK. Collagen IV in the developing lens capsule. *Matrix Biol* 2002;21:415-23.
- Kelman CD. Phaco-emulsification and aspiration. A new technique of cataract removal. A preliminary report. *Am J Ophthalmol* 1967;64:23-35.
- Kelman CD. Phaco-emulsification and aspiration. A progress report. *Am J Ophthalmol* 1969;67:464-77.
- Kelman CD. Cataract emulsification and aspiration. *Trans Ophthalmol Soc U K* 1970;90:13-22.
- Kelman CD. Phacoemulsification in the anterior chamber. *Ophthalmology* 1979;86:1980-2.
- Kim JS, Chung SH, Joo CK. Clinical application of a Scheimpflug system for lens density measurements in phacoemulsification. *J Cataract Refract Surg* 2009;35:1204-9.
- Kim P, Sutton GL, Rootman DS. Applications of the femtosecond laser in corneal refractive surgery. *Curr Opin Ophthalmol* 2011;22:238-44.
- King, D. Eye, lens, iris and ciliary body. SIU SOM, 2004. [Accessed 30<sup>th</sup> October, 2016]. Available at <http://www.siumed.edu/~dking2/ssb/EE012b.htm>
- Kinoshita JH. Carbohydrate metabolism of lens. *AMA Arch Ophthalmol* 1955;54:360-8.
- Kinoshita JH. Pathways of Glucose Metabolism in the Lens. *Invest Ophthalmol* 1965;4:619-28.

- Kirkwood BJ, Hendicott PL, Read SA, Pesudovs K. Repeatability and validity of lens densitometry measured with Scheimpflug imaging. *J Cataract Refract Surg* 2009;35:1210-5
- Klein BE, Klein R, Lee KE. Incidence of age-related cataract: the Beaver Dam Eye Study. *Arch Ophthalmol* 1998;116:219-25.
- Koch DD, Ali SF, Weikert MP, Shirayama M, Jenkins R, Wang L. Contribution of posterior corneal astigmatism to total corneal astigmatism. *J Cataract Refract Surg* 2012;38:2080-7.
- Koch PS, Katzen LE. Stop and chop phacoemulsification. *J Cataract Refract Surg* 1994;20:566-70.
- Kojima M, Wegener A, Hockwin O. Imaging characteristics of three cameras using the Scheimpflug principle. *Ophthalmic Res* 1990;22 Suppl 1:29-35.
- Kong XD, Liu N, Shi HR, Dong JM, Zhao ZH, Liu J, Li-Ling J, Yang YX. A novel 3-base pair deletion of the CRYAA gene identified in a large Chinese pedigree featuring autosomal dominant congenital perinuclear cataract. *Genet Mol Res* 2015;14:426-32.
- Kratz RP, Mazzocco TR, Davidson B, Colvard DM. A comparative analysis of anterior chamber, iris-supported, capsule-fixated, and posterior chamber intraocular lenses following cataract extraction by phacoemulsification. *Ophthalmology* 1981;88:56-8.
- Krwawicz T. Intracapsular Extraction of Intumescent Cataract by Application of Low Temperature. *Br J Ophthalmol* 1961;45:279-83.
- Krwawicz T. Further Experience with Intracapsular Cataract Extraction by Application of Low Temperature. *Br J Ophthalmol* 1963;47:36-8.
- Kuroda T, Fujikado T, Maeda N, Oshika T, Hirohara Y, Mihashi T. Wavefront analysis in eyes with nuclear or cortical cataract. *Am J Ophthalmol* 2002a;134:1-9
- Kuroda T, Fujikado T, Maeda N, Oshika T, Hirohara Y, Mihashi T. Wavefront analysis of higher-order aberrations in patients with cataract. *J Cataract Refract Surg* 2002b;28:438-44.
- Kuroda T, Fujikado T, Ninomiya S, Maeda N, Hirohara Y, Mihashi T. Effect of aging on ocular light scatter and higher order aberrations. *J Refract Surg* 2002;18:S598-602

- Kuszak JR. The ultrastructure of epithelial and fiber cells in the crystalline lens. *Int Rev Cytol* 1995;163:305-50.
- Kuszak JR, Bertram BA, Macsai MS, Rae JL. Sutures of the crystalline lens: a review. *Scan Electron Microsc* 1984:1369-78.
- Kuszak JR, Costello MJ. Embryology and anatomy of human lenses, in Duane's *Clinical Ophthalmology*. ed.: 2002: Philadelphia: Lippincott; 2002:1 - 20.
- Kuszak JR, Ennesser CA, Bertram BA, Imherr-McMannis S, Jones-Rufer LS, Weinstein RS. The contribution of cell-to-cell fusion to the ordered structure of the crystalline lens. *Lens Eye Toxic Res* 1989;6:639-73.
- Kuszak JR, Macsai MS, Bloom KJ, Rae JL, Weinstein RS. Cell-to-cell fusion of lens fiber cells in situ: correlative light, scanning electron microscopic, and freeze-fracture studies. *J Ultrastruct Res* 1985;93:144-60.
- Kuszak JR, Macsai MS, Rae JL. Stereo scanning electron microscopy of the crystalline lens. *Scan Electron Microsc* 1983:1415-26.
- Kuszak JR, Zoltoski RK, Tiedemann CE. Development of lens sutures. *Int J Dev Biol* 2004;48:889-902.
- Laganowsky A, Benesch JL, Landau M, Ding L, Sawaya MR, Cascio D, Huang Q, Robinson CV, Horwitz J, Eisenberg D. Crystal structures of truncated alphaA and alphaB crystallins reveal structural mechanisms of polydispersity important for eye lens function. *Protein Sci* 2010;19:1031-43.
- Lampi KJ, Ma Z, Hanson SR, Azuma M, Shih M, Shearer TR, Smith DL, Smith JB, David LL. Age-related changes in human lens crystallins identified by two-dimensional electrophoresis and mass spectrometry. *Exp Eye Res* 1998;67:31-43.
- Lang GK. *Ophthalmology: a pocket textbook atlas*. 2 ed. New York: Thieme; 2007.
- Lee J, Kim MJ, Tchah H. Higher-order aberrations induced by nuclear cataract. *J Cataract Refract Surg* 2008;34:2104-9.
- Leinfelder PJ. Metabolism of the lens and the occurrence of cataract. *Trans Am Ophthalmol Soc* 1953;51:301-5.
- Li DW, Liu JP, Wang J, Mao YW, Hou LH. Expression and activity of the signaling molecules for mitogen-activated protein kinase pathways in human, bovine, and rat lenses. *Invest Ophthalmol Vis Sci* 2003;44:5277-86.

- Li WC, Kuszak JR, Dunn K, Wang RR, Ma W, Wang GM, Spector A, Leib M, Cotliar AM, Weiss M, et al. Lens epithelial cell apoptosis appears to be a common cellular basis for non-congenital cataract development in humans and animals. *J Cell Biol* 1995;130:169-81.
- Liang JN, Li XY. Interaction and aggregation of lens crystallins. *Exp Eye Res* 1991;53:61-6.
- Lim SA, Hwang J, Hwang KY, Chung SH. Objective assessment of nuclear cataract: comparison of double-pass and Scheimpflug systems. *J Cataract Refract Surg* 2014;40:716-21.
- Lin H, Ouyang H, Zhu J, Huang S, Liu Z, Chen S, Cao G, Li G, Signer RA, Xu Y, Chung C, Zhang Y, Lin D, Patel S, Wu F, Cai H, Hou J, Wen C, Jafari M, Liu X, Luo L, Zhu J, Qiu A, Hou R, Chen B, Chen J, Granet D, Heichel C, Shang F, Li X, Krawczyk M, Skowronska-Krawczyk D, Wang Y, Shi W, Chen D, Zhong Z, Zhong S, Zhang L, Chen S, Morrison SJ, Maas RL, Zhang K, Liu Y. Lens regeneration using endogenous stem cells with gain of visual function. *Nature* 2016;531:323-8.
- Lo WK, Harding CV. Structure and distribution of gap junctions in lens epithelium and fiber cells. *Cell Tissue Res* 1986;244:253-63.
- Lorente R, and Mendicute J. *Cirurgía del cristalino (Volume 1)*. ed.: 1<sup>st</sup> Madrid - España: Macline S.L. - Sociedad Española de Oftalmología 2008.
- Mackic JB, Jinagouda S, McComb JG, Weiss MH, Kannan R, Kaplowitz N, Zlokovic BV. Transport of circulating reduced glutathione at the basolateral side of the anterior lens epithelium: physiologic importance and manipulations. *Exp Eye Res* 1996;62:29-37.
- Maeda K. Assessment of Corneal Optical Quality for Premium IOLs with Pentacam. *Highlights of Ophthalmology* 2011;39:2-5.
- Magno BV, Freidlin V, Datiles MB. Reproducibility of the NEI Scheimpflug Cataract Imaging System. *Invest Ophthalmol Vis Sci* 1994;35:3078-84.
- Magno BV, Lasa MS, Freidlin V, Datiles MB. Comparison of linear, multilinear and mask microdensitometric analyses of Scheimpflug images of the lens nucleus. *Curr Eye Res* 1994;13:825-31.
- Maisel H. Cytoskeletal proteins of the ageing human lens. *Ciba Found Symp* 1984;106:163-76.

- Majumder, P.D. Anatomy of Lens. eOphtha, 2008. [Accessed 30<sup>th</sup> October, 2016]. Available at <http://www.eophtha.com/eophtha/anatomy/anatomyoflens3.html>
- Makley LN, McMenimen KA, DeVree BT, Goldman JW, McGlasson BN, Rajagopal P, Duniyak BM, McQuade TJ, Thompson AD, Sunahara R, Klevit RE, Andley UP, Gestwicki JE. Pharmacological chaperone for alpha-crystallin partially restores transparency in cataract models. *Science* 2015;350:674-7.
- Marcantonio JM, Duncan G. Calcium-induced degradation of the lens cytoskeleton. *Biochem Soc Trans* 1991;19:1148-50.
- Marsack JD, Thibos LN, Applegate RA. Metrics of optical quality derived from wave aberrations predict visual performance. *J Vis* 2004;4:322-8.
- Marshall J, Beaconsfield M, Rothery S. The anatomy and development of the human lens and zonules. *Trans Ophthalmol Soc U K* 1982;102 Pt 3:423-40.
- Mathias RT, Kistler J, Donaldson P. The lens circulation. *J Membr Biol* 2007;216:1-16.
- Mathias RT, Rae JL. The lens: local transport and global transparency. *Exp Eye Res* 2004;78:689-98.
- Mathias RT, Rae JL, Baldo GJ. Physiological properties of the normal lens. *Physiol Rev* 1997;77:21-50.
- Mazzocco TR, Kratz RP, Davidson B, Colvard DM. Secondary posterior chamber intraocular lens implants. *J Am Intraocul Implant Soc* 1981;7:341-3.
- McLean P, Gonzalez AM, Sochor M, Hothersall JS. Lens metabolism and cellular effects of aldose reductase. *Diabet Med* 1985;2:189-93.
- Mecham RP, Hinek A, Cleary EG, Kucich U, Lee SJ, Rosenbloom J. Development of immunoreagents to ciliary zonules that react with protein components of elastic fiber microfibrils and with elastin-producing cells. *Biochem Biophys Res Commun* 1988;151:822-6.
- Mertens EL. Is a Robust Growth of Premium IOL Use in the Cards? *Cataract and Refractive Surgery Today Europe* 2015;15:42.
- Mescher A, Mescher AL, Anthony L. The Eye & Ear: Special Sense Organs, in Junqueira's Basic Histology. ed.:14<sup>th</sup>. New York: McGraw Hill Medical; 2015:479 - 510.

- Mierzejewski A, Kalluzny JJ, Kaluzny B, Eliks I. [Cataract phacoemulsification techniques: "divide and conquer" versus "stop and chop"--comparative evaluation of operation course and early results]. *Klin Oczna* 2004;106:612-7.
- Ming, P.Y. Eye doctor trivia. 2013. [Accessed 30<sup>th</sup> October, 2016]. Available at [http://eyesurgerysingapore.blogspot.pt/2013\\_09\\_01\\_archive.html](http://eyesurgerysingapore.blogspot.pt/2013_09_01_archive.html).
- Molebny VV, Panagopoulou SI, Molebny SV, Wakil YS, Pallikaris IG. Principles of ray tracing aberrometry. *J Refract Surg* 2000;16:S572-5.
- Mrochen M, Kaemmerer M, Mierdel P, Krinke HE, Seiler T. Principles of Tscherning aberrometry. *J Refract Surg* 2000;16:S570-1.
- Mukhopadhyay B, Sharma KR. Cataract surgery in susruta samhita. *Anc Sci Life* 1992;11:169-73.
- Nagy Z, Takacs A, Filkorn T, Sarayba M. Initial clinical evaluation of an intraocular femtosecond laser in cataract surgery. *J Refract Surg* 2009;25:1053-60.
- Netter FH. Atlas of human anatomy. ed.: 5th. Philadelphia: Saunders Elsevier; 2011.
- Netto MV, Ambrósio R, Jr., Shen TT, Wilson SE. Wavefront analysis in normal refractive surgery candidates. *J Refract Surg* 2005;21:332-8.
- Nieves-Moreno M, Asorey-Garcia A, Santos-Bueso E, Garcia-Sanchez J. [History of cataract surgery (I): from destruction to removal]. *Arch Soc Esp Oftalmol* 2015a;90:e3-5.
- Nieves-Moreno M, Asorey-Garcia A, Santos-Bueso E, Garcia-Sanchez J. [History of cataract surgery (II): from the removal of the lens to phacoemulsification]. *Arch Soc Esp Oftalmol* 2015b;90:e22-4.
- Nixon DR. Preoperative cataract grading by Scheimpflug imaging and effect on operative fluidics and phacoemulsification energy. *J Cataract Refract Surg* 2010;36:242-6
- Obuchowska I, Mariak Z. [Jacques Daviel--the inventor of the extracapsular cataract extraction surgery]. *Klin Oczna* 2005;107:567-71.
- Oliveira CM, Ferreira A, Franco S. Wavefront analysis and Zernike polynomial decomposition for evaluation of corneal optical quality. *J Cataract Refract Surg* 2012;38:343-56.

- Ortiz D, Alió JL, Ruiz-Colech J, Oser U. Grading nuclear cataract opacity by densitometry and objective optical analysis. *J Cataract Refract Surg* 2008;34:1345-52
- Oshika T, Klyce SD, Applegate RA, Howland HC. Changes in corneal wavefront aberrations with aging. *Invest Ophthalmol Vis Sci* 1999;40:1351-5.
- Osnes-Ringen O, Berg KH, Moe MC, Zetterstrom C, Roger M, Nicolaissen B. Cell death pattern in lens epithelium of cataract patients. *Acta Ophthalmol* 2016;94:514-20.
- Pan AP, Wang QM, Huang F, Huang JH, Bao FJ, Yu AY. Correlation among lens opacities classification system III grading, visual function index-14, pentacam nucleus staging, and objective scatter index for cataract assessment. *Am J Ophthalmol* 2015;159:241-7 e2.
- Park J, Yum HR, Kim MS, Harrison AR, Kim EC. Comparison of phaco-chop, divide-and-conquer, and stop-and-chop phaco techniques in microincision coaxial cataract surgery. *J Cataract Refract Surg* 2013;39:1463-9.
- Paterson CA. Distribution and movement of ions in the ocular lens. *Doc Ophthalmol* 1972;31:1-28.
- Paterson CA, Delamere NA. ATPases and lens ion balance. *Exp Eye Res* 2004;78:699-703.
- Paterson CA, Maurice DM. Diffusion of sodium in extracellular space of the crystalline lens. *Am J Physiol* 1971;220:256-63.
- Patterson JW. Characterization of the equatorial current of the lens. *Ophthalmic Res* 1988;20:139-42.
- Pei X, Bao Y, Chen Y, Li X. Correlation of lens density measured using the Pentacam Scheimpflug system with the Lens Opacities Classification System III grading score and visual acuity in age-related nuclear cataract. *Br J Ophthalmol* 2008;92:1471-5.
- Pepose JS, Applegate RA. Making sense out of wavefront sensing. *Am J Ophthalmol* 2005;139:335-43.
- Piatigorsky J. Lens crystallins and their genes: diversity and tissue-specific expression. *FASEB J* 1989;3:1933-40.
- Pinero DP, Sanchez-Perez PJ, Alio JL. Repeatability of measurements obtained with a ray tracing aberrometer. *Optom Vis Sci* 2011;88:1099-105.

- Rada J, Johson J. Sclera, in *Cornea. Fundamental, diagnosis, and management*. ed.: 3<sup>rd</sup>. Philadelphia: Elsevier Mosby; 2011.
- Ratkay-Traub I, Juhasz T, Horvath C, Suarez C, Kiss K, Ferincz I, Kurtz R. Ultra-short pulse (femtosecond) laser surgery: initial use in LASIK flap creation. *Ophthalmol Clin North Am* 2001;14:347-55, viii-ix.
- Reddy VN. Glutathione and its function in the lens--an overview. *Exp Eye Res* 1990;50:771-8.
- Reddy VN, Giblin FJ. Metabolism and function of glutathione in the lens. *Ciba Found Symp* 1984;106:65-87.
- Reddy VN, Varma SD, Chakrapani B. Transport and metabolism of glutathione in the lens. *Exp Eye Res* 1973;16:105-14.
- Reinstein DZ, Archer TJ, Silverman RH, Rondeau MJ, Coleman DJ. Correlation of anterior chamber angle and ciliary sulcus diameters with white-to-white corneal diameter in high myopes using artemis VHF digital ultrasound. *J Refract Surg* 2009;25:185-94.
- Ridley H. Further observations on intraocular acrylic lenses in cataract surgery. *J Int Coll Surg* 1952;18:825-33.
- Ridley H. Further observations on intraocular acrylic lenses in cataract surgery. *Trans Am Acad Ophthalmol Otolaryngol* 1953;57:98-106.
- Ridley H. Late surgical results of use of the intraocular acrylic lens. *J Int Coll Surg* 1956;26:335-41.
- Riordan-Eva P. Anatomy & Embriology of the Eye, in P. Vaughan & Asbury's *General Ophthalmology*. ed.: 18<sup>th</sup>. New York: McGraw-Hill Medical; 2011:1-26.
- Rocha KM, Nose W, Bottos K, Bottos J, Morimoto L, Soriano E. Higher-order aberrations of age-related cataract. *J Cataract Refract Surg* 2007;33:1442-6.
- Roper KL. Suturing in cataract surgery, with a transitional history of cataract: its early treatment; healing of the cataract wound; and the factors that have advanced the development of modern suture technics. *Trans Am Ophthalmol Soc* 1954;52:587-749.
- Rosales P, Marcos S. Pentacam Scheimpflug quantitative imaging of the crystalline lens and intraocular lens. *J Refract Surg* 2009;25:421-8.



- Rosenberg EA, Sperazza LC. The visually impaired patient. *Am Fam Physician* 2008;77:1431-6.
- Rovati L, Docchio F. Autofluorescence methods in ophthalmology. *J Biomed Opt* 2004;9:9-21.
- Rozema JJ, Van Dyck DE, Tassignon MJ. Clinical comparison of 6 aberrometers. Part 1: Technical specifications. *J Cataract Refract Surg* 2005;31:1114-27.
- Sachdev N, Ormonde SE, Sherwin T, McGhee CN. Higher-order aberrations of lenticular opacities. *J Cataract Refract Surg* 2004;30:1642-8.
- Salomao MQ, Esposito A, Dupps WJ, Jr. Advances in anterior segment imaging and analysis. *Curr Opin Ophthalmol* 2009;20:324-32.
- Sasaki K. Cataract classification systems in epidemiological studies. *Dev Ophthalmol* 1991;21:97-102.
- Sasaki K, Shibata T, Obazawa H, Fujiwara T, Kogure F, Obara Y, Itoi M, Kato K, Akiyama K, Okuyama S. [A cataract classification and grading system]. *Nippon Ganka Gakkai Zasshi* 1989;93:796-800.
- Scheimpflug T. Improved Method and Apparatus for the Systematic Alteration or Distortion of Plane Pictures and Images by Means of Lenses and Mirrors for Photography and for other purposes. GB Patent 1904;1196.
- Scheuring S, Buzhynskyy N, Jaroslowski S, Goncalves RP, Hite RK, Walz T. Structural models of the supramolecular organization of AQP0 and connexons in junctional microdomains. *J Struct Biol* 2007;160:385-94.
- Sethna SS, Holleschau AM, Rathbun WB. Activity of glutathione synthesis enzymes in human lens related to age. *Curr Eye Res* 1982;2:735-42.
- Sharma KK, Santhoshkumar P. Lens aging: effects of crystallins. *Biochim Biophys Acta* 2009;1790:1095-108.
- Shepherd JR. In situ fracture. *J Cataract Refract Surg* 1990;16:436-40.
- Shestopalov VI, Bassnett S. Three-dimensional organization of primary lens fiber cells. *Invest Ophthalmol Vis Sci* 2000;41:859-63.
- Shestopalov VI, Bassnett S. Development of a macromolecular diffusion pathway in the lens. *J Cell Sci* 2003;116:4191-9.
- Simon SA, Zampighi G, McIntosh TJ, Costello MJ, Ting-beall HP, Robertson JD. The structure of junctions between lens fiber cells. *Biosci Rep* 1982;2:333-41.

- Sinjab MM. Five Steps to Start Your Refractive Surgery: A Case-Based Systematic Approach. ed.: 1<sup>st</sup>. New Dehli – India. Jaypee Brothers Medical Publishers; 2014.
- Slavi N, Rubinos C, Li L, Sellitto C, White TW, Mathias R, Srinivas M. Connexin 46 (cx46) gap junctions provide a pathway for the delivery of glutathione to the lens nucleus. *J Biol Chem* 2014;289:32694-702.
- Smith AF, Smith JG. The economic burden of global blindness: a price too high! *Br J Ophthalmol* 1996;80:276-7.
- Standring S. Gray's Anatomy: The Anatomical Basis of Clinical Practice. ed.: 41<sup>st</sup>. Edinburgh – Scotland. Elsevier; 2016.
- Steinberg EP, Tielsch JM, Schein OD, Javitt JC, Sharkey P, Cassard SD, Legro MW, Diener-West M, Bass EB, Damiano AM, et al. The VF-14. An index of functional impairment in patients with cataract. *Arch Ophthalmol* 1994;112:630-8.
- Stifter E, Sacu S, Benesch T, Weghaupt H. Impairment of visual acuity and reading performance and the relationship with cataract type and density. *Invest Ophthalmol Vis Sci* 2005;46:2071-5.
- Storr-Paulsen A, Norregaard JC, Ahmed S, Storr-Paulsen T, Pedersen TH. Endothelial cell damage after cataract surgery: divide-and-conquer versus phaco-chop technique. *J Cataract Refract Surg* 2008;34:996-1000.
- Su SP, McArthur JD, Truscott RJ, Aquilina JA. Truncation, cross-linking and interaction of crystallins and intermediate filament proteins in the aging human lens. *Biochim Biophys Acta* 2011;1814:647-56.
- Tan AC, Loon SC, Choi H, Thean L. Lens Opacities Classification System III: cataract grading variability between junior and senior staff at a Singapore hospital. *J Cataract Refract Surg* 2008;34:1948-52.
- Taylor VL, al-Ghoul KJ, Lane CW, Davis VA, Kuszak JR, Costello MJ. Morphology of the normal human lens. *Invest Ophthalmol Vis Sci* 1996;37:1396-410.
- Thibos LN. Principles of Hartmann-Shack aberrometry. *J Refract Surg* 2000;16:S563-5.
- Thibos LN, Applegate RA, Schwiegerling JT, Webb R, science VSTMV, its a. Standards for reporting the optical aberrations of eyes. *J Refract Surg* 2002;18:S652-60.

- Thibos LN, Hong X. Clinical applications of the Shack-Hartmann aberrometer. *Optom Vis Sci* 1999;76:817-25.
- Thorpe HE. Chymotrypsin: An Aid to Intracapsular Cataract Extraction. *Trans Am Ophthalmol Soc* 1959;57:254-89.
- Varadaraj K, Kumari S, Shiels A, Mathias RT. Regulation of aquaporin water permeability in the lens. *Invest Ophthalmol Vis Sci* 2005;46:1393-402.
- Varadaraj K, Kushmerick C, Baldo GJ, Bassnett S, Shiels A, Mathias RT. The role of MIP in lens fiber cell membrane transport. *J Membr Biol* 1999;170:191-203.
- Varma SD, Srivastava VK, Richards RD. Photoperoxidation in lens and cataract formation: preventive role of superoxide dismutase, catalase and vitamin C. *Ophthalmic Res* 1982;14:167-75.
- Vasavada A, Singh R. Step-by-step chop in situ and separation of very dense cataracts. *J Cataract Refract Surg* 1998;24:156-9.
- Vasavada AR, Desai JP. Stop, chop, chop, and stuff. *J Cataract Refract Surg* 1996;22:526-9.
- Wang L, Santaella RM, Booth M, Koch DD. Higher-order aberrations from the internal optics of the eye. *J Cataract Refract Surg* 2005;31:1512-9.
- Waring IV GO. Diagnosis and Treatment of Dysfunctional Lens Syndrome. *Cataract and Refractive Surgery Today* 2013;13:36 - 38.
- Waring IV, GO. Replacement of dysfunctional lens may pose multiple benefits. Published June 14, 2015. [Accessed 30<sup>th</sup> October, 2016]. Available at <http://ophthalmologytimes.modernmedicine.com/ophthalmologytimes/content/tags/acufocus/replacement-dysfunctional-lens-may-pose-multiple-benefits?page=full>
- Wegener A, Hockwin O, Laser H, Strack C. Comparison of the Nidek EAS 1000 system and the Topcon SL-45 in clinical application. *Ophthalmic Res* 1992;24 Suppl 1:55-62.
- Wegener A, Laser-Junga H. Photography of the anterior eye segment according to Scheimpflug's principle: options and limitations - a review. *Clin Exp Ophthalmol* 2009;37:144-54.
- Weiner X, Baumeister M, Kohnen T, Bühren J. Repeatability of lens densitometry using Scheimpflug imaging. *J Cataract Refract Surg* 2014;40:756-63.

- Wong AL, Leung CK, Weinreb RN, Cheng AK, Cheung CY, Lam PT, Pang CP, Lam DS. Quantitative assessment of lens opacities with anterior segment optical coherence tomography. *Br J Ophthalmol* 2009;93:61-5.
- Wong WL, Li X, Li J, Cheng CY, Lamoureux EL, Wang JJ, Cheung CY, Wong TY. Cataract conversion assessment using lens opacity classification system III and Wisconsin cataract grading system. *Invest Ophthalmol Vis Sci* 2013;54:280-7.
- World Health Organization. Vision 2020 – The Right to see. The Global Initiative for the Elimination of Avoidable Blindness. 2016. [Accessed 30<sup>th</sup> October, 2016]. Available at <http://www.who.int/pbd/Vision2020>.
- World Health Organization. Universal Eye Plan A Global Action Plan 2014-2019. 2013. [Accessed 30<sup>th</sup> October, 2016]. Available at <http://www.who.int/mediacentre/factsheets/fs282/en/>.
- Zhang WZ, Augusteyn RC. Ageing of glutathione reductase in the lens. *Exp Eye Res* 1994;59:91-5.
- Zhu XJ, Zhou P, Zhang KK, Yang J, Luo Y, Lu Y. Epigenetic regulation of alphaA-crystallin in high myopia-induced dark nuclear cataract. *PLoS One* 2013;8:e81900.
- Zinn KM, Mockel-Pohl S. Fine structure and function of ocular tissues. The lens and zonules. *Int Ophthalmol Clin* 1973;13:143-55.



ROLE OF THE SCHEIMPFLUG-BASED LENS DENSITOMETRY IN  
PREOPERATIVE ASSESSMENT OF AGE-RELATED NUCLEAR CATARACTS

FERNANDO ANTÓNIO FARIA-CORREIA

Ano: 2017  
2 Exemplares (1ª Edição)

Produção Gráfica: [www.ajnet.net](http://www.ajnet.net)  
T 252 681 975 / 220 991 392